University of Windsor

Scholarship at UWindsor

1-1-2006

Effects of applied pressures and calcium contents on microstructure and tensile properties of squeeze cast magnesium-aluminum-calcium alloys.

Mohsen Masoumi
University of Windsor

Follow this and additional works at: https://scholar.uwindsor.ca/etd

EFFECTS OF APPLIED PRESSURES AND CALCIUM CONTENTS ON MICROSTRUCTURE AND TENSILE PROPERTIES OF SQUEEZE CAST Mg-Al-Ca ALLOYS

by

Mohsen Masoumi

A Thesis
Submitted to the Faculty of Graduate Studies and Research
through Engineering Materials
in Partial Fulfillment of the Requirements for
the Degree of Master of Applied Science
at the University of Windsor

Windsor, Ontario, Canada

Canada

ABSTRACT

In this study, the effect of applied pressure levels and calcium contents on the microstructure and tensile properties of squeeze cast magnesium alloys AMC50X has been investigated. The results indicate that the tensile properties of AMC501 alloy including ultimate tensile strength (UTS), yield strength (YS), and elongation (E_f) increase as the applied pressure increases from 3 MPa to 90MPa. The improvement in tensile properties can be attributed to casting densification. As the calcium content of AMC50X increases from 0 to 4%, the UTS and E_f decrease dramatically at room temperature, but the yield strengths of the alloys improve slightly. At 150 $^{\circ}$C, however, the UTS of the alloys increases with increasing the Ca content. The variation of E_f and YS of the alloys at 150 $^{\circ}$C are similar to those at room temperature. The results of microstructural analysis indicate that calcium addition has a grain refining effect on the base alloy AM50A.

iii

DEDICATION

I dedicate this thesis to my dear parents, who I owe all my achievement in my life time to their support and effort.

iv

ACKNOWLEDGEMENTS

TABLE OF CONTENTS

viii

CHAPTER IV. RESULTS AND DISCUSSION

x

LIST OF TABLES

xi

LIST OF FIGURES

xv

xvi

CHAPTER I

INTRODUCTION

1.1 Background

Squeeze casting is a process by which molten metal solidifies under pressure within closed dies positioned between the plates of a hydraulic press. The applied pressure and the instant contact of the molten metal with the die surface produce a rapid heat transfer condition that yields a pore-free fine-grain casting with mechanical properties approaching those of a wrought product [1-11]. Although squeeze casting is now the accepted term for this process, squeeze casting also known as liquid pressing [12], extrusion casting [13], liquid forging [14], pressure crystallization [15], and squeeze forming [16].

Although squeeze casting and its variants have been used as a commercial process in the USSR for some time, the process has only recently found commercial applications in the western industrialised world [2-4].

Squeeze casting has its origin in work by Chernov [17], which in 1878 suggested that steam pressure might be applied to molten metal during solidification in a permanent mold. However, the first recorded attempt to study the effect of pressure on the solidification behaviour of liquid metals and alloys was not carried out until 1931 by Welter [18] on Al-Si alloys. The possibility of combining traditionally casting and forging was initially examined in details in the USSR during the late 1930's, principally by Plyatskii [13]. After extensive work, the process parameters governing the technique were successfully resolved, and by the mid 1960's 150 large batch plants were operating in the USSR [2]. After the publication of Plyatskii's authoritative book on squeeze casting

1

in 1965, western interest in the process was awakened, which resulted in active research and commercial production in many countries including the USA, Japan and Britain [2].

The squeeze casting process is easily automated to produce near-net to net-shape high quality components. Aluminium, magnesium, and copper alloy components are readily manufactured using this process. Several ferrous components with relatively simple geometry-for example, nickel hard crusher wheel inserts- have also been manufactured by squeeze casting processes. Despite the shorter die life for complex ferrous castings requiring sharp corners within the die or punch (tooling), the process can be adopted for products where enhanced properties and/or saving in labour or material costs are desired [1, 2].

Squeeze casting is simple and economical, efficient in its use of raw material, and has excellent potential for automated operation at high rates of production. The process generates the highest mechanical properties attainable in a cast product [2].

Magnesium is a plentiful element, comprising 2.7% of the earth's crust, one of the lightest among all the engineering materials with a density of $1.74g/Cm^3$; 35% lighter than aluminum and over four times lighter than iron or steel. Magnesium is frequently used as an alloying element in aluminum to improve the corrosion resistance and machinability. Recent attention has focused on the use of magnesium alloys for weight saving in the transportation and aerospace industries, but still keeping the high strength to weight ratio.

Magnesium alloys meet the demand for a combination of light weight, good machinability and handling, high recycling potential, and are designed as engineering materials. Magnesium has been increasingly used for various automotive applications in

2

the past decade [19]. To increase the use of magnesium to further reduce the weight of vehicles, the next generation of magnesium automotive applications needs to be expanded in a more aggressive sense [19]. One of the potential areas is in the powertrain system where the operating temperature could approach or exceed 200 °C with the presence of cyclic thermal and mechanical loadings. However there is a major limitation on the use of magnesium in power train system. This is primarily due to the inadequate creep resistance and the poor corrosion resistance that the conventional die casting magnesium AM and AZ alloys inherently provide. Efforts to improve the creep strength of magnesium die casting alloys at temperature exceeding 120 °C have resulted in the introduction of alloy containing Si, RE, Ca and Sr elements or mixture of them. These alloying elements form inter-metallic constituents that stabilize the grain boundaries. In these alloys, Aluminum must be kept at relatively low levels [20].

Ca is a cheap and light element which can contribute to high temperature properties [21-25]. Small addition of calcium significantly improves the creep and stress resistance of AM50 [26-28]. The addition of 1.7% Ca dramatically lowers the creep rate of the die-cats AM50 magnesium alloy for about three orders of magnitude [29, 30].

But the addition of calcium to magnesium alloy is not trouble free. The addition of calcium increases the casting defects such as sinks, solder drag and cracks in high pressure die casting [31, 32].

Therefore it seems necessary to develop alternative manufacturing processes for potential high temperature magnesium-aluminium-calcium (Mg-Al-Ca) alloys, such as squeeze casting. Hence process-related casting defects can be minimized while the advantages of Mg-Al-Ca are made full use.

3

1.2 Objectives of the research

This project is divided into two sections. In an effort to develop a squeeze casting process for potential high temperature magnesium-aluminium-calcium alloy, the first objective of this study was to investigate the effect of applied pressure levels on microstructure, mechanical properties and soundness of castings (including porosity and cracks). The other objective of this work are to investigate the effect of calcium contents on microstructure and tensile properties of Mg-Al-Ca alloys in room and elevated temperature for determining Ca role in the squeeze cast alloys.

1.3 Organization of the thesis

This thesis contains six chapters. Chapter 1 has provided a general background of squeeze casting. Chapter 2 is the literature review which looks into the process of squeeze casting and metallurgical aspect of magnesium alloys, especially those with high potential for high temperature applications. The experimental procedures used in this research work are described in chapter 3. Chapter 4 reports and discusses the results of the effect of pressure levels and calcium contents on microstructure and tensile properties of Mg-Al-Ca alloys. The conclusions of the present study are summarized in chapter 5. Finally, chapter 6 wraps up the thesis with recommendation for future work.

4

CHAPTER II

LITERATURE REVIEW

2.1 Squeeze casting

2.1.1 Process description

Squeeze casting has been developed based on the principal of pressurized solidification, in which finished castings can be produced in a single process from molten metal to solid components within reusable dies. As shown in Figure 2.1, squeeze casting involves several steps:

1- A suitable die set is installed on the bed of a hydraulic press. The die set is preheated to the required working temperature. During the heating-up period, the die set is usually sprayed with a commercial graphite lubricant.

2- A metered quantity of molten metal is poured into an open female die cavity. Then, an upper male die or punch is lowered, coming into contact with the liquid metal.

3- The pressure is applied shortly after molten metal begins to solidify and maintained until all the molten metal has solidified. The upper punch returns to its original position and the casting is ejected.

The high pressure applied (typically 50 to 200 MPa) is enough to suppress gas porosity except in extreme cases, for which standard degassing treatments are used [1-3, 9, 10, 14]. The tendency toward shrinkage porosity is limited by using a bare minimum of superheat in the melt during pouring. This is possible in squeeze casting because of melt fluidity, is not necessary for die filling. In heavy sections of the casting, which are particularly prone to incidence of shrinkage porosity, the applied pressure squeezes liquid

5

or semi-liquid metal from hot spots into incipient shrinkage pores to prevent pores from forming. Alloys with wide freezing ranges accommodate this form of melt movement very well, resulting in sound castings with a minimum of applied pressures [1].

Because of the magnitude of pressures involved, squeeze casting takes place in metal dies sufficiently thick to withstand the applied pressures. The dies are usually made from high quality die steels, which are heated and lubricated [3, 4]. Currently H13 tool steel is a widely used material for die construction; but generally dies should have good hot hardness, high temper resistance, adequate toughness, and especially a high degree of cleanliness and uniform microstructure [4, 33]. To facilitate release of the casting, draft angles are chosen to be 0.5 degrees on external walls of the die, and 1 to 2 degrees on the punch surface and on die details around which the casting tends to contract after solidification [33].

2.1.2 Types of squeeze casting

In general, two different kinds of squeeze casting techniques, known as "direct" and "indirect", have been developed based on different approaches of metal metering and metal movement.

2.1.2.1 Direct squeeze casting

The direct squeeze casting technique is characterized by a direct pressure imposed onto the casting without any gating system as illustrated in Figure 2.1. The pressure is applied in two stages to prevent the melt from spraying out through the necessary gap between the piston and mold. A few seconds after the pressure is applied, all pores in the

6

solidifying material are closed [7]. Since the pressure is directly applied to the entire surface of the molten metal during solidification, this technique gives fully densified components and extremely fast heat transfer, which yields fine grain structure [1-3, 9, 10]. It means that the cycle times for squeeze castings are generally much shorter than those for either gravity or low pressure die castings. For instance it has been reported that a cycle time of only two minutes is required for the production of an aluminium alloy car wheel, in comparison with six minutes for low pressure process [3]. As a result of high heat transfer, enhanced mechanical properties are attained.

The process is mainly suited to chunky components having a small aspect ratio i.e. the width and height of the casting are of similar dimensions [2]. The major advantages of direct squeeze casting over other processes can be itemized as follows [5, 34]:

- Material having neither gas porosity nor shrinkage porosity is produced;

- No feeder or risers are required and therefore no metal wastage occurs;

- The inherent "castability" of the alloy is of little or no concern since the applied pressure obviates the need for the customary high fluidity, which enables both common casting and wrought alloys to be squeeze cast to finished shape;

- Control of the microstructure is possible solely by control of the dominant process parameters such as the pouring temperature and mould temperature;

- Because there are no internal (or external) defects on a properly produced squeeze cast component; costly post-solidification examination by non-destructive testing techniques is of very limited value;

- Squeeze castings can have mechanical properties as good as, and in some cases even better than, wrought products of the same composition; and

7

- Squeeze castings provide the most effective and efficient route to produce near-net-shape composite components for engineering applications.
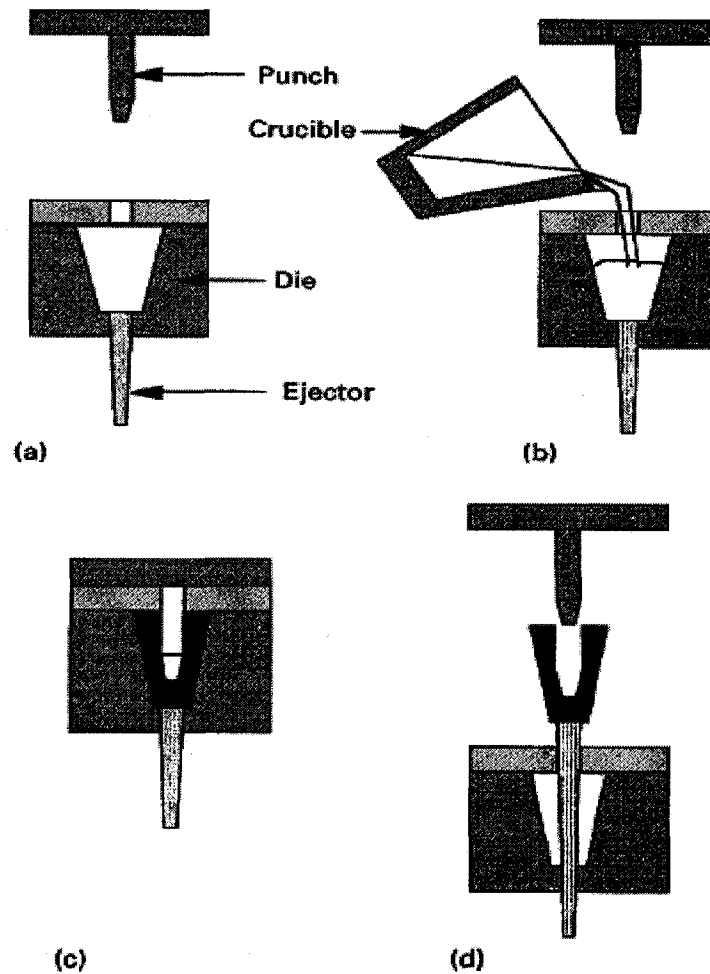
Figure 2.1: Schematic diagram of direct squeeze casting process[6]

a) step1, preheated, lubricating tooling ;

b) step2, transfer melt into die cavity;

c) step3, solidify melt under pressure; and

d) step 4, eject casting.

8

2.1.2.2 Indirect squeeze casting

In the indirect technique as shown in Figure 2.2, the pressure is exerted on a gate, which transmits the load to the component. This technique is really a hybrid process between low pressure die casting and high pressure die casting. The melt is pushed through a relatively large feeder compared to pressure die casting [7, 9 and 10]. The gate velocity of the melt is usually between 0.5 m/sec [7] and 3 m/sec [10] compared to 30 m/sec for pressure die casting. This requires a gate three to five times larger than in conventional high pressure die casting [2]. The low flow rate ensures a controlled filling of the mould without trapping air [7, 9 and 10]. Due to the fact that the pressure is imposed at a distance from the component, it is difficult to maintain high pressure on the component throughout its solidifying and cooling periods. This indicates that it is difficult to cast long freezing range alloys with the indirect technique. Also, metal yield is much lower than that achievable with direct squeeze casting owing to the necessity of using a gating system. The advantage of the indirect technique is that, due to presence of a gating system, a highly accurate external metering system is not necessary. Variations in metal volume are adjusted in the gate. Although it seems that the direct squeeze cast offers more opportunities for a wide range of alloys for the production of high strength, full integrity metal casting and metal matrix composite components but more indirect squeeze casting machines presently is in operation than direct. This is probably because the indirect process has been successfully commercialized. To achieve a sound structure the aspect ratio is usually kept below 5:1 [2].

The major advantage of indirect squeeze casting is that, because the casting forms inside a closed die, the dimensions of the casting are relatively easier to control than in

9

direct process. Thus, the use of a highly accurate external metering system is not necessary [3]. The slow filling of the die enables the use of lost cores, which in the case of pressure die casting are often broken or washed away [7]. In practice, indirect squeeze casting has two disadvantages [3, 5]:

- Material utilisation is inefficient and very much less than the high levels achievable with direct squeeze casting because of the necessity of using a runner and gating system [5, 7]. The biscuit and runners have to be machined off the casting and internally recycled in the same manner as high pressure die casting practice.

- Because of the complexities of the necessary runner systems and due to the fact that the external pressure on the metal is applied at a great distance from the casting, it follows that it is difficult to maintain a high pressure on the casting throughout its freezing and cooling periods. This means that long freezing range alloys cannot be cast by indirect squeeze casting, which limits the process to conventional casting alloys. The high strength, 'wrought' aerospace alloys are extremely difficult, if not impossible, to cast defect-free using the indirect squeeze casting process.

Of the two philosophies for squeeze casting (direct and indirect), it appears that the direct process offers more opportunities for utilisation of a wide range of alloys for production of high strength, full integrity castings, and metal matrix composite components.

10
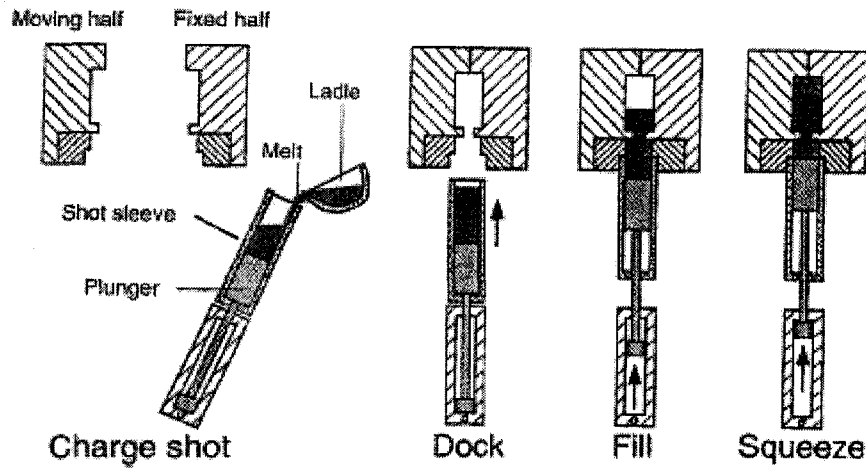
Figure 2.2: Schematic diagram showing the operation of a typical vertical injection indirect squeeze casting machine [4].

2.1.3 Process Parameters

There are a number of variables that are generally controlled for the soundness and quality of the castings. The variable ranges discussed in the following sections may differ with alloy system and part geometry being squeeze cast.

2.1.3.1 Alloy composition

The most important process parameter is the alloy itself. The composition and physical characteristics of the alloy are of paramount importance due to their direct effects on the die life. These include the melting temperature and thermal conductivity of the alloy together with the combined effect of the heat-transfer coefficient and soldering onto the die material. Furthermore, the alloy dictates the selection of casting parameters such as die temperature, which has a direct consequence on the die life [4].

11

2.1.3.2 Melt volume and quality

In the direct process, due to lack of runners and gating to accommodate any excess metal, precision control of the metal volume is required when filling the die cavity, which ensures dimensional control [1, 2]. However this has appeared to be difficult even by using automatic ladling or commercial metering pumps, especially for small components or multi-dies. A technique suggested to solve the problem is to pour excess metal into the die and allowing the component to be oversized in a non-critical direction or to include an overflow system [2]. In addition for the same reason, that is, no gating system, more attention has to be paid to the melt quality, in terms of dross, in the direct than in the indirect processes. However, in both direct and indirect squeeze castings, the presence of absorbed gases in the melt is less critical than that in any other casting processes, owing to the nature of squeeze casting where the imposed pressure is usually sufficiently high to suppress gas evolution and retain gases solution.

2.1.3.3 Pouring temperature

Pouring temperature depends on several factors, such as liquidus temperatures, freezing ranges of metals and die complexity. Normally, high superheat above the liquidus is required for narrow freezing range metals due to their relatively fast solidification rates. In general, a low pouring temperature for wide freezing range alloys is more effective in yielding good metallurgical quality [3, 33]. However, too low pouring temperatures can result in the insufficient fluidity, which leads to incomplete die fill and cold laps. On the other hand, too high pouring temperature might cause extrusion of liquid metal between the interfaces of die, punch and casting, which jams the tooling.

12

Also shrinkage porosity might occur in thick sections of the casting. A high pouring temperature can reduce the die life significantly [35].

At pouring temperatures above the liquidus temperature, columnar grain structure is reported in Al-Si alloys; grains are equiaxed when poured at the equilibrium temperature. This refinement is attributed to the under-cooling that is a result of increasing the liquidus temperature with pressure, via the Clapeyron effect [11].

Ha [36] reported an equiaxed grain structure for squeeze cast AZ91 Mg poured at 680 °C and an ingot-type structure for squeeze castings at 730 °C. Rozak [20] observed a finer equiaxed grain size in squeezed cast AZ91 Mg at 735 °C than at 700 °C, attributed to changes in the inoculation efficiency.

For aluminium alloys, the casting temperature may range between 10 to 100 °C above liquidus temperatures, with the lower limit applicable to alloy like 7075 and A390 aluminum that have extended freezing ranges, and the upper limit to narrow freezing range alloy such as 3003 and A413 aluminium [33]. The value for magnesium may be higher than aluminium due to a lower specific heat capacity [2]. Superheats varying from 30-140 °C have been used in the previous study for magnesium alloys [6].

2.1.3.4 Tooling temperature

Operating die temperatures need to strike a balance between the need for sufficient heat to prevent premature solidification of metals, thermal fatigue in the tooling, and cold laps on the surface of the casting. There is a tendency for welding to occur between the casting and the mould if the die temperature is too high. Ranging from 200 to 300 °C is normally used [1-4, 6]. The lower range is more suitable for thick section casting. In general, the smaller die castings require the higher die temperatures [9].

13

Temperatures above 300 °C are not recommended for aluminium alloys. Although it has been reported that, although a low die temperature around 150 °C can result in an equaxied grain structure for magnesium alloy AZ91D, the detailed values for magnesium alloys are still unknown [36]. To provide a stable die temperature during production, water or oil cooling line in the die may be necessary [2].

The punch temperature is often kept 15 to 30 °C below the die temperature to maintain sufficient clearance between them for adequate venting. Excess punch-to-die clearance allows molten metal to be extruded between them, and therefore eroding the surface of die [1].

2.1.3.5 Time delay and temperature for pressure application

Time delay is the duration between the actual pouring of the metal and the instant at which the punch contacts the molten pool and starts the pressurization. Because increased pouring temperatures may required to fill these sections adequately upon pouring, a time delay allows for cooling of the molten pool before closing of the dies to avoid shrink porosity [1]. This time varies depending on melt temperature and component geometry. Times differ greatly but generally range from a few seconds for small ferrous components to approximately one minute for large aluminium alloy components [2]. For magnesium alloys, the effect of this time delay on the properties and structures of the castings is still unknown and needs to be investigated [6].

There is no universal agreement regarding the temperature for pressure application, i.e. if the metal should be fully liquid or partially solid. Bidulya [38] and Weinberg [39] suggested that pressure should be applied when the metal is near the "zero fluidity temperature", i.e. at dendiritic coherency when the melt loses its fluid flow

14

properties. However, the melt should be mainly liquid according to Williams et al [34] for squeeze casting to be fully effective.

2.1.3.6 Pressure level

The density of the squeeze casting is increased by applied pressures exerted on solidifying metal [10, 14]. Pressure levels of 50 to 200 MPa are normally used as 70 MPa is generally applied, depending on the part geometry and required mechanical properties. The improvement in mechanical properties with pressure is expected to level off as porosity is eliminated and maximum structural refinement occurs; e.g., grain size approaches minimum. Hence there is an optimum pressure for each of the systems after which no additional advantages in mechanical properties obtained [1, 4, 14, 40 and 41]. Factors affecting the pressure are: [33]

- flow stress of the alloy near its freezing temperature;
- the growth morphology of the alloy crystallites; and
- the freezing range of the alloy.

2.1.3.7 Pressure duration

Pressure duration varying from 30 to 120 second has been found to be satisfactory for castings weighing 9 Kg (20Lb) [1]. Franklin and Das [42] recommend pressurization time of about 1 second per mm of the section thickness. However, the pressure duration is dependent on part geometry, alloy type and heat transfer condition [2]. As the time of pressure application is increased, finer dendrite is produced [14]. However applied pressure after complete solidification does not contribute any property enhancements and only increases cycle times [1]. It is only necessary to apply pressure until the

15

solidification is completed, since slightly longer times may be used to avoid hot tearing. Prolong holding times provide little benefit, and may cause wall cracking or problems with punch redrawal, due to thermal contraction of the casting on the rigid punch [2].

2.1.3.8 Lubrication

Lubrication for aluminium, magnesium, and copper alloys, a good grade of colloidal graphite spray lubricant has proved satisfactory when sprayed on the warm dies prior to casting. Excess build-up on narrow webs and fin areas should be avoided where vent holes or slots are used [1, 2, 4]. Care must be taken to prevent plugging these vents. At the pressure applied during squeeze casting, the coat may strip from the die surface and cause surface contamination in the component. Limiting the lubricant thickness to 50 microns, should prevent this to occur [2].

For ferrous castings, ceramic-type coatings are required to prevent welding between the casting and the metal die surfaces [1, 33].

2.1.3.9 Press speed

Press speed in most practical purposes, a punch impact speed of 0.5m/sec may be used without detrimental effects. In the situation where there is a large distance between punch and die, a two speed action may be used, i.e., a rapid approach of the punch to the metal surface followed by a slower impact speed.

2.1.3.10 Ingate size (indirect squeeze casting)

The ingate size for indirect squeeze casting is an important consideration since it must remain open until the casting is solidified and pressure is maintained on the

16

solidifying casting. The volume of metal entering the die cavity has to be sufficient to fill the cavity before localized solidification occurs. This is best accomplished with a larger ingate to attain rapid filling without excessive velocity and the inertial type of flow that occurs at high metal velocities. The fan type of ingate helps to accomplish this rapid fill without high velocity [9]. The velocity of the melt at ingates is usually between 0.5 m/sec [7] to 3 m/sec [10] compared to 30 m/s for pressure die casting [7]. The low flow rate ensures a controlled filling of the mould without trapping air with a proper venting [7, 9 and 10].

2.1.4 Effect of Applied pressure

2.1.4.1 Reduction of porosity

Pressure applied to liquid metal prior to and during solidification tends to reduce or eliminate the gas related porosity. Increased pressure increases the solubility of gases in the melt. These gases do not evolve during solidification, due to the difficulties in nucleation of bubbles against the pressure [2]. For the other main cause of void related defects, solidification shrinkage, the effect of pressure is to force feed the liquid or semi-solid metal into the voids, producing a fully dense material [2].

2.1.4.2 Equilibrium diagrams

Equilibrium phase diagrams depict conditions of slow cooling rates under atmospheric pressure. However, these are not the conditions encountered during squeeze casting. The application of pressure causes the melting point of most alloys to increase in a manner which obeys the Clasius-Clapeyron equation:

17

$$\frac{\Delta T}{\Delta P} = \frac{T_f(V_l - V_s)}{\Delta H_f}$$

where ΔH_f is latent heat of fusion, V_s and V_l are specific volume of solid and liquid phases, T_f is melting temperature at atmospheric pressure, ΔT and ΔP are the variation of temperature and pressure, respectively.

The majority of metals show a rise of 2-6 $^\circ$C for every 100 MPa of external pressure applied [43]. For pure magnesium, Sekhar [44] calculated dT/dP which is about 0.0647 $^\circ$C/MPa. Such change in freezing temperature is expected due to reduction in interatomic distance with increasing pressure and thus restriction of atomic movement, which is prerequisite for melting/freezing [4]. The inter-solubility of constituent elements together with the solubility of impurity and trace elements is also expected to increase with pressure [4].

Pressure application also distorts phase diagrams. Figures 2.3 and 2.4 illustrate the distortion of Mg-Al and Al-Si phase diagrams due to pressure application and rapid cooling rates. When the melting point of a component in an alloy is changed by pressures, the eutectic point is shifted in the direction of higher concentrations of the component whose melting point is least affected [45]. In the case of Al-Si alloys (Figure 2.3), it moves towards the higher silicon content [46], while in Mg-Al alloys (Figure 2.4), the eutectic moves towards the Mg concentration [2]. Lipchin [47] and Taha et al [48] reported that the solubility of silicon in aluminium increased by squeeze casting. The volume fraction of silicon in an aluminium dendrite increased from 3 to 7.8% with an increase in solidification pressure from 41 to 69 MPa [48]. Recent experiments on pure

18

binary Al-Si alloys of compositions 7% and 14% squeeze cast at 150 MPa have indicated an upward movement of the liquidus and eutectic temperatures of 9 K and 2.25 K respectively at a pressure of ~150 MPa [3, 4].

2.1.4.3 Reduction of grain size

The effect of solidification under pressure on grain size can be illustrated by reference to Figure 2.4. Alloy X is well above the liquidus line at T1 at atmospheric pressure. The application of pressure causes the liquidus line to move (dotted line) but it still is below the T1, and the melt does not start to solidify until the temperature has reached the new liquidus line. Nucleation and growth processes commence at the new liquidus line, but without significant grain refinement. If, however, the initial alloy temperature is at T2 when pressure is applied, the liquidus line moves above this point and super-cooling occurs. The grain refining effect is proportional to the degree of under-cooling, and a true squeeze casting consists of fine equiaxed grains as a result of correct pressurisation applied at the appropriate time. Further, the dendrite arm spacing becomes smaller, constituent particles tends to remain small and a more homogeneous distribution of structural components takes place [14, 42]. Also the applied pressure has a marked effect on heat transfer during the solidification of the castings (which will be discussed in details in the following subsection) [4, 6].

19
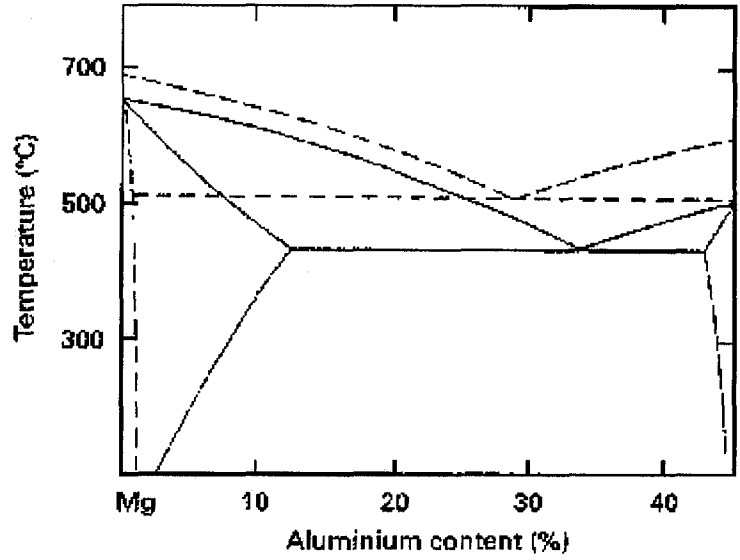
Figure 2.3: Deviation from equilibrium conditions in the Mg-Al phase diagram due to high applied pressure[44].
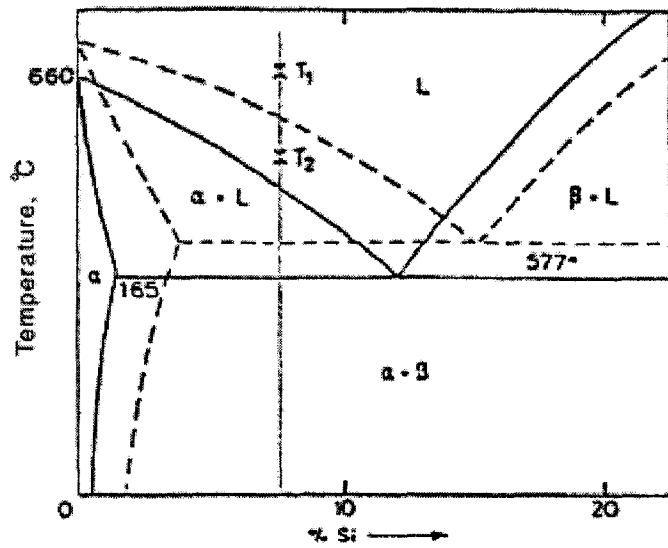
Figure 2.4: Effect of pressure (100 MPa) on the Al-Si phase diagram [46].

20

2.1.5 Effect of applied pressure on microstructure

The effects of squeeze casting on solidification are manifested in the microstructural refinements: grain structure, porosity, segregation, and secondary phases. In addition to the densification achieved, there are several reasons why squeeze casting produces casting with superior properties. The applied pressure has a marked effect on heat transfer during the solidification of the castings. Due to contraction of most metals and thermal expansion of the mold during solidification, the detachment of the casting from the die wall takes place once the initial solid shell of the casting has sufficient strength to hold the remaining molten metal. Consequently, an air gap is formed between the die walls and casting, which considerably increases resistance to heat transfer. In squeeze casting, the applied pressure on the casting forces the initial solid shell to remain in contact with the die for a certain period of time before any detachment could occur. If the applied pressure is sufficiently high, the intimate metal-die contact can be maintained via the plastic deformation of the casting throughout solidification. This leads to very fast heat transfer, high cooling rates and an increase in casting temperature gradients [4, 6]. Murthy and Satyanarayan [49] found an increase in the cooling rate from 6 K/sec in permanent mould casting to 300 K/sec in squeeze casting. Due to higher cooling rate in squeeze casting, dendrite arm spacing is much finer in comparison with that resulting from other casting process [9, 14]. The study by Fujii et al [50] on squeeze casting of an aluminium alloy indicates that the solidification time is only a half the time in gravity castings; the heat transfer coefficient is four times higher than that in gravity castings; and temperature gradients in the casting increase with applied pressure. Even moderately applied pressure causes intimate contact between the solidifying casting and the die for a

21

tenfold increase in heat transfer rate over permanent mold casting. This results in relatively fine grains in the casting. Fine grain size is also promoted by the large number of nuclei formed because of the low pouring temperature and the elevated pressure [1, 2, and 4]. Furthermore, because die filling in squeeze casting does not require high melt fluidity, a number of wrought alloys can be squeeze cast. Again, pressurized solidification with rapid heat transfer tends to minimize the segregation that wrought alloys are usually prone to [2, 34].

The high solidification rate also distorts the equilibrium phase diagram by modifying the solubility of solute atoms. Lipchin observed that pressure during solidification increase the solubility of the second component during solidification. Only in the Al-Mg, Al-Zn, and Mg-Al systems does the solid solubility of the second phase decreased with an increase in applied pressure of squeeze casting [47].

2.1.5.1 Aluminum alloys

In the case of Al-Si alloys, fibrous silicon is the likely morphology. A typical squeeze cast microstructure of LM24 Al-Si alloys (Al- 8.5wt.%Si-3.5wt.%Cu) is shown in Figure 2.5, together with conventionally cast to highlight the differences in silicon morphology and grain structure [4].

Reddy and Murthy [14] reported a low pouring temperature, high specific pressure and minimum dwell time results in high densities, fine dendrites arm spacing, isotropic microstructure of squeeze castings compared to those of sand or metal mould castings.

Pressurised solidification modifies eutectic silicon in aluminium-silicon alloys. Taha et al [48] reports a decrease in the size and number of eutectic silicon particles with increases in pressures up to 69 MPa. The eutectic silicon in a squeeze cast unmodified

22

A356 Al alloy was a globular shape; but the shape was elongated when sand cast [51]. Sobczak [52] also reportd a globular shape of eutectic silicon in squeeze cast Al-12%Si alloy without modifiers after a 3-hr, 300 °C heat treatment.

Murthy [49] reported that, in case of aluminum-silicon alloys, pressure solidification leads to (a) an increase in volume fraction of α-phase with an increase in pressure, (b) fragmentation of primary dendrites, (c) decrease in the volume fraction of eutectic, and (d) refinement of β-silicon of the eutectic.

Balan [53] showed that microstrucre refinement takes place when pressure is applied to the solidifying metal. The primary dendrites become finer for aluminum LM6 alloy (Al-11.5wt.%Si) with increasing pressure. The volume fraction of the primary dendrites increases from 34.0 to 39.8% when the pressure is increased from 0 to 75 MPa. The dendrite arm spacing similarly decreased from 30 to 5μm over the same pressure range.

Chemical grain refinement has no significant effect on squeeze casting. However, by the addition of modifier, i.e. in an Al-Si alloy, uniform and much smaller silicon particles can be obtained [2].

2.1.5.2 Magnesium alloys

Yong et al [41] reported a sixfold reduction in cell size for RZ5 (Zn4.2%, RE 1%, Zr 0.7%) magnesium alloy as the pressure increases from 0.1 to 60 MPa. The reduction in cell size was attributed to the intimate contact between the melt and die wall that promoted rapid heat transfer, as the applied pressure was increased.

23
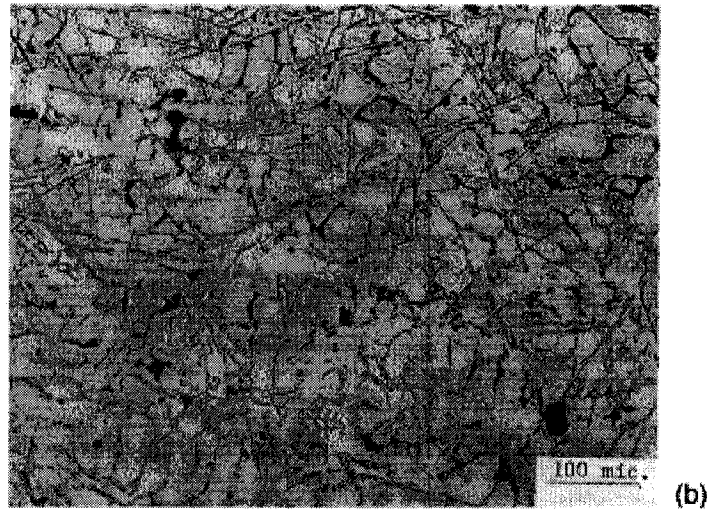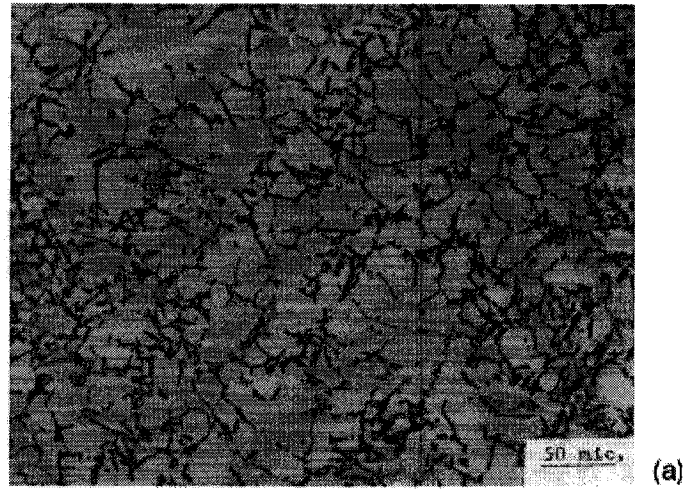
Figure 2.5: Optical micrograph showing the as cast structure of LM24 Al-Si alloy [4]

(a) Squeeze cast LM24 and (b) conventional as-cast LM24.

24

2.1.6 Mechanical properties

Squeeze casting is amenable to the use of a very wide range of alloys. Alloys that respond to heat treatment can quite successfully be put through the necessary solution treatment and age hardening.

It should be noted that the squeeze cast properties are superior in all respects to those given by conventional casting processes. The proof stresses are improved by squeeze casting, and of particular significance is marked improvement in the elongation to failure [2, 4, and 40]. In general, the fine structure and superior mechanical properties of squeeze casting components are due to the following factors: (i) changes in undercooling of the molten alloy, (ii) changes in the composition and percentages of the forming phases of the solidifying alloy, (iii) changes in the heat transfer coefficient between the metallic mould and solidifying alloy, and (iv) changes in the density of the alloy due to reduction of porosity [4]. These improvements reflect both the fine-grained structure and more importantly the elimination of microporosity in the squeeze cast material. In general, a squeeze cast component compares extremely well forgings. In the most cases, there is a good comparison between the isotropic squeeze cast property and the longitudinal forging property [34].

The mechanical properties improvement with pressure is expected to level off as porosity is eliminated and maximum structural refinement occurs; e.g., grain size approaches minimum. The increase in strength and ductility beyond these refinements must occur via refinement at the substructural level, e.g., at higher dislocation densities with increasing squeeze cast pressures. Lipchin and Bykov [43] observe higher dislocation densities in squeeze casting with higher applied pressures.

25

2.1.6.1 Aluminum alloys

Squeeze cast commercial Al alloys are assessed and compared with sand cast gravity die cast, and die forged material of the same composition by Yue and Chadwick [5]. Table 2.1 gives typical mechanical properties for Al-Si casting alloys. Tremendous improvements in properties can be achieved with fully heat treated squeeze castings. For instance, the cheap LM24 alloy (Al-8.5wt.%Si-3.5wt.%Cu) can provide better mechanical strength than the more expensive LM25 (Al-7wt.%Si -0.3wt.%Mg) and A357 (Al-7wt.%Si-0.5wt.%Mg) alloys when squeeze cast and fully heat treated, However the elongation shows the opposite [5]. For LM24 (Al-8.5wt.%Si-3.5wt.%Cu) in particular, which is normally considered to be non-heat treatable, the fully heat treated squeeze cast material exhibits a 0.2% proof stress three times higher and ultimate tensile strength (UTS) twice as high as the specified standard requirements [3]. Using the squeeze casting technique, the usually deleterious iron aluminide crystals do not grow into massive plate like forms but remain very small and uniformly distributed throughout the matrix and hence do not exhibit their usual embrittling effects [3, 5, and 34].

Murthy [49] reported an UTS increase from 157 to 226 MPa while elongation values increased from 8 to 18 percent for LM6 (Al-11.5wt.%Si) as the pressure increase from 41.2 to 247.2 MPa.

Balan et al [53] studied the effect of applied pressure (0-75 Mpa) on LM6 Al-Si alloy (Al-11.5wt.%Si) and reported an increase of about 3.4% in density, 63% in UTS, 2.6% in percentage elongation and 50% in hardness with increasing applied pressures. Such remarkable improvement was mainly due to microstructural alternation through the

26

refinement of the primary α-phase and modification of the silicon phase [53]. Similar results were obtained for pure aluminium [54].

Table 2.1 Typical mechnaincal properties of commercial Al-Si alloys cast by different Process [5].

Alloy		0.02% PS [MPa]	UTS [MPa]	Elongation [%]
A357	Typical chill cast (FHT)	248	313	7
	Squeeze cast (FHT)	283	347	9.3
LM24	Minimum requirement	100	180	1.5
	Typical chill cast	110	200	2
	Squeeze cast(as cast)	126	233	2.7
	Squeeze cast(FHT)	330	368	2
LM25	Typical chill cast (as cast)	90	180	5
	Squeeze cast (as cast)	104	214	5.3
	Typical chill cast (FHT)	240	310	3
	Squeeze cast (FHT)	274	331	7

FHT = fully heat treatment

Das et al [55] showed when Al-4.5wt.%Cu and Al-3.75wt.%Mg were squeezed cast under a pressure of 188 MPa, the UTS and percent of elongation increased 50% and 128% respectively for Al-4.5wt.%Cu and 38% and 138% for Al-3.75wt.%Mg, in comparison with the gravity die cast pressure. In addition to grain refinement and freedom from porosity, the improvement in the tensile properties of squeeze cast Al-4.5wt.%Cu alloy can be attributed to a fine dispersal of the intermetalic compound

27

$CuAl_2$ and the disappreance of the Cu-rich layer around α-Al, which are directly related to the influence of pressures and cooling rates on phase diagram. For Al-3.75wt.%Mg alloy, the absence of β constituent, Mg_2Al_3, which usually is present in sand casting and gravity die casting, is responsible for tensile properties improvement.

The dynamic properties of squeeze cast alloys are also superior to conventionally cast material. For example LM24 (Al-8.5wt.%Si-3.5wt.%Cu) in its squeeze cast and fully heat treated condition exhibit better fatigue behaviour than the more expensive high purity alloy as shown in Figure 2.6. This superior behaviour is again due to a combination of the absence of large plates of embrittling (Fe Al Si) compounds, the refinement of the primary and eutectic constituents and the total absence of porosity [3].

The dynamic and static properties given above were obtained on direct squeeze cast material. The properties of the direct squeeze castings are 25-30% greater than those of the indirect squeeze castings. These differences are due, presumably, to the greater refinement of the microstructure in the direct squeeze casting alloy and to the total absence of porosity in the direct squeeze cast alloy [3].

Das et al [55] showed the fatigue life of the Al-4.5wt.%Cu alloy has an improvement of 75% over the sand cast alloy and the Al-3.75wt.%Mg showed a 30% improvement on the sand cast alloy.

It has been observed that squeezed cast and fully heat treated high strength aluminium alloys (wrought alloys) exhibit mechanical properties between those of the longitudinal (L) and short transverse (ST) properties of wrought material. Unlike the direct chill (DC) cast material in which the grain structure is not fully controllable, squeeze-cast material can be produced having isotropic behaviour as illustrated in

28

Table 2.2. This is due to the fine grain micro-structure and thereby the isotropic yielding behaviour [2, 3, and 5]. Hashemi et al [40] reported the tensile properties of heat treated squeeze cast specimens Al-Zn approaches those of wrought aluminium alloys obtained by other processes.
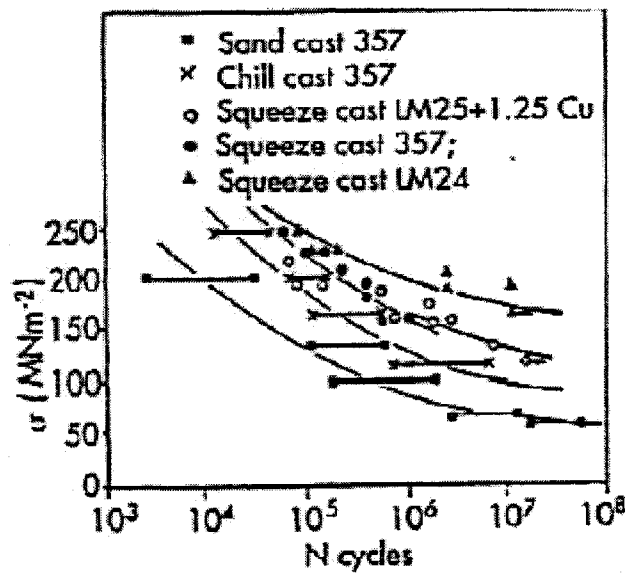
Figure 2.6: Fatigue behaviour of some aluminum alloys cast by different techniques [3].

Table 2.2 Comparison of tensile properties of fine grained squeeze cast Al-4.5%Cu with wrought alloy of similar composition [2].

Alloy		0.02% PS[MPa]	UTS [MPa]	Elongation[%]
Al-Cu4.5%	Squeeze cast (FHT)	184	346	22
2025	Wrought properties	225	400	19

FHT = fully heat treatment

29

2.1.6.2 Magnesium Alloys

Rozak [37] compared the tensile properties of squeeze cast AZ91 magnesium and A356 aluminium alloys with those of the permanent mold cast alloys. AZ91 is one of the most common magnesium casting alloys, which contains~9% Aluminium and ~1% Zinc. The samples were squeeze cast with 138 MPa pressure, heat treated to a T6 condition as shown in Table 2.3 [11]. The increase in tensile properties is due to highly refined structure.

Table 2.3 Tensile properties of cast A356 and AZ91D [11].

Alloy	Casting condition	Yield strength (MPa)	Tensile strength (MPa)	Elongation (%)
A356	Squeeze	248	290	5.7
A356	Permanent mold	206	282	10
AZ91D	Squeeze	144	303	9.7
AZ91D	Permanent mold	124	262	6.2

The variation in properties of AZ91 in the as cast and in the fully heat treated condition for sand, gravity die casting and squeeze cast materials is shown in Figures 2.7 and 2.8. The squeeze cast alloy shows the highest value of ultimate tensile strength, 0.2% proof stress and elongation-to-failure.

A full heat treatment increases the ultimate tensile strength of the squeeze cast material from 200 to 260 MPa with an associated decrease of elongation of only 1% [5]. Luo and Hu [56] showed that the ductility of the squeeze casting specimens of AZ91D

30

has been significantly improved over the die cast parts through the elimination of porosity. Yong et al [57] showed the squeeze casting improves the mechanical properties of the Mg-4.2%Zn-Re by 15 to 40 % over those obtained by gravity die casting [4]. Further improvements can be expected for compositions outside casting specifications, which are difficult to cast. Squeeze casting can then make use of the extra solute content to improve the properties by enhanced precipitation hardening in the porosity free matrix.

The extruded magnesium wrought alloy AZ31 (~3% Aluminium and ~1% Zinc), in the longitudinally direction shows an UTS value higher than squeeze cast specimens. However, the squeeze cast value is probably better than the properties in the extruded, short transverse direction [2].

Yong et al [41], reported an approximately 50% increase in UTS for RZ5 (Zn4.2%, RE 1%, Zr 0.7%) magnesium alloy as the pressure increase from 0.1 to 60 MPa. The improvement in tensile properties was attributed to reduction in porosity and cell size.

Zhou et al [58] compared the tensile properties of squeeze cast AM50A magnesium with those of high pressure die cast. She reported a significant improvement in elongation (281%) and UTS (75%) of the squeeze cast AM50A over the die cast. The improvement in tensile properties was attributed to the extremely low of porosity present in the squeeze cast specimens.

31
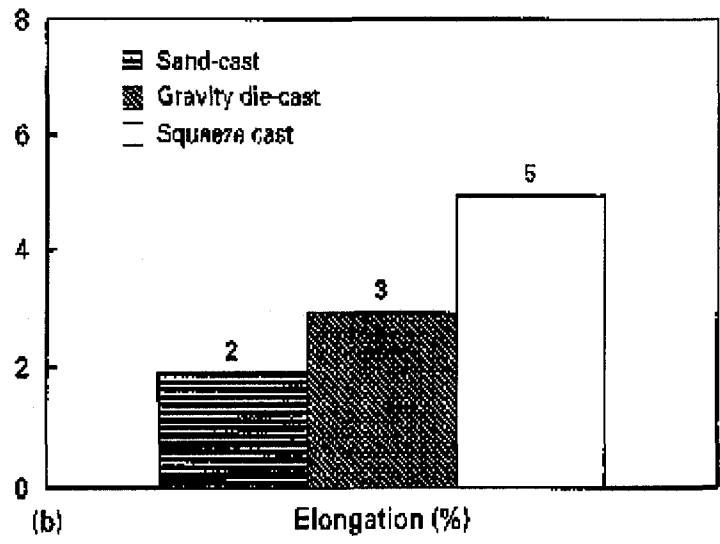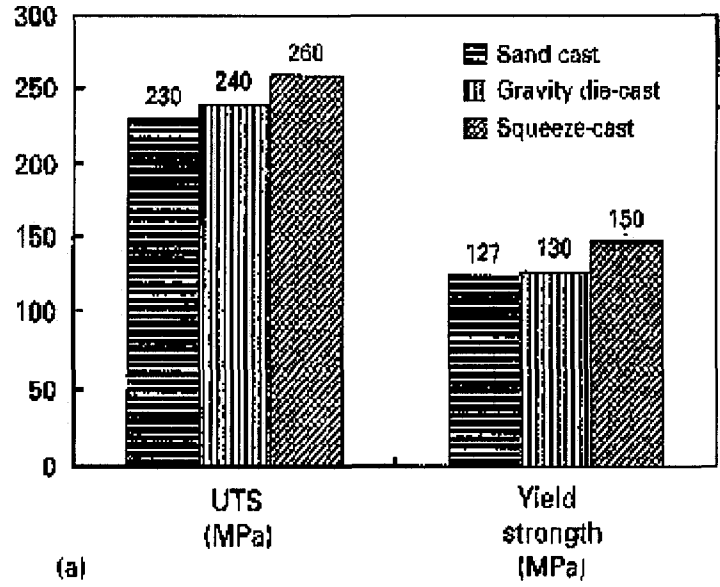
Figure 2.7: Mechanical properties of cast AZ91 in fully heat treated condition

a) UTS and yield strength, (b) elongation [5].

32
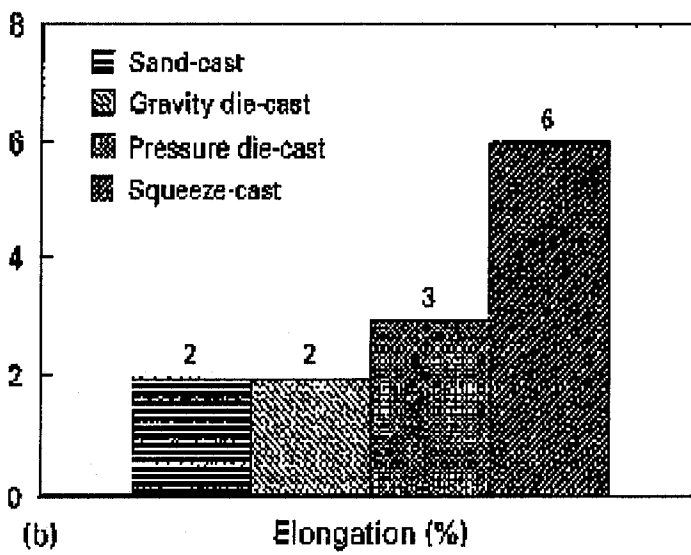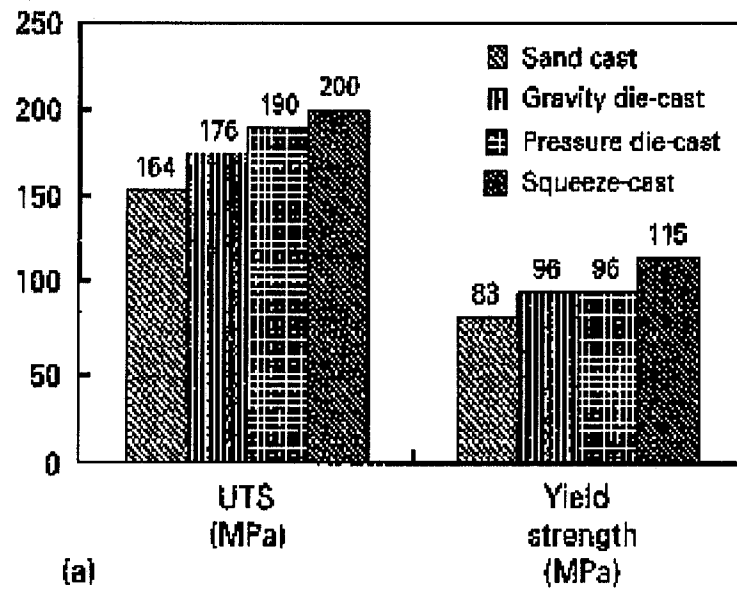
Figure 2.8: Mechanical properties of cast AZ91 in the as-cast condition

a)UTS and yield strength, b) elongation [5].

33

2.2 Metallurgical aspects of magnesium casting alloys

2.2.1 Crystal structure of pure magnesium

Magnesium has a hexagonal close-packed structure (hcp) with lattice dimensions of c= 5.199A and a=3.202A. The axial ratio c/a= 1.6237 is close to the theoretical close-packing c/a=1.63 obtained for incompressible spheres. Of all the hcp metals, only magnesium has an atom that approaches true spherical shape [59].

2.2.2 Mass characteristics

The density of magnesium at 20 °C is 1738 kg/m^3. At melting temperature (650 °C) the density in the solid state is about 1650 kg/m^3 and in liquid state it is about 1580 kg/m^3 [59].

Volume change on freezing

Volumetric shrinkage of 4.2% occurs on freezing (1.5% liner shrinkage) [59].

Volume change on cooling

Volumetric shrinkage of 5% occurs on cooling from the solid form 650 to 20 °C (1.7% liner shrinkage)

2.2.3 Effects of alloying elements on magnesium alloys

Pure magnesium has poor mechanical properties and like other structural metals, such as Al, Zn or Fe. It has to be alloyed in order to improve its overall mechanical properties and make it attractive for engineering applications. Given below is a summary of the effect of some alloying elements and their effect on the metallurgical behavior of magnesium [59]:

34

Aluminum: improves strength and hardness, and it widens the freezing range and makes the alloys easier to cast. When present in amount in excess of 6% the alloy becomes heat treatable, but commercial alloys rarely exceeding 10% aluminum. An alminum content of 6% yields the optimum combination of strength and ductility.

Beryllium: Be although only slightly soluble in Mg, adding up to about 0.001% Be decreases the tendency for the surface of the molten metal to oxidize during melting, casting and welding. It can be used successfully in die-cast and wrought alloys, but must be used judiciously in sand casting alloys because of its grain-coarsening effect.

Calcium: Ca is a special alloying ingredient added in very small amounts by some manufacturers to assist in metallurgical control. It serves a dual purpose: when added to casting alloys immediately prior to pouring, it reduces oxidation in molten condition as well as during subsequent heat treatment of the casting, and it improves the roll-ability of Mg sheet. The addition of Ca must be controlled to below about 0.3%, however, or the sheet is susceptible to cracking during welding. In the following subsection, the effect of this element will be discussed more in details.

Copper: Cu adversely affects the corrosion resistance of Mg alloys if present in quantities exceeding 0.05%, however it improves high-temperature strength.

Iron: Fe is one of the more harmful impurities in Mg alloys in that it greatly reduces the corrosion resistance if present in even small amounts. In ordinary commercial grade alloys, the iron content can average as high as 0.01 to 0.03%. For max resistance to corrosion, however 0.005% is specified as the upper limit for Fe content.

Manganese: Mn does not have much effect on tensile strength, but it does increase yield strength slightly. Its most important functions are to improve the saltwater resistance of

35

Mg-Al and Mg-Al-Zn alloys by removing Fe and other heavy metal elements into relatively harmless inter-metallic compounds, some of which separate out during melting. Commercial alloys containing Manganese rarely over 1.5% and in the presence of Al, the solid solubility of Manganese is reduced to about 0.3%.

Nickel: Ni like iron is one of the more harmful impurities in Mg alloys in that it greatly reduces the corrosion resistance if present in even small amounts. In ordinary commercial grade alloys, the iron content can average as high as 0.01 to 0.03%. To maximize corrosion resistance, however, 0.005% is specified as the upper limit for Ni content.

Rare earth metals: RE are added to Mg alloys either as misch-metal or as didymium. Misch-metal is a natural mixture of the rare earth containing about 50% Ce, the reminder being principally lanthanum and neodymium, didymium is a natural mixture of approximately 85% neodymium and 15% praseodymium. Additions of the rare earth increase the strength of Mg alloys at elevated temperature. They also reduce weld cracking and porosity in casting because they narrow the freezing range of the alloys.

Silicon: the addition of Si to Mg alloys has been found to increase fluidity of the metal in the molten state. However, it reduces corrosion resistance of Mg alloys if Fe is also present in the alloy.

Silver: Ag addition improves the mechanical properties of Mg alloys by increasing response to age hardening.

Thorium: addition increases the creep strength of Mg alloys at high temperature up to 370 °C. The most common alloys contain 2 to 3% thorium in combination with Zn, Zr or Mn. Thorium improves the weldability of alloys containing Zn.

36

Tin: Sn is useful when alloyed with Mg in combination with small amount of Al. Sn serves to increase the ductility of the alloy and makes it better for hammer forging because it reduces the tendency for the alloy to crack while being hot worked.

Zinc: Zn is often used in combination with Al to produce improvement in room-temperature strength; however, it increases hot-shortness when added in amount greater than 1% in Mg alloys containing 7 to 10% Al. Zn is also used in combination with Zr, rare earths or thorium to produce precipitation hardenable Mg alloys having good strength. Zn also helps overcome the harmful corrosive effect of iron and Ni impurities that might be present in Mg alloys.

Zirconium: Zr has a powerful grain refining effect on Mg alloys. It is thought that because the lattice parameters of α-Zr (a = 0.323nm, c = 0514nm) are very close to those of Mg (a = 0.32nm, c = 052nm), Zr-rich solid particles produced early in the freezing of the melt provide sites for the heterogeneous nucleation of Mg grains during solidification. Zr is added to alloys containing Zn, rare earth, thorium or a combination of the elements where it serves as a grain refiner (up to its limit of solid solubility). However, it can not be used in alloys containing Al or Mn because it forms stable compounds with these elements and thus removed from solid solution. It also forms stable compounds with any Fe, Si, C, N, O and mainly it present in the melt. Because only the portion of the Zr content available for grain refining is that which is in solid solution, the soluble Zr content, rather than the total Zr content, is the value important to the alloy.

Yttrium: Yt has a relatively high solid solubility in Mg (12.4%) and is added with other rare earth elements to promote creep resistance at temperatures up to 300 $^{\circ}$C. about 4 to 5% Zr is added to Mg to form commercial alloys such as WE54 (Mg-5wt.%Y-4wt.%RE)

37

and WE43 (Mg-4wt.%Y-3wt.%RE) where it imparts good elevated-temperature properties up to about 250 °C.

Lithium: Li has relatively high solid solubility (5.5%) in Mg. Because of its low relatively density of 0.54, it has attracted interest as an alloying element in Mg alloys to lower the density to values even lower than that of unalloyed Mg. Moreover, only some of 11% Li is needed to form the phase, which has a bcc crystal structure (rather than a Hcp structure), thereby improving formability of wrought products. The addition of Li decreases strength, but increases ductility. Mg-Li alloys are also amenable to age hardening although they tend to overage at only slightly elevated temperature (e.g. 60 °C).

2.2.4 Conventional magnesium alloys for die casting

Table 2.4, shows the nominal compositions of Mg alloys for die castings. The current commercial Magnesium die-casting alloys contain aluminum as the main alloying element, which improves the cast-ability, strength, and corrosion resistance. In addition, they also contain manganese to improve their corrosion resistance. Zinc additions to one of the most common die casting alloys, AZ91, around 0.7% result in minor improvement in strength and corrosion resistance. AZ91 has excellent cast-ability and high strength combined with moderate ductility, and it should always be considered the first choice for an application unless it is ruled out by specific property requirements [59].

Because ductility and fracture toughness are gradually reduced with increasing Al content, the AM series of alloys with reduced aluminum content and reduced Zn contents are now used extensively for automotive safety-related components. To some extent,

38

since the castability is diminished as the Al content is reduced, the alloys having the highest Al content with the required mechanical properties should be chosen [59].

A high purity version of AZ91, i.e., AZ91D, is also now available for die casting. Because tight limits have been placed on levels of Cu, Ni, and Fe impurities allowed in AZ91D, this alloy has saltwater corrosion rates 100 times lower than sand cast AZ91C, making it comparable to the rates of aluminum casting alloys [59].

Table 2.4 Nominal compositions (wt.%) of Mg alloys for castings [59].

	AE42	AM20	AM50A	AM60A	AS21	AS41A	AZ91A	AZ91B	AZ91D(a)
Al	4	2.1	4.9	6	2.2	4.25	9	9	9
Zn	-	-	-	-	-	-	0.7	0.7	0.7
Mn	0.2	0.4	0.4	0.4	0.2	0.2	0.15	0.15	b
Si	-	-	-	-	1.0	1.0	-	-	-
Rare earth	2.5	-	-	-	-	-	-	-	-

a) high purity alloy having very low limits for Cu, Ni and Fe

b) if Fe>0.005 then the iron to Mn ratio must be <0.032

Higher levels of Cu are allowed in AM60A than in AM60B. Therefore, AM60B has better saltwater corrosion resistance than AM60A. The only difference between AZ91A and AZ91B is that a higher level of Cu is allowed in AZ91B than AZ91A.

Manganese content in Magnesium die-casting alloys varies from one alloy to another, depending on the mutual solubilities of iron and manganese in presence of other

elements. A basic requirement for the high-purity alloys is that the iron content of die cast parts is limited to a max of 0.005 wt.%.

Be is added to the Mg die casting alloys to level of 5 to 15 ppm to reduce the oxidation in molten metal.

2.2.5 Magnesium alloys for high temperature applications

The most commonly used magnesium AM and AZ alloys exhibit poor creep resistance. The previous work [20] attributes the poor elevated temperature creep resistance of both AM and AZ alloys to the discontinuous precipitation of the $Mg_{17}Al_{12}$ (β-phase). This is because the $Mg_{17}Al_{12}$ (β-phase) with relatively low melting temperature of 455 °C is metallurgically unstable and may soften considerably at operating temperature of powertrain components over 150 °C. Dargusch et al [60] metallographically observed that the grain boundary sliding in these alloys and suggested that the decomposition of supersaturated α-Mg solid solution is mainly responsible for the poor creep resistance of the alloys. The discontinuous precipitation of the β-$Mg_{17}Al_{12}$ phase resulting from decomposition triggers and promotes grain boundary processes such as sliding and migration [19].

Efforts to improve the creep strength of magnesium die casting alloys at temperature exceeding 120 °C have resulted in the introduction of alloy containing Si, RE, Ca and Sr elements or mixture of them. These alloying elements form inter-metallic constituents that stabilize the grain boundaries. In these alloys, aluminum must be kept at relatively low levels [19]. In the following sections, each of these alloy systems will be discussed.

40

2.2.5.1 Mg-Al-Si alloy

The first development in creep resistant Mg die-casting alloys for automotive applications was the development of Mg-Al-Si die casting alloys for air cooled engines by Volkswagen in the 70's. Silicon addition in AS alloys leads to the formation of the Mg_2Si precipitates that has low density(1.9 g/cm^3), high hardness(460$HV_{0.3}$), low thermal expansion coefficient(7.5×10^{-6} k^{-1}), and perhaps most importantly, unlike the β-$Mg_{17}Al_{12}$ phase, it has a high melting temperature (1085 ^{o}C). Si lacks the ability to tie up Al rendering it ineffective in hindering the formation of β-phase and discontinuous precipitation for a given level of Al. These alloys hence have two types of intermetallics, the β-$Mg_{17}Al_{12}$ and the Mg_2Si phase with high temperature stability, which is deemed to pin dislocations and grain boundaries, thereby imparting increased creep resistance to the alloy [20]. The Mg_2Si that has a face centered cubic crystal structure[61] and is a metallurgically stable phase that forms in Chinese script morphology under slow cooling conditions, which would exhibit very low ductility. In the diecast alloy, a fine distribution of the strengthening phase, Mg_2Si, is achieved with resultant high temperature resistance and a satisfactory level of toughness [62]. Despite that the creep resistance achieved is moderate, the alloys are difficult to diecast.

The AS41 (Mg-4wt.%Al-1wt.%Si) and AS21 (Mg-2wt.%Al-1wt.%Si) alloys are the two standardized Mg-Al based heat-resistant alloys in use that display some improvement in creep properties in the range 130-150 ^{o}C. Both the alloys rely on the reduced Al content (reduced presence of low-melting $Mg_{17}Al_{12}$). AS41 offers better heat and wear resistance than AZ91D, but with reduced fluidity of its melt. AS41 has moderate castability, but due to lower Al content, the castability of AS21 becomes even a

41

bigger problem [63]. Forester [64] suggested that silicon improves the fluidity of Mg alloys when 4% Al is present, making AS41 more castable than AS21. Considerable amount of data on the Mg_2Si has reported by Beer et al [61]. However, silicon addition must be accompanied by a reduction in Al content to lower the amount of $Mg_{17}Al_{12}$ in the microstructure in order to improve the creep resistance. Creep mechanisms for alloy AS21 were studied by Dargush et al [60, 65].

The improved creep resistance of the AS21 over AZ91D was attributed to the smaller amount of creep-induced precipitates and grain boundary pinning provided by the Mg_2Si precipitates.

Blum et al [66] have reported that, at high stresses, AS21 displays smaller maximum deformation resistance compared to AZ91 whereas under low stress the opposite is true. It is also interesting to note, as reported by Aune and Ruden [67], that up to 200 °C, alloys of the AZ, and AS series all appear to exhibit the same relative decrease in strength as the temperature is increased, and that at all temperatures, AZ91 shows superior yield strength. It is also revealed that, as 200 °C is approached except for AS41, these alloys would display similar levels of ductility. It is possible to obtain a compromise between castability and creep resistance in this alloy system by going to an AS31 composition. Recently a modified version of AS21x with small additions of rare earth elements has been developed. Rare earth additions at trace levels do not affect the creep resistance but improve the corrosion resistance as well as castability [68].

2.2.5.2 Mg-Al-RE alloys

A major development in creep resistant Mg alloys has been the emergence of rare-earth (RE) containing alloys (AE42 and AE41). This group of Mg-Al-RE alloys involves

42

at least one, and in general a mixture of the REs as precipitates forming alloying addition in their composition. Rare earth alloying additions are expensive and therefore a cheaper substitute known as misch metal, a mixture of several rare earth elements that is enriched in one of the constituents is generally used. This alloy system exhibits major improvement in creep resistance due to the complete suppression of the formation of the β-$Mg_{17}Al_{12}$ phase and the presence, instead, of the Al-RE containing intermetallics [69]. In a review by Aune and Westengen on mechanical properties of various Mg alloys, it has been shown that the ultimate strength increases with Al and RE content in the alloy, and that tensile yield strength primarily depends on the amount of RE and attains a limiting maximum level [69]. For a given RE content, the creep strength decreases with increasing Al content, while for a given Al content it increases with increasing amount of RE addition [70].

There have been a number of studies aimed at identifying the second phases in AE alloy family. Polmear [71] has claimed that Mg-Al alloys containing RE addition are suitable only for diecasting since slow cooling rates lead to the formation of coarse Al_2RE particles. $Mg_{12}Ce$ type particles were also detected at grain boundaries during creep. Both of these precipitates, unless they coarsen, are considered to inhibit grain boundary sliding and thus being beneficial for creep resistance [71]. Precipitation of Al_4RE compound in the alloy AE42 has also been reported [64, 72-74].

Depending on the composition, precipitates of other types of compounds have also been mentioned in the literature. Pettersen et al [74] suggested that, when RE/Al weight ratio is above 1.4, all of the aluminum is tied up as $Al_{11}RE_3$ in which case further precipitation of other phases such as another type of Al-Re phase or $Mg_{12}RE$ becomes

43

possible. In samples produced by cold chamber diecasting, they observed $Al_{11}RE_3$ and $Al_{10}RE_2Mn_7$ formation at grain boundaries. Their TEM observation has revealed that the major phase was $Al_{11}RE_3$ (a body-centered orthorhombic cell with lattice parameters a=4.5A b= 13.2A and C=9.9A.). No special orientation relationship was found between this phase and Mg-matrix. EDS measurements gave an atomic ratio Al:RE= 3.3±0.6 which is claimed to be in good agreement with the proposed stoichiometric ratio 11:3. The relative amounts of REs were reported to be (at %) La27±2, Ce51±2, Pr6±1, Nd16±1. This phase ($Al_{11}RE_3$) was found to co-exist with a minor phase $Al_{10}RE_2Mn_7$. Diffraction patterns from this phase were indexed according to a hexagonal system with lattice parameters a=9 A^0 and c=13.1 A^0. This structure was found in agreement with the published data for $Al_{10}Ce_2Mn_7$ phase.

Dargusch et al [60] studied creep in AE42 alloy and have observed that just as AZ91 and AS21 alloys, the activation energy was in the range of 30-40 kJ/mol, indicating the same creep mechanism of creep-induced-precipitation resulting in grain-boundary migration. $Mg_{17}Al_{12}$ was not observed but Al-super-saturation was noted. The difference between AZ and AS alloys and the AE was that the onset of the second creep mechanism at the high stress region at 150 °C was not seen in AE42 up to 100 MPa and that the creep strain was lower than AZ91 and AS21.

In a more recent paper by Powell et al [75] on the microstructural evolution of AE42, it was reported that two intermetallics $Al_{11}RE_3$, Al_2RE and particularly no $Mg_{17}Al_{12}$ where present in the diecast structure. Creep testing at 150 °C and 175 °C showed a change in microstructure and in the relative amounts of these phases (Table 2.5). These are consistent with the reaction by which $Al_{11}RE_3$ decomposes to Al_2RE and

44

frees Al, which then reacts with Mg to form $Mg_{17}Al_{12}$, which is accepted as being responsible for poor creep resistance in Mg alloys [75]. To see if stress played a role on the decomposition of $Al_{11}RE_3$, samples were exposed to the same thermal history but without the applied stress [74]. The same microstructural changes were observed and it was concluded that $Al_{11}RE_3$ suffered merely from thermal instability at 175 °C. A relationship was discovered between the relative amounts of $Al_{11}RE$ and Al_2RE and the La:Nd (below 0.7 Al_2RE was seen and above 0.7 $Al_{11}RE_3$ seemed to form).

Formation of either $Al_{11}RE_3$ or Al_2RE maybe sensitive to individual rare earth elements and that this might influence the stabilization of the $Al_{11}RE_3$ phase in AE42 alloy. AE42 alloy was perceived to have issues with cost, castability and fatigue strength and was not considered for widespread automotive use for long time.

Table 2.5 Change in amounts of phases [75].

Temperature (°C)	Mg (%)	$Al_{11}RE_3$ (%)	Al_2RE (%)	$Mg_{17}Al_{12}$ (%)
As-cast 25	97.5	1.8	0.8	0
150	97.7	1.5	0.8	0
175	97	1.2	1.3	0.6

2.2.5.3 Mg-Al-Ca alloy

Ca addition, as a cheaper and lighter alternative to RE elements, also contributes to high temperature properties [76, 21-25]. When Ca is added to Mg-Al binary alloys, the type of precipitating compound is found to depend on the Ca/Al mass ratio. When this

ratio is more than ~0.8 presence of both Mg_2Ca and Al_2Ca were detected that resulted in considerable increase in hardness, while below this ratio only Al_2Ca was observed to have formed. Both types of precipitates were observed to form along the grain boundaries with an increasing volume fraction as the Al and Ca content increases [24].

Sohn et al [26, 27] mentioned that, in addition to the α-Mg solid solution phase, the microstructure of AMC alloys contain Al_2Ca phase. EDS analysis results for the AMC5009 alloy indicated that the gray area (B) in Figure 2.9 contained calcium (~2 wt.%) as well as aluminum. Higher calcium concentration (~3 wt.%) was detected as the width of secondary phase becomes narrower (C). As the calcium concentration increased, the proportion of sharp, well-defined phase boundaries in AMC alloys increased. This suggests that calcium segregated at the phase boundaries that are characterized by well-defined image and sharp contrast change in an etched specimen. By X-ray diffraction and TEM for the as-cast AMC5009 alloy, thin films (200~500nm) of Al_2Ca phase were identified at grain boundaries of α-Mg solid solution. The rounds, white particles observed within matrix were identified as an intermetallic phase containing aluminum and manganese.

Powell [77] reported that below 1 wt.% Ca addition to AM50, only α-Mg was identified in the XRD pattern. At the above 1 wt.% Ca, a secondary phase was also identified, Mg_2Ca, with certain shifts in both a and c parameters. The amount increased as the Ca level in the melt was increased. The formation of $(Mg, Al)_2Ca$ has been reported for AC53 alloy (Mg-5wt.%Al-3wt.%Ca), in which no other phases were identified and no evidence of Al_4Ca or $Mg_{17}Al_{12}$ was detected [78].

46
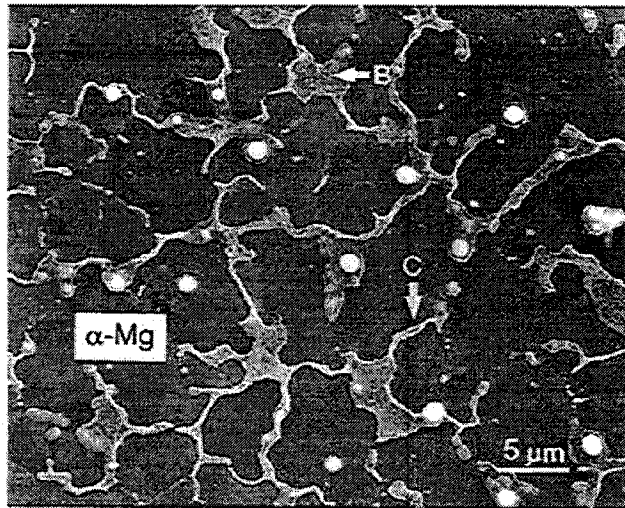
Figure 2.9: SEM micrograph showing as-cast microstructure of AMC5009 [26].

2.2.5.3.1 Effect of calcium on Creep resistance of Mg-Al-Ca alloy

Hollrigl-Rosta et al [21] attempted the use of Mg-Al-Ca alloys in 1970's, and claimed an improvement in creep resistance with addition of about 1% calcium to magnesium alloy AZ81. Small addition of calcium significantly improves the creep and stress resistance of AM50 [26-28]. The addition of 1.7% Ca dramatically lowers the creep rate of the die-cats AM50 magnesium alloy for about three orders of magnitude [29, 30]. As shown in Table 2.6, 100 hours tensile creep extensions of the AC52 (Mg-5wt.%Al-2wt.%Ca) and AC53 (Mg-5wt.%Al-3wt.%Ca) alloys range from 40 to 80% less than that of AE42 at 150 °C [77]. AC52 has slightly better creep resistance than AC53 [77]. The improvement in creep was related to presence of calcium intermetallic. The formation of low melting point eutectic phase, $Mg_{17}Al_{12}$, which is generally present in aluminum containing magnesium alloys, is completely suppresses in the presence of calcium. The $Mg_{17}Al_{12}$ is not seen either in the as-cast structure or in the creep deformed microstructure of the alloys. Al_2Ca is generally present along the grain boundary in the diecast

47

microstructure. It is likely that thermally-stable phase at grain boundaries impedes grain boundary sliding and diffusion related dislocation climb at high temperatures, and can partly explain the improved creep resistance in the new AC series alloys [27-29].

Table 2.6 Total 100-hour creep extension (%) of magnesium alloys [77].

alloy	150 °C, 82 MPa	175 °C, 82 MPa	200 °C, 82 MPa
AE42	0.11	0.12	----
AC2	0.05	0.06	0.26
AC3	0.07	0.09	0.28

2.2.5.3.2 Effect of calcium on mechanical properties of Mg-Al-Ca alloy

Berkmortel et al [31] investigated the effect of calcium content on mechanical properties of the die cast AM50 alloy at room temperature. As demonstrated, the addition of calcium into the alloy slightly increases its yield strength but decreases the ultimate strength. The effect of calcium on elongation is more complex. A small amount of calcium (<0.3%) had no obvious effect on the elongation. The elongation value decreases sharply with increasing calcium content above 0.3%. When the calcium content reaches 0.8%, the elongation decreases to less than 50% of that of AM50 alloy (Figure 2.10).

Pekguleryuz and Renaud [28] investigated the effect of calcium content on mechanical properties of AM50 at elevated temperature and compared them with AZ91D and AE42. Their results (in table 2.7) show that the strength of the AC alloys increases with increasing calcium content. AC508 (5%Al, 0.8%Ca) and AC51 (5%Al, 1%Ca) have

48

(at 150 °C) ultimate tensile strength and yield strength values comparable to AE42 and AZ91D alloys. Elongation at 150 °C is better than AZ91D and but less than AE42.

Powell et al [77] studied the tensile properties of AC52 (Mg-5wt.%Al-2wt.%Ca) and AC53 (Mg-5wt.%Al-3wt.%Ca) and compare it with AM50. The results are shown in Table 2.8. All of the ACX alloys have a higher yield and tensile strength than AM50, due to the calcium addition; AC53 is stronger than AC52 at both room and 175 °C. However calcium addition reduces the total elongation of the alloys.
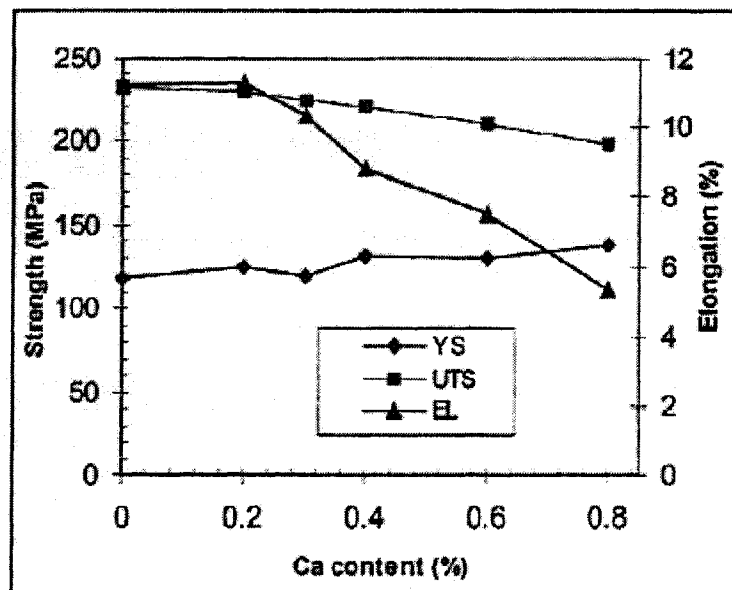
Figure 2.10: Effect of calcium content on mechanical properties of AC alloys (note the AC (0%Ca) is the AM50 alloy) [31].

49

Table 2.7 Tensile properties of AC51 at 150 °C [29].

Property	Alloys				
	AC506	AC508	AC51	AZ91D	AE42
Yield strength (MPa)	95	102	112	110	107
Ultimate Tensile (MPa)	156	161	165	159	160
Elongation (%)	8.4	7.4	8.4	6.7	36

Table 2.8 Mechanical properties of AM50 and ACX alloy at room temperature
and 175 °C [77].

Alloy	Temperature	Ultimate tensile strength (MPa)	Yield strength (Mpa)	Elongation (%)
AM50	Room	214	116	17
	175	126	90	14.2
AC52	Room	228	161	13.3
	175	171	133	22.6
AC53	Room	240	186	9.1
	175	190	151	14.5

50

2.2.5.3.3 Effect of calcium on diecastability of Mg-Al-Ca alloy

Berkmortel et al [31] found that casting defects in the AC series alloy casting increased with increasing calcium content from zero to 0.8%Ca. Above 0.3% calcium, visual defects were far more predominant. Through the visual analysis they found that the most prominent defects were sinks, solder drag and cracks. Figures 2.11 and 2.12 show crack and solder drag defects in production of transfer case [31]. Very few flow/fill related defects, such as cold shut, were observed. This indicates that Ca-alloyed AM50 alloys have certain fluidity and are capable of filling the die cavity. In their research, they observed that AZ91D casting have the least defect, closely followed by AE42. AM and AC series alloys have more defects, especially cracks. The tendency of forming primarily cracks in the AC alloys is greatly affected by the calcium content. A small addition of calcium (0.2-0.3 wt.%) to AM alloy may decrease its tendency of forming cracks. But additions of calcium greater than 0.4% appears influences on crack formation significantly.
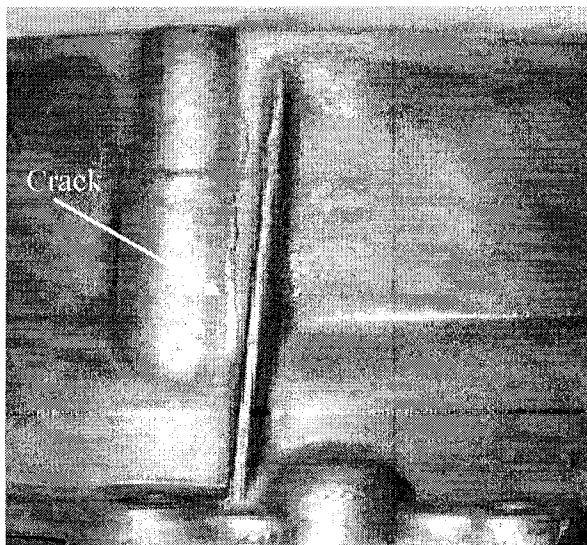

Figure 2.11: Casting defect (cracking) present in a die cast transfer case [31].
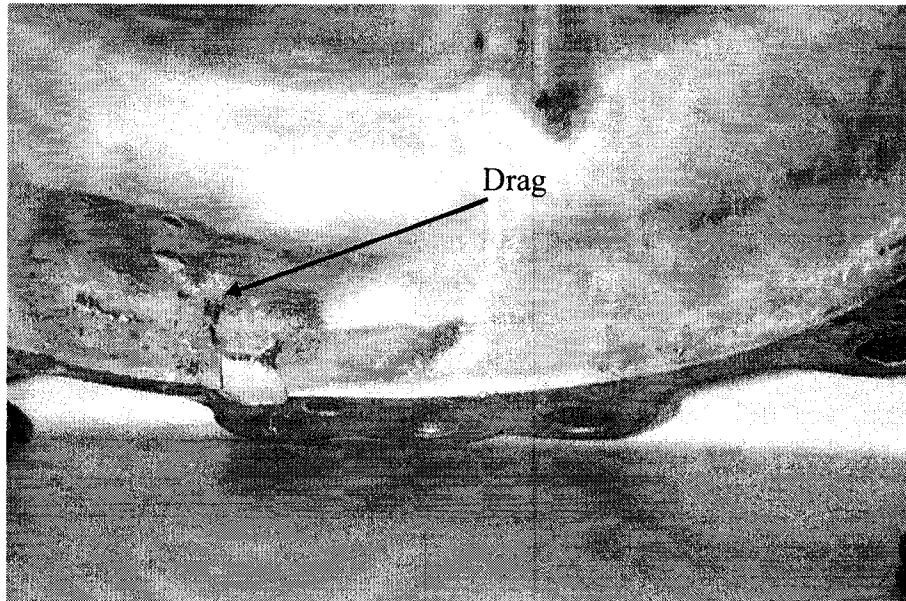
51

Figure 2.12: Casting defects, solder drag/tear, present in a die cast transfer case [31].

Limited studies revealed that the cracks were mainly inter-granular. In addition, it was found that cracks were initiated from the magnesium grain boundaries where a large amount of second phase (MgO and/or Al_2Ca) was presented. It is therefore proposed that cracks were initiated by the thermal stress caused by the difference in shrinkage rate between the second phase material and the magnesium matrix during solidification. This is further compounded by an increased susceptibility to hot cracking [31].

Pekguleryuz [24] revealed that calcium additions greater than 0.8% adversely affected die-castability due to extensive hot-cracking and die-sticking. Also, it was reported some die-sticking problems when the Ca level reached 1%. Die-sticking at that level was eliminated by the use of die lubricants and the proper casting temperature [28]. Powell et al [77] reported excellent diecastability for AC52 and AC53 alloys for small parts and simple shapes. All casting showed smooth surfaces and no evidence of

52

cracking. Also it was mentioned that resistance to ignition of ACX alloys during melting is greater (compared to AZ91D and AE42) and casting could reduce the need to use sulfur hexafluoride as a protective gas.

Powell et al [32] studied the die castability of Mg-Al-Ca-Sr alloys (AXJ) and compared with that of AM50. The optimum overall castability of the AXJ alloys was found to occur at nominally 2%Ca. at lower Ca levels (0.9%), cold shuts, staining, hot cracking, die sticking, and soldering defect ratings returned to AM50 levels. When the Ca level was increased to 2.6% Ca, hot cracking and die sticking ratings also improved. At all levels, Ca increased the occurrence of hot cracking slightly above that of AM50. The effects of Al and Sr content on casting quality were negligible. The excellent fluidity of the AXJ compared with that of AM50 was also shown by the extensive flash that was observed during casting.

2.2.5.4 Mg-Al-Sr system

Mg-Al-Sr alloys are a new addition to the creep-resistant magnesium alloys. The resistance to creep deformation of the Mg-Al-Sr alloys seems to be due to dispersoid (second phase) strengthening. SEM and EDX analysis shows that strontium in the alloy combines with Al, which impedes the formation of the $Mg_{17}Al_{12}$ phase. The absence of $Mg_{17}Al_{12}$ in microstructure is probably one of the main reasons for the superior creep resistance of the Mg-Al-Sr alloys [79].

Various alloy compositions such as AJ51 (Mg-5wt.%Al-1wt.%Sr), AJ52 (Mg-5wt.%Al-2wt.%Sr) and AJ62 (Mg-6wt.%Al-2wt.%Sr) have been studied. AJ52 shows the highest creep resistance, while AJ62x gives an excellent combination of creep performance and castability [80].

53

Pekguleryuz et al [79, 81] report that the alloys show different microstructures based on the Sr/Al ratio. For Sr/Al ratio below about 0.3, Al_4Sr intermetallic is the only secondary phase in the structure. When the Sr/Al ratio is higher, a secondary intermetallic phase (a ternary Mg-Al-Sr) is also observed. Sr/Al controls the formation of $Mg_{17}Al_{12}$ as well. When the Sr/Al ratio is very low, there would be insufficient amount of Sr to bind all Al and excess Al would form the $Mg_{17}Al_{12}$phase. Further studies on the ternary Mg-Al-Sr phase are needed. The superior creep resistance of the AJ52 and AJ62 alloys is attributed to the existence of the secondary phase in addition to Al_4Sr. Al_4Sr is a tetragonal phase and no phase coherency with the primary Mg phase has yet been reported.

Table 2.9 Tensile properties of diecast magnesium alloys [79].

alloy	Tensile strength (MPa)			Yield strength (MPa)			Elongation%		
	R.T	150 °C	175 °C	R.T.	150 °C	175 °C	R.T.	150 °C	175 °C
AZ91	239	170	138	157	105	89	4.7	18	20.5
AE42	226	142	121	135	87	81	9.2	22.5	23.1
AS41	249	153	127	132	94	85	8.9	16.8	18
Mg-5%Al 1.8%Sr	202	164	148	145	108	103	4	13.6	14.8
Mg-5%Al- 1.2%Sr	233	149	133	138	102	97	8.8	16.4	21.4
A380	290	255	248	155	149	154	3.2	6.4	7.1

R.T : Room Temperature.

54

Tensile yield strength and the ultimate strength of Mg-Al-Sr At 150-175 °C were reported to be higher than AE42 [79, 84] and AS41 [79]. Tensile yield and ultimate strength of the alloys at 175 °C also surpassed AZ91D. Ductility of the Mg-5wt.%Al-1.8wt.%Sr was comparable to AZ91D. The results are summarized in Table 2.9 [79]. These alloys also show higher creep resistance than all magnesium alloys and aluminum alloy A380 at 150 °C and 175 °C and under 35 MPa tensile loading. The Mg-5wt.%Al-1.8wt.%Sr showed the most creep resistance [79].

The Mg-Al-Sr alloys exhibited better creep resistance than AS41 and AZ91D. The performance is comparable to the AE42 and A380 for temperature up to 175 °C [79, 82].

The Mg-5wt.%Al-1.4wt.%Sr alloy shows slightly higher defect content than the AZ91D counterparts in die castings. The physical properties of the Mg-Al-Sr1.4% presented a real challenge to the die cast industry. Compared to traditional alloys such as AM50, the alloy requires less energy to cool from liquidus to solidus. This caused continuous problems with metal transfer and when in production would require additional energy in the form of heat to be present in the transfer of metal from the holding furnace to the shot sleeve. High shot speeds in an attempt to offset the limited solidification time led to soldering problems. In fact, slow shot speeds seemed to help metal flow but further compounded the need for additional heat. Nevertheless good castability is attainable with process optimization for Mg-5wt.%Al-1.4wt.%Sr alloy. Mg-5wt.%Al-2.1wt.%Sr has a better dicastability than Mg-5wt.%Al-1.4wt.%Sr alloy [82].

Argo et al [83] investigated the diecastability of Sr-alloyed Mg-5wt.%Al alloys by die casting valve covers. It has been indicated that die casting of the 1.4wt.%Sr-alloyed

55

Mg-5wt.%Al alloy required a die temperature of 30 °C to 50 °C, a melt temperature of 40 °C to 70 °C higher than those in normal operation of diecasting alloy AM50. Examination of casting quality manifests that hot tears and cold shuts occurred in the geometry transition areas such as ribs and boltholes, as well as the flat surface of castings. The observation also showed that casting defects tended to disappear as die temperature increased. However, the high die and melt temperature may lead to a shorten tool life. Despite the quality issue present in the castings, the study concluded that the alloy is castable in a production die-casting environment with the optimized die design and process parameters.

2.2.5.5 Mg diecasting alloys with combined additions of alkaline earth and/or rare earth elements

In recent years, many Al-containing Mg alloy systems have been developed with combined additions of rare-earth and alkaline earth elements. Nissan patent on an Mg-Al-Ca-RE alloy and later a Honda alloy [84] ACM522 (Mg-5wt.%Al -2wt.%Ca -2wt.%RE) both claim improved creep resistance over AE42 alloy. ACM522 is based on specific Al/RE/Ca ratios to ensure Al-RE precipitates in addition to Al-Ca intermetallics. This alloy is used by Honda in oil pans for their hybrid car. The microstructures of these alloys exhibit a combination of Al-RE and Al-Ca intermetallic mixtures. The Mg-8wt.%Al-2.5wt.%RE-1.6wt.%Ca-1.3wt.%Mn alloy Al_2Ca coupled eutectic phase as well as needle shaped Al-RE (Ca, Mn) itermetallics and Al-Mn-RE intermetallics[84]. Another alloy system based on Mg-Al-Ca-RE with optional additions of Sr and Zn is a patent by Dead Sea Magnesium [86]. Two alloy formulations code-named MRI153 MRI230 were reported to exhibit good elevated temperature performance [86] at 150 °C and 180 °C

56

respectively. Furthermore MRI153 exhibits good diecastability similar to AZ91alloy. The alloy system of this patent is quite complex, having a number of elements and would lend itself to further development to find optimum combinations of strength, creep resistance and castability.

2.2.6 Summary

From the literature review, it can be seen that the addition of calcium significantly improves the creep and stress resistance of Mg-Al alloys. But serious casting defects present in the Mg-Al-Ca alloys, produced by conventional high pressure diecasting processes limits its potential for high temperature automotive applications.

In terms of manufacturing, little research work has been carried out to produce Mg-Al-Ca alloys by other promising casting processes, such as squeeze casting. Also limited studies have been done on microstruicture and mechanical properties of squeeze cast Ca-containing magnesium alloys. Therefore a systematic research in understanding the castability, microstructure and mechanical properties of squeeze cast Mg-Al-Ca alloys are needed for potential applications of the alloys.

CHAPTER III

EXPERIMENTAL PROCEDURE

3.1 Casting

3.1.1 Melting unit

Melting of magnesium alloy AM50A was carried out in a 2.6 KW, 50/60 HZ electrical furnace with a maximum temperature of 1200 °C (Figure 3.1). Raw materials supplied in bar ingot form were cut into smaller pieces and melted in a crucible made of mild steel with a maximum holding capacity of 1.4 liters of molten metal (Figure 3.2). The temperature of the melt was closely monitored by both the control panel of the furnace and a hand held digital thermometer. To minimize temperature drop, the molten metal was poured directly from the crucible into the mould cavity.
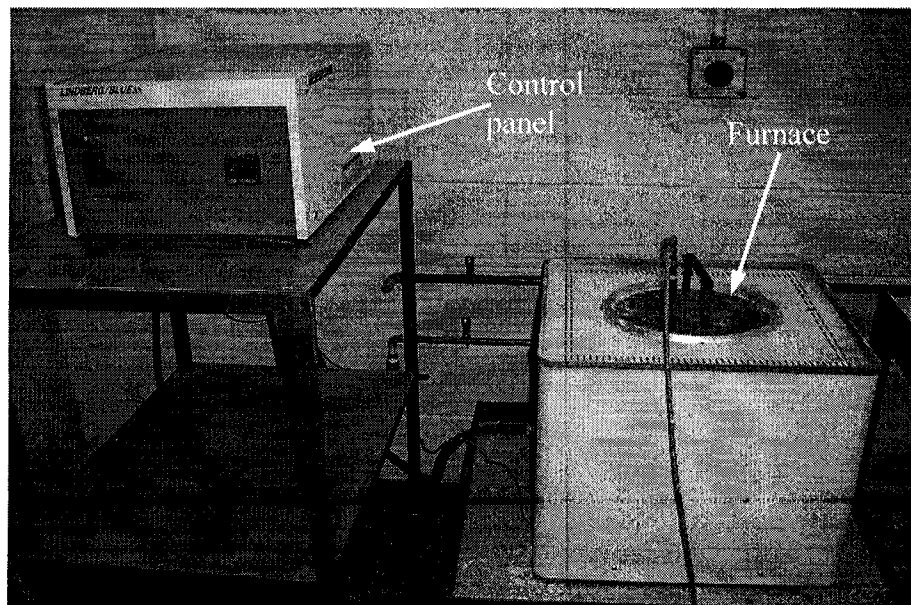
Figure 3.1: Melting furnace.

58

3.1.2 The Die sets

The aim of this project was to study the effects of pressure levels and calcium contents on the microstructure and mechanical properties of Mg-5wt.%Al-Xwt.%Ca alloy. A simple cylindrical configuration of casting coupons was adopted for this purpose. A set of cylindrical male and female dies was used to produce coupons with a diameter of 0.1 m and height of 0.15 m. Figure 3.3 shows the geometry of a squeeze cast cylindrical coupon. Both the die and its insert were made of grade H13 chromium molybdenum hot work steel due to its strength at high temperature and its wear resistance. The plunger and its head were made of steel grades 4140 and D8 respectively. A close tolerance of 0.1 mm was designed for the gap between the plunger head and the die in order to prevent any flash of molten metal during squeeze casting.

Figure 3.2: Mild steel crucible.

59
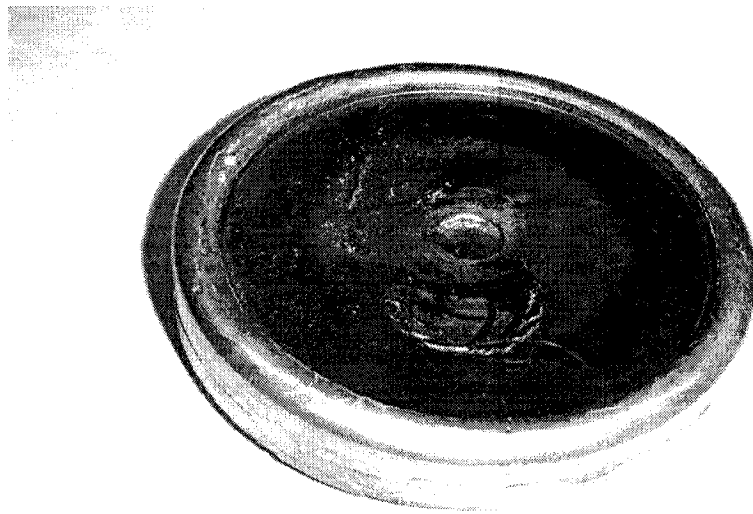
Figure 3.3: Schematic diagram showing a squeeze cast cylindrical coupon.

Die sets were preheated by Acrolab ceramic band heaters (Acrolab Ltd. Windsor, Ontario, Canada) prior to squeeze casting. Both the top and bottom dies were heated by two separate band heaters with electric powers of 220V, 6KW and 2KW, respectively at 220V. During heating, the die was kept being closed to reduce heat loss.

3.1.3 The hydraulic press

A 75 ton, vertical hydraulic press was used for direct squeeze casting. Figure 3.4 shows the hydraulic press, together with die set in position.

The die which was mounted on the bottom base platen is approximately 1.1 meters above the floor level. This height facilitated the pouring of molten metal during casting. For safety, a transparent polycarbonate shield was built around the press to protect operators from any injury resulting from the spill of molten metal during pressing.

60
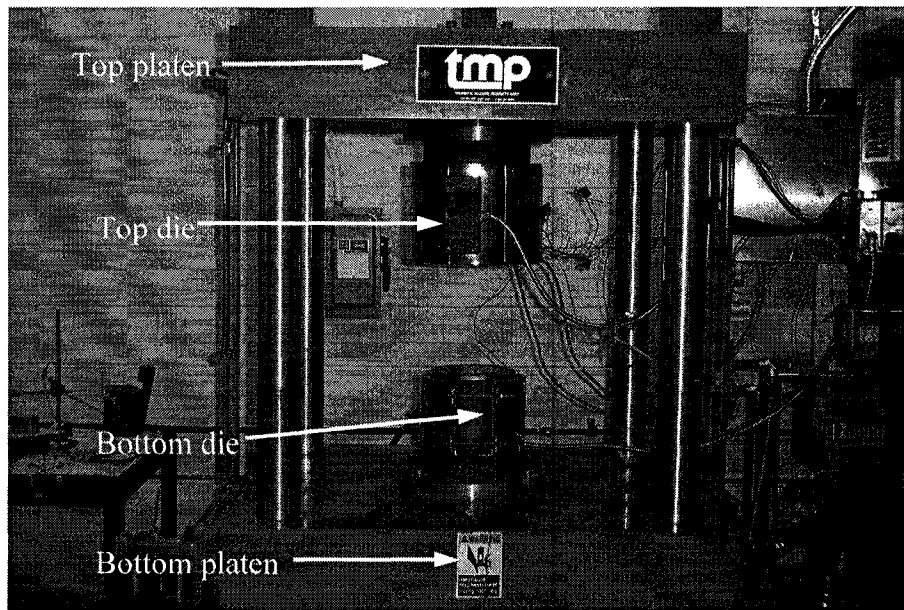
Figure 3.4: Squeeze cast machine and die.

When the press was activated, the bottom platen attached to the main ram (plunger) moved upwards and closed the die. Upon the completion of pressure build up in the hydraulic system, the plunger applied a pre-selected pressure to melt in the die cavity. The operation can be controlled either automatically or manually.

The press is also equipped with several level sensors to control the closing speeds of the platens.

3.1.4 Melting and pouring of molten metal

A magnesium alloy designated as AM50A was used in the study as parent alloy; it was provided by Ford Motor Company. A master alloy of magnesium-calcium (70wt.%Mg- 30wt%Ca), supplied by Timminco, was used to produce the desired alloy with different percentages of calcium. Raw materials were supplied in cast ingot bars.

61

Sufficient metal for each melt was prepared from these bars; initially melting was carried out in a mild steel crucible. The results of chemical analysis of the alloy samples taken from the squeeze cast coupons with different levels of calcium content are summarized in Table 3.1.

During the course of melting, no flux was used either to protect or to refine the melt. However, to protect the melt from any excessive oxidation or possible burning, a protective gas mixture of sulfur hexafluoride, SF_6, in a carrier gas of carbon dioxide, CO_2, was used.

Table 3.1 Chemical compositions of the squeeze cast alloys.

Alloy	Symbol	Aluminum (wt.%)	Calcium (wt.%)	Manganese (wt.%)
Mg-Al5%-Ca0%	AM50A	4.8	0	0.32
Mg-Al5%-Ca1%	AMC501	4.71	0.98	0.28
Mg-Al5%-Ca2%	AMC502	4.7	1.78	0.3
Mg-Al5%-Ca3%	AMC503	4.5	2.7	0.31
Mg-Al5%-Ca4%	AMC504	4.4	3.6	0.31

The molten metal was heated to a temperature of 760 °C, which is higher than the pouring temperature (720 °C) to have sufficient superheat for skimming and transferring. The molten metal temperature was closely monitored by a hand held digital thermometer. Once the melt temperature reached the desired temperature of 760 °C, the crucible was

moved out of the furnace and transferred to the die. The molten metal was poured directly from the crucible into the die cavity to avoid any large temperature drop. Transferring and pouring of the molten metal were done manually and attempts were made to pour at an equal and fairly rapid rate.

3.1.5 Casting conditions

The casting procedure can be summarized as follows:

1) Pre-heating the die set to the required casting temperature (300 $^\circ$C). Before its course of heating up, the die set was normally brushed with a die release agent, i.e., a water based graphitic die spray, supplied by Acheson Colloids Company;

2) Selecting the pressure level;

3) Installing the safety transparent shield;

4) Skimming the melt in the crucible and install a plate in crucible to allow the pouring of melt. This plate reduces the possibility of surface oxide entering the die cavity;

5) Pouring molten metal into the die cavity;

6) Activating the press by pushing the automatic cycle button. The bottom platen ascended rapidly until reaching a point, at which the top and bottom die was ready for closing;

7) Changing the platen movement with slow pressing speeds for die closing;

8) Building up pressure to a desired level in the hydraulic system upon die closing;

9) Holding up for a preset dwell time (60 seconds);

10) Retracting the punch to its original position;

63

11) Ejecting the casting from die; and

12) Repeating the cycle.

Two process parameters were investigated in this research: the pressure levels, and the calcium contents of the alloys.

The first series of experiments was aimed at investigating the effect of applied pressure on microstructure and mechanical properties. In the first series of experiments, applied pressures of 3, 10, 30, 60 and 90 MPa were employed to squeeze cast the alloys with the calcium content of 1 wt.%.

In second series, the effects of calcium contents were investigated on microstructure and mechanical properties. The alloys with various calcium contents of 0, 1, 2, 3, and 4% were squeeze cast under a constant applied pressure of 30 MPa.

3.2 Mechanical Testing

The mechanical properties of squeeze cast Mg-Al-Ca alloys were evaluated by tensile testing, which was performed at both ambient temperature and 150 °C on an Instron machine equipped with a computer data acquisition system. Following ASTM B557 [87], subsize flat tensile specimens (25 mm in gage length, 6 mm in width, and 6 mm in thickness) were machined from the center of squeeze cast disc as shown in Figure 3.5. Figure 3.6 shows schematically the dimensions of tensile specimen. The tensile properties, including 0.2% yield strength (YS), ultimate tensile strength (UTS), and elongation to failure (E_f), were obtained based on the average of three tests.
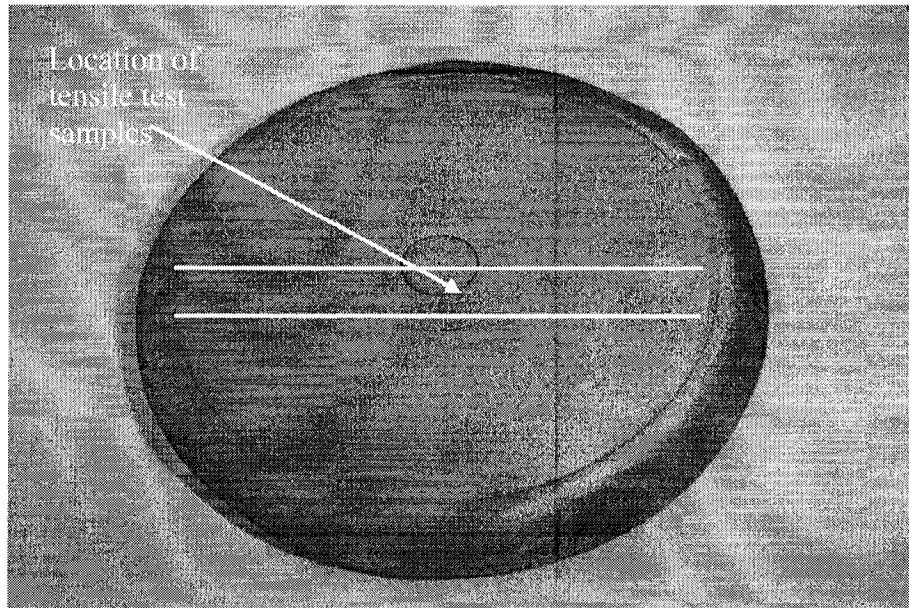
a) Top view
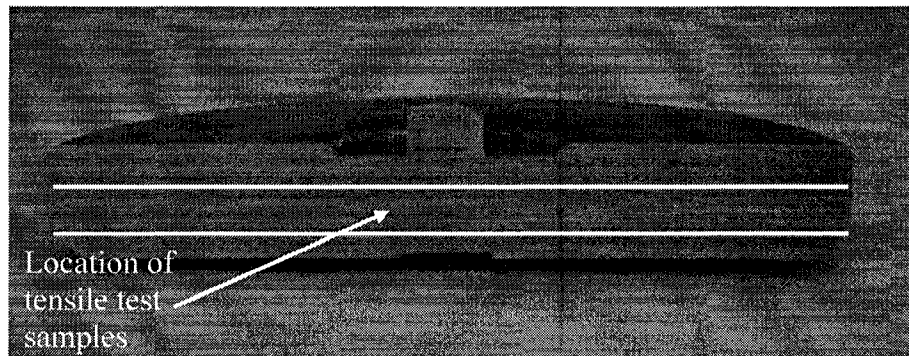
b) Side view

Figure 3.5: Schematic diagram showing the location of die cast coupons from in which the samples were taken for tensile test, a) top view and b) side view.

65
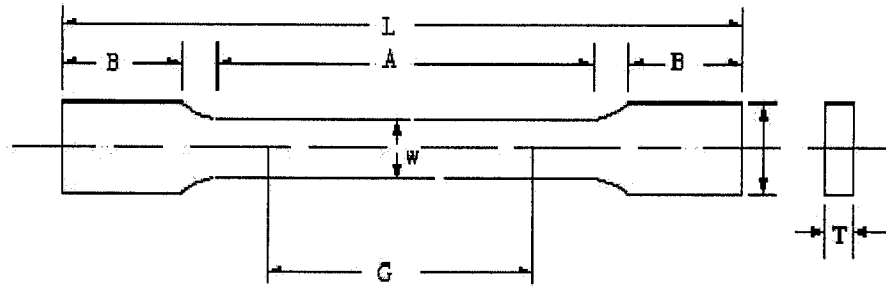
Figure 3.6: Schematic illustration of Tensile Test Specimen.

G- Gage length: 25±0.1 mm   W- Width: 6±0.1 mm

T- Thickness 6±0.1 mm   R-Radius of fillet, min: 6 mm

L- Overall length, min: 100 mm   A-Length of reduced section: 32 mm

B- Length of grip section, min: 30 mm   C-Width of grip section: 10 mm

3.3 Metallography

3.3.1 Specimen preparation

The castings were sectioned, mounted, and polished from the center of the squeeze cast disc and prepared following the standard metallographic procedures. Samples were cut from the castings and were mounted by Buehler Simplimet 3 mounting press. Mounted samples were ground on series of SiC papers in the sequence: 180, 320, 400 and 600 grit. Samples were then polished on a DP-PAN polishing cloth with 1μm Al_2O_3 suspension. Polished specimens were washed with water, liquid soap and ethyl alcohol, and then dried using cold air; hot air is noted to leaves a brownish oxide on the surface.

Considerable time was spent optimizing the polishing and etching conditions. The best etchant used was the glycol, consisting of 1 ml HNO_3, 75 ml di-ethylene glycol, and 25 ml H_2O. Etching was performed by swabbing the sample for 10 to 15 seconds, and

66

then washing the specimen surface with running water and ethanol. Figure 3.7 shows the location of squeeze cast discs from which metallographic samples were taken for microstructural analysis.

3.3.2 Optical and Electron Microscopy

A Buehler optical image analyzer 2002 system was used to determine the primary characteristics of the specimens. Figure 3.8 shows the Buehler optical image analyzer 2002 system. The grain size was measured by image analyzer according the ASTM E112-96 [88].

The detailed features of the microstructure were characterized at high magnifications by A JSM-5800LV scanning electron microscope (SEM) with a maximum resolution of 100nm in a backscattered mode/1μm in X-Ray diffraction mapping mode, and maximum useful magnification of 30,000. In order to maximize composition reading of the Energy Dispersive Spectroscopy (EDS) data, etchant was applied to specimen for microscopy examination. Fractured surfaces of tensile specimens were also analyzed by the SEM to ascertain the nature of fracture mechanisms. In addition, the longitudinal section of tensile tested specimen passing through the fractured surface were polished and examined in an effort to understand the extent of damage beneath the fractured surface. Figure 3.10 shows scanning Electron Microscope (Joel Model JSM-5800LV).
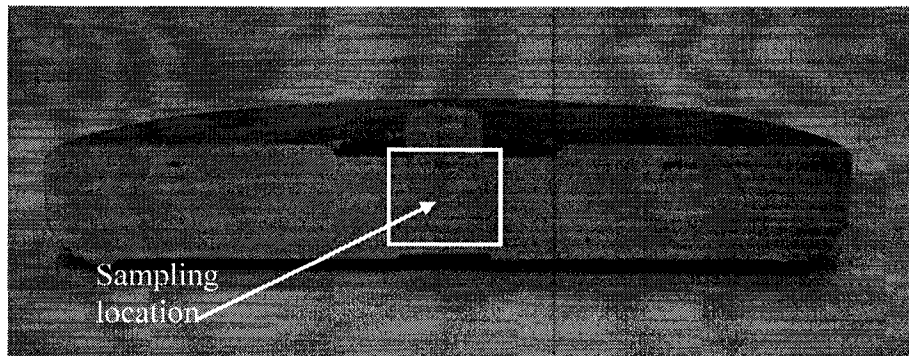
Figure 3.7: Schematic diagram showing the location of die cast coupons from which

the samples were taken for microstructural analysis.
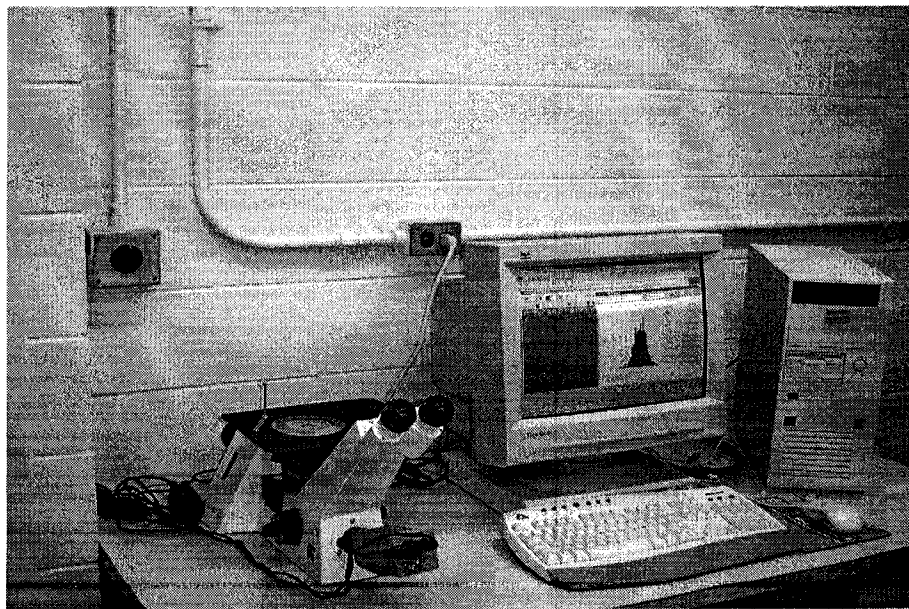
Figure 3.8: Buehler optical image analyzer model 2002.

Figure 3.9: Scanning electron microscope (Joel Model JSM-5800LV).

3.4 Density Measurement

Specimens for density measurement were taken from the place close to which metallographic samples were taken from. Following the measurement of specimen weight in air and distilled water, the actual density (D_a) of each specimen was determined using Archimedes principle based on ASTM standard D3800 [89]:

$$D_a = W_a D_w/(W_a-W_w)$$

Where W_a and W_w are the weight of the specimens in air and in water, respectively, and D_w is the density of water. Figure 3.10 shows the lab set up of the density measurement. The porosity of each specimen was calculated by the following equation:

$$\%Porosity = [(D_t-D_a)/D_t]\ 100\%$$

where D_t is the density of alloy AMC501 squeeze cast under 90MPa, since the standard density of densified AMC alloys is not available.

69

Figure 3.10: Experimental setup for density measurement.

CHAPTER IV

RESULTS AND DISCUSSION

4.1 Introduction

In this chapter, the results of the microstructural analysis and tensile properties of squeeze cast Mg-Al-Ca alloy are presented. The influence of both pressure levels and calcium contents on tensile properties are discussed.

The results in this chapter will be presented in the following sequence:

1. Microstructure analysis including optical microstructure and SEM;

2. Tensile test results; and

3. SEM-based microstructural studies of tensile fracture regions and fracture surfaces.

4.2 Effect of Pressure Levels on Tensile Properties and Microstructure of Squeeze Cast Mg-Al-Ca Alloys

To investigate the effect of applied pressures on microstructure and mechanical properties of squeeze cast Mg-Al-Ca alloys, five different levels of applied pressures, 3, 10, 30, 60 and 90 MPa, were employed while the calcium content of the alloys was kept constant at 1 wt.%. It should be mentioned that the lowest hydraulic pressure, available in the squeeze cast machine used in this study, was 3 MPa.

4.2.1 Surface cracking of Mg-Al-Ca alloys

As discussed in the preceding section, Ca addition to magnesium alloys enables them to easily form surface cracks [24, 28, 31, and 32]. In attempt to understand the effect of pressure levels on the formation of surface cracks, direct observations on the surfaces of cast Mg-Al-Ca alloys with and without applied pressures were made.

Figure 4.1 clearly shows evidently that surface cracks in a star shape formed in the AMC501 alloy when no external pressure was applied. However, an applied pressure, as low as 3 MPa, tended to eliminate the occurrence of surface cracking in the alloy as illustrated in Figures 4.2 and 4.3. Examination of squeeze cast AMC501 alloy reveals that the elimination of surface cracks taking place in the AMC501 alloy becomes achievable with the help of an applied external pressure.
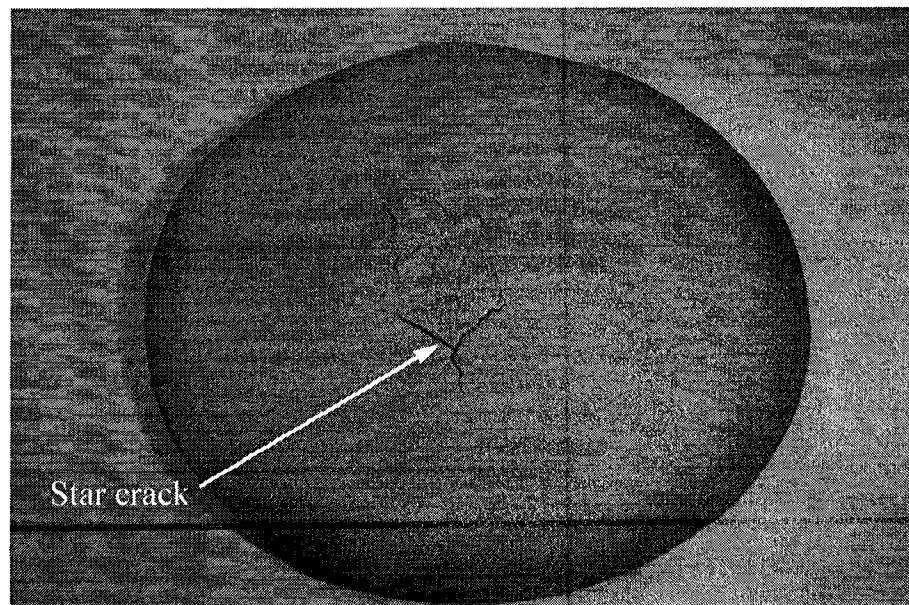
Figure 4.1: Crack formation in AMC501 alloy solidified under no applied pressure.

72
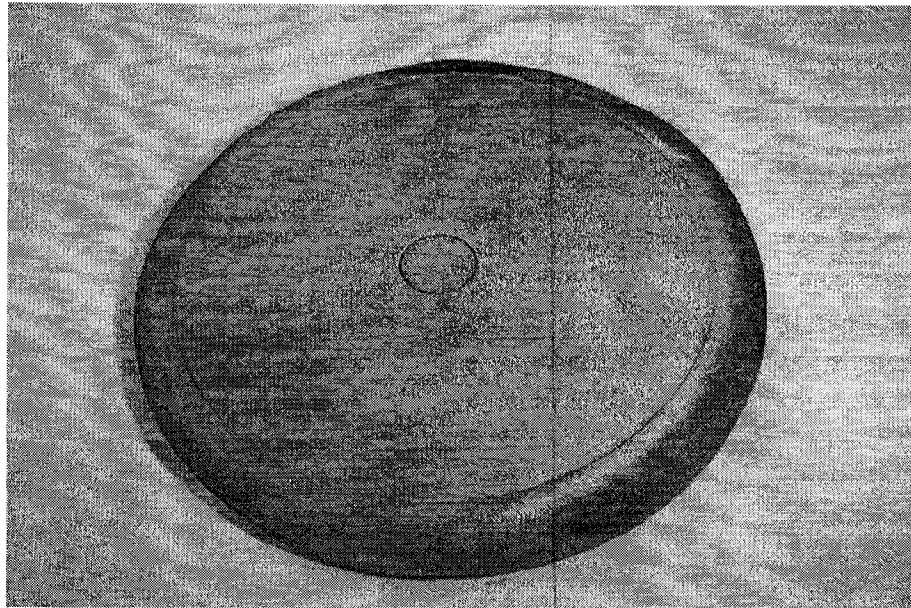
Figure 4.2: No Crack foramtion in AMC501 alloy solidified under 3 MPa applied

pressure.
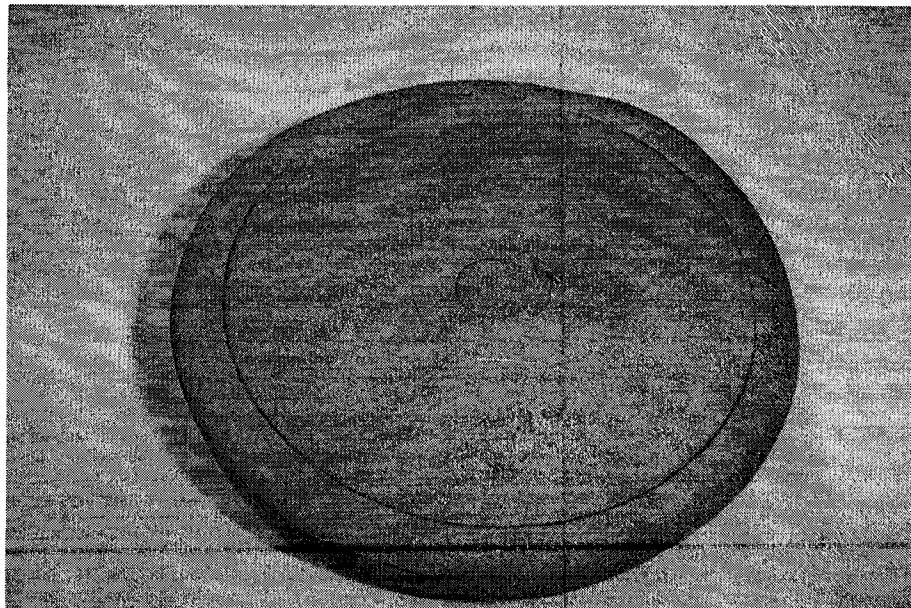
Figure 4.3: No crack formation in AMC501 alloy solidified under 30 MPa applied

pressure.

73

4.2.2. Microstructure Analysis

Figures 5.4 to 5.8 show the optical microstructure of the Mg-5%Al-1%Ca alloy squeeze cast under the pressure of 3, 10, 30, 60, 90 MPa in the as-cast condition, respectively. It can be seen that the secondary phase (intermetallic Al_2Ca particles) are precipitated around grain boundaries. The third phase present is an intermetallic of Al-Mn which has round shape.

As the pressure increases from 3 to 90 MPa, the grain sizes of the alloy were noted to vary only from 40.2μm to 39μm. This experimental observation indicates that an increase in applied pressure leads to no reduction in grain size, which is on the contrary to the results given in references 9, 14, 41 and 50. However, no effect of applied pressure on grain size may be attributed to casting geometry-related heat transfer taking place during squeeze casting.

The heat transfer at the casting /die interface can be determined by:

$$Q = h (T_c - T_d) A \qquad [5-1]$$

where Q is the heat transferred in time unit

h is heat transfer coefficient ($W\ m^{-2}\ K^{-1}$);

T_c is the casting temperature at the casting-die interface;

T_d is die temperature; and

A is contact area of the interface between casting and die.

In general, during squeeze casting heat transfer coefficient (h) across the interface between the casting and die is enhanced with applied pressure which eliminates air gaps at casting/die interface. However, due to high aspect ratio (the ratio of casting diameter to

74

its height) of the current casting, the side surface area of the casting is much smaller than its top and bottom surface area. According to Equation 5-1, the top and bottom surfaces of the casting play a dominating role in heat transfer during the process compared to its side surface. Despite the application of external pressure eliminating the air gap present between the casting side surface and die wall, the resulting enhancement on heat transfer at the side interface is limited due to its high aspect ratio.
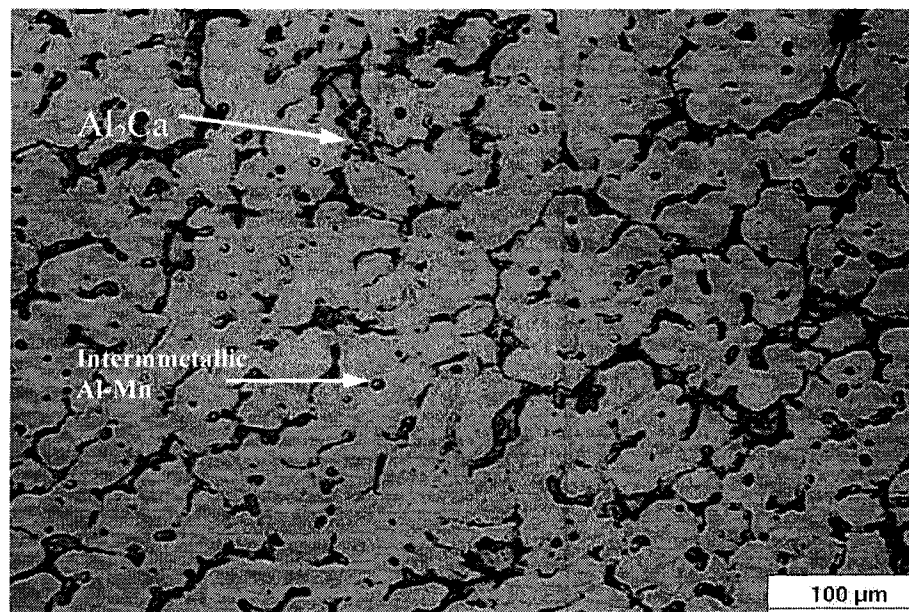
Figure 4.4: Optical micrograph showing microstructure of alloy AMC501 squeeze cast under 3 MPa.
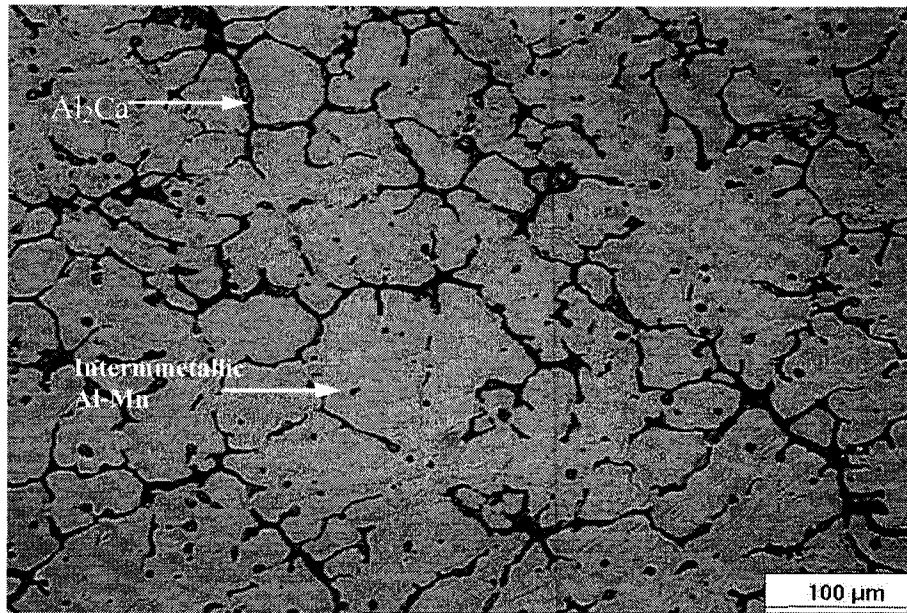
Figure 4.5: Optical micrograph showing microstructure of alloy AMC501 squeeze cast under 10 MPa.
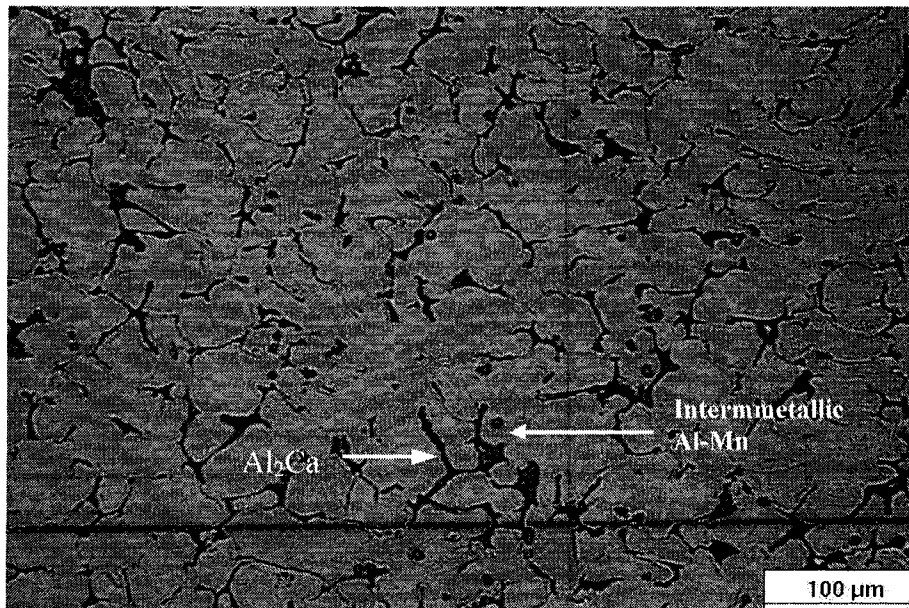
Figure 4.6: Optical micrograph showing microsturcture of alloy AMC501 squeeze cast under 30 MPa.

76
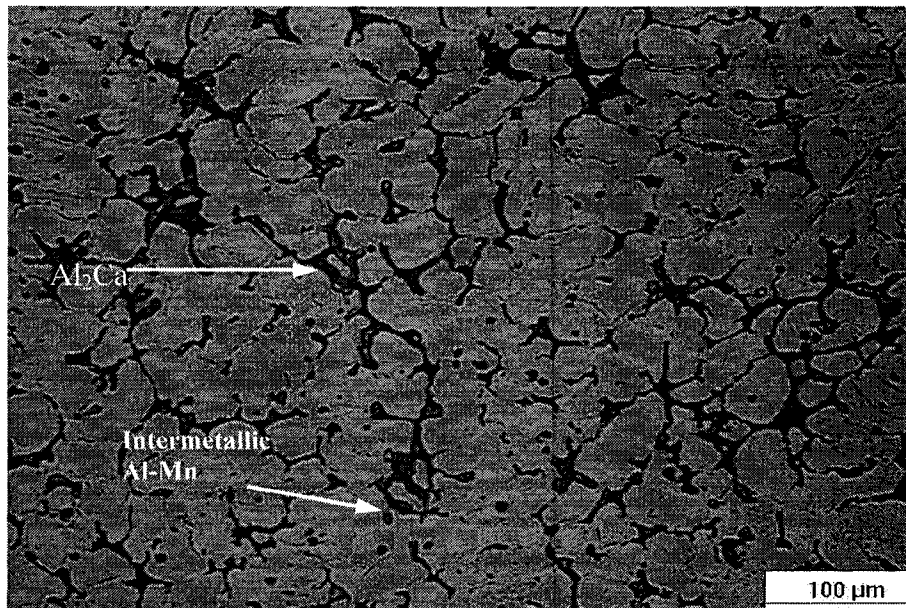
Figure 4.7: Optical micrograph showing microstructure of alloy AMC501squeeze cast

under 60 MPa.
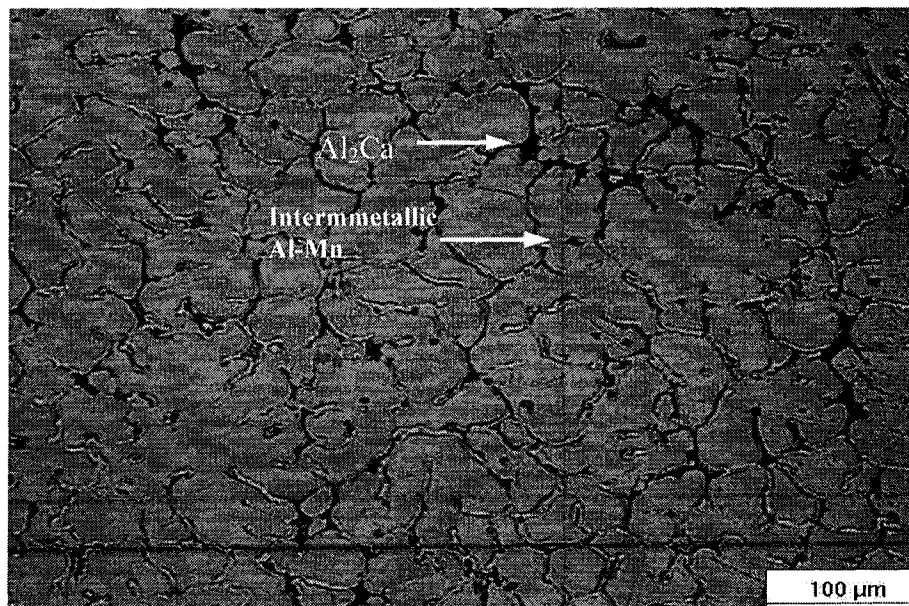
Figure 4.8: Optical Micrograph showing microstructure of alloy AMC501 squeeze cast

under 90 MPa.

77

4.2.3 Material densification

Figures 4.9 and 4.10 present the density and porosity measurements of alloy AMC501 samples squeeze cast under different pressure levels of 3, 10, 30, 60, and 90 MPa. It is evident from Figures 4.9 and 4.10 that the density of squeeze cast AMC501 samples increases and its porosity decreases with an increase in applied pressures. The densification and porosity reduction of squeeze cast AMC501 should be attributed to the fact that the applied pressure enables the melt to feed the microshrinkage forming in the last solidifying region of casting, capable of deforming the solidifying metal, and also suppresses gas nucleation, and significantly decreases the size of entrapped gas. As a result, the alloy becomes highly densified with considerable low amount of porosity.

The SEM results given in Figures 4.11-4.14 further support the porosity measurement. Relatively low pressures (3 and 10 MPa) are incapable of completely eliminating porosity in the alloy as depicted in Figures 4.11 and 4.12. As the applied pressure increases to and beyond 30 MPa, no porosity was observed in the squeeze cast alloy (Figures 4.13 and 4.14).

78
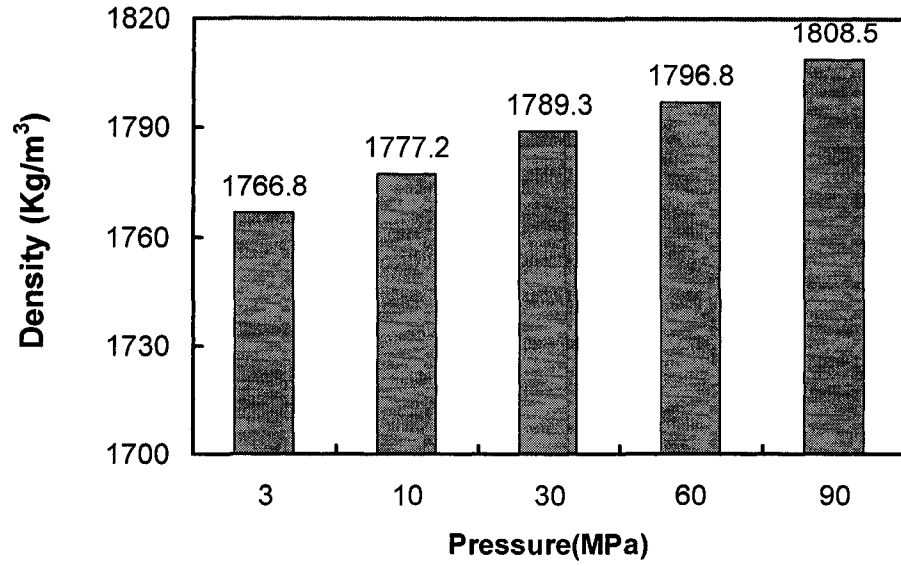
Figure 4.9: Effect of applied pressure on density of alloy AMC501.
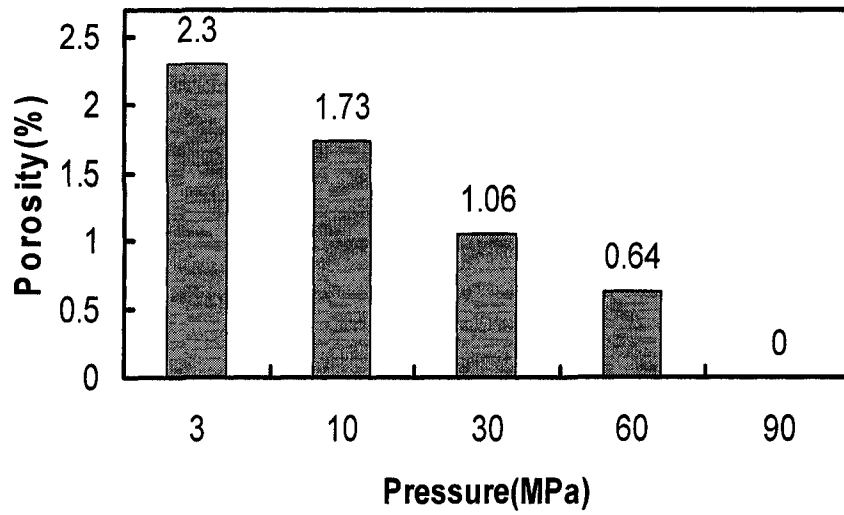
Figure 4.10: Porosity versus applied pressure.

79
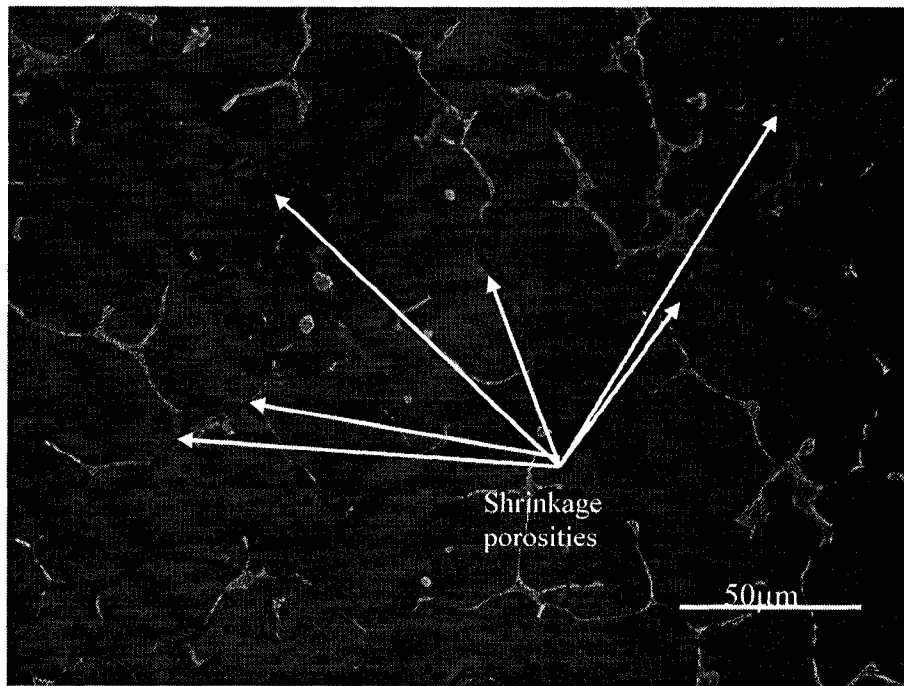
Figure 4.11: Shrinkage porosities in samples cast under 3MPa.
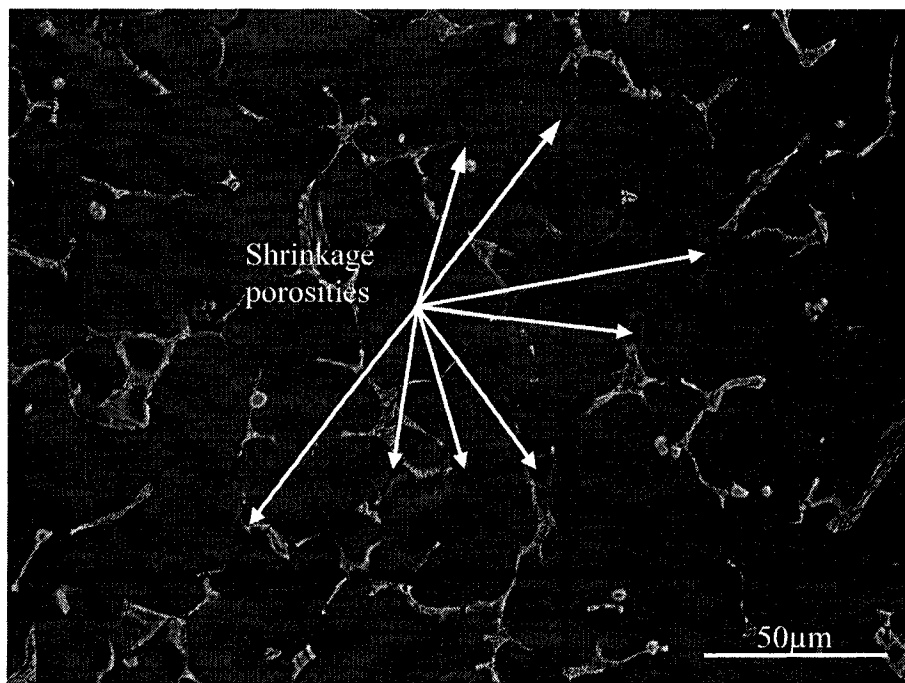
Figure 4.12: Shrinkage porosities in samples cast under 10MPa.

80
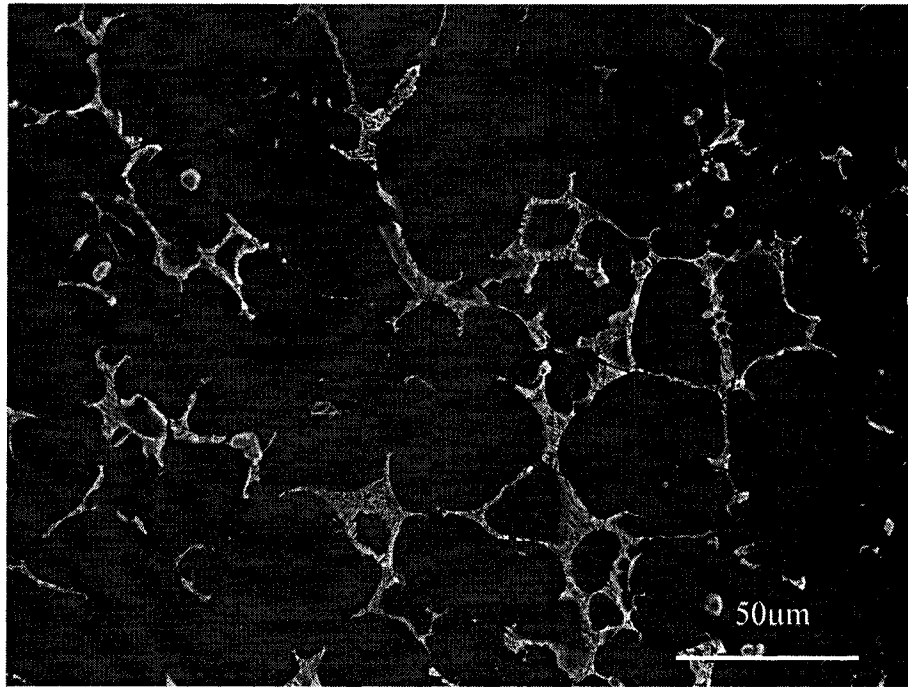
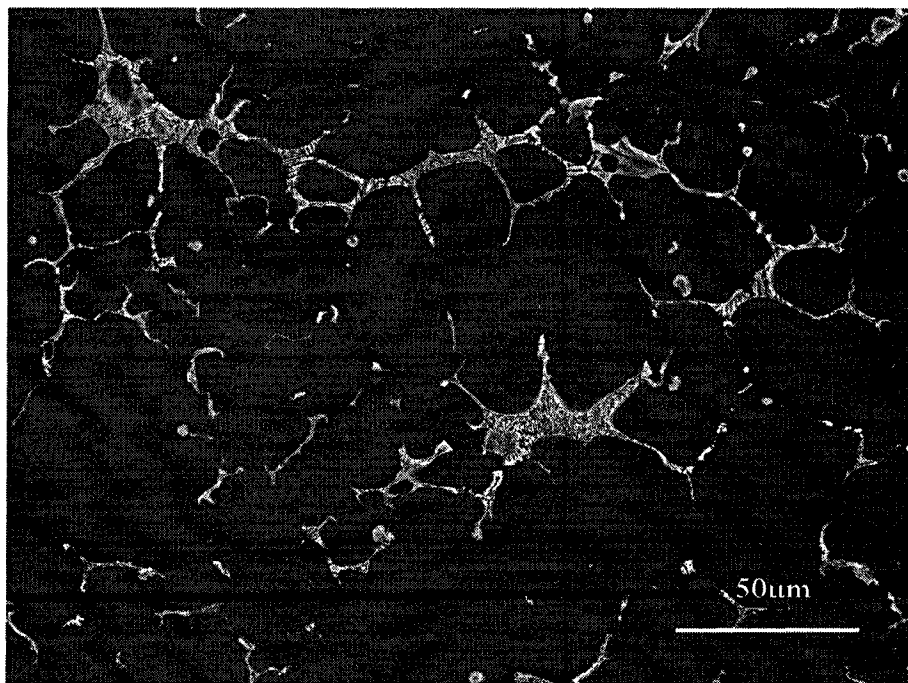Figure 4.13: No shrinkage porosities in samples cast under 30MPa.

Figure 4.14: No shrinkage porosities in samples cast under 60MPa.

81

4.2.3 Tensile properties

Figure 4.15 shows representative engineering stress and strain curves of squeeze cast Mg-5wt,%Al-1wt.%Ca alloy under the applied pressures of 3 and 90 MPa at room temperature. For these two pressures, the stress variation with the strain follows almost the same pattern. Under tensile loading, the alloy deformed elastically first. Once yield points reaches, plastic deformation of the alloy starts. However, the ultimate tensile strength (UTS) and elongation of the sample cast under 3MPa are much lower than those cast under 90MPa.

The effect of applied pressures on tensile properties of squeeze cast AMC501 alloy, is shown in Table 4.1 and Figure 4.16. It is observed from the results that an increase in pressure levels brings a significant improvement in the ductility and some improvement in UTS and yield strength (YS). The elongation, UTS and YS of the alloy for 90 MPa is 5.42%, 183.7MPa and 90.2 MPa, respectively, which result in increases of 66% in elongation, 20% in UTS and 13% in YS over those specimens cast under 3 MPa. Since no significant microstructural change was observed under different pressure levels, the improvement in mechanical properties by the pressure increase should be attributed to materials densification and porosity reduction. The slight increase in yield strength might be attributed to higher dislocation densities in samples squeeze cast under higher applied pressures, as suggested in reference 29.

One of the major characteristics of the plastic deformation of metals is the fact that the shear stress required to produce slip continuously increases with increasing shear strain. The increase in the stress required to cause slip because of previous plastic deformation is known as strain hardening or work hardening. Strain hardening is

82

attributed to the interaction of dislocations with other dislocations and with other barriers to their motion through the lattice [93]. Figure 4.17 gives true strain stress curves of AMC501 cast under 3 and 90 MPa. To elucidate the strain-hardening behaviour of the AMC501 alloy cast under 3 and 90 MPa, a plot of strain-hardening rate ($d\delta/d\varepsilon$) versus true plastic strain (ε), is given in Figure 4.18, which is derived from true strain-stress curves. It can be seen from Figure 4.18 that as the applied pressure in casting process rises, the strain hardening rate of the alloys increases. It suggests that AMC alloys cast under high pressure content are able spontaneously to strengthen themselves increasingly to certain extent, in response to large plastic deformation prior to fracture. The high strain hardening rates of the alloy cast under higher applied pressure may be attributed to high dislocation densities in samples squeeze cast under high applied pressures, suggested in reference 29.
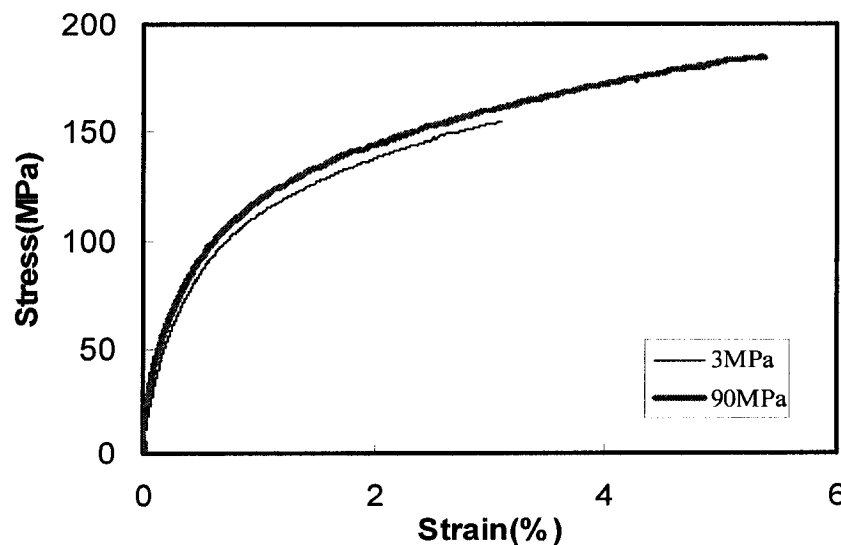
Figure 4.15: Engineering stress-strain curves of AMC501 under 3 and 90MPa.

83

Table 4.1 Effect of pressure levels on UTS, YS and Elongation.

Pressure level(MPa)	UTS(MPa)	0.2%YS(MPa)	Elongation (%)
3	153.7±6.6	80±2	3.26±0.6
10	169±3	83.5±3.75	4.37±0.45
30	176.9±0.8	86±1	5.02±0.1
60	180±3.5	88±4.5	5.16±0.05
90	183.7±0.95	90.5±2.5	5.42±0.05
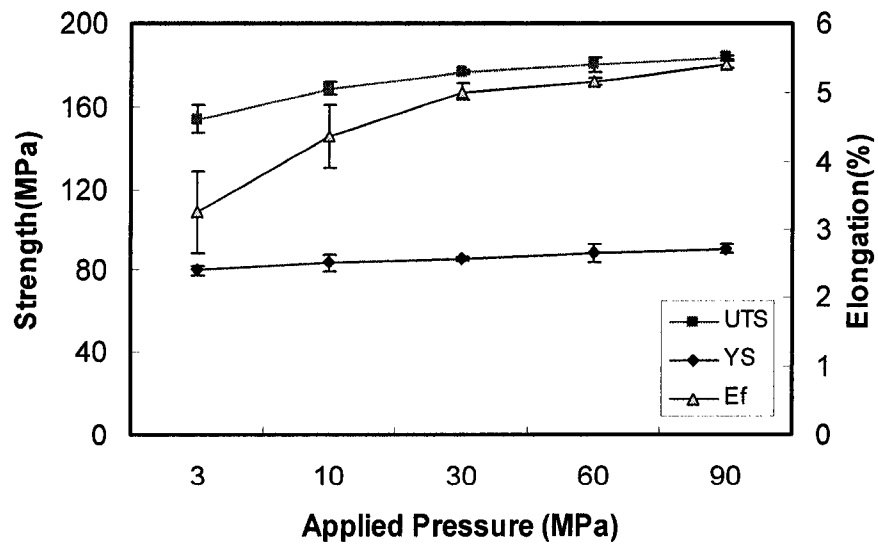
Figure 4.16: Effect of pressure levels on UTS, YS and Elongation of AMC501 alloy.
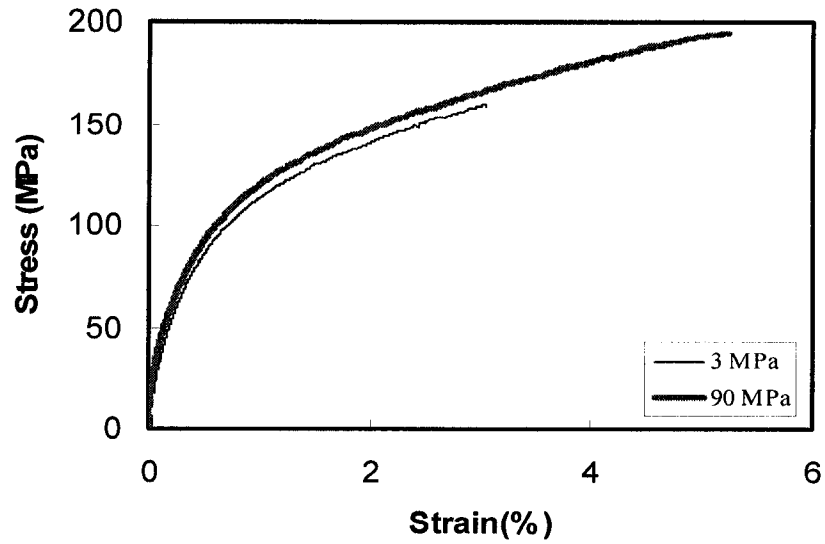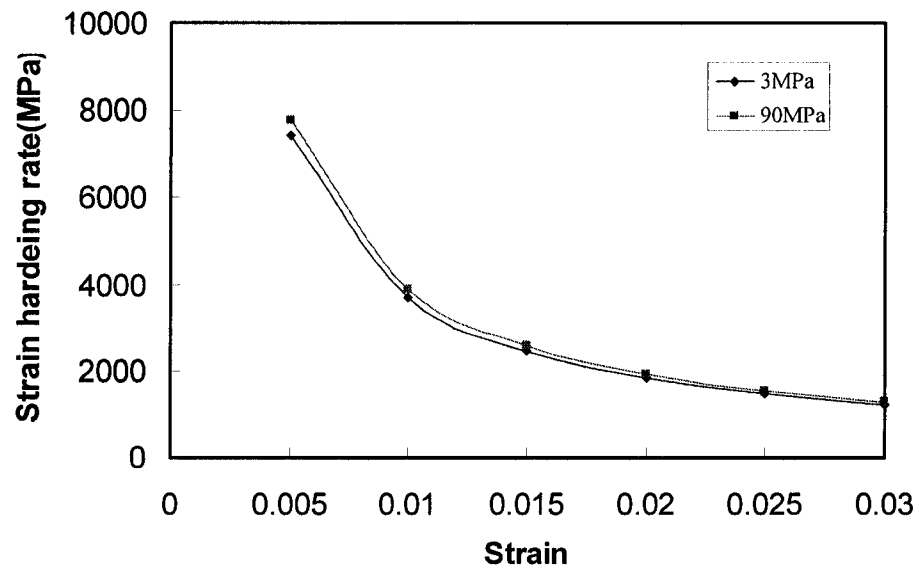
Figure 4.17: True stress-strain curves of AMC501 cast under 3 and 90MPa.

Figure 4.18: Strain hardening rate versus strain of AMC501 cast under 3 and 90MPa.

85

4.2.5 Fracture behaviour

The tensile fractured surfaces of squeeze cast AMC501 are shown in Figures 4.19 and 4.20. The observed fracture mode of the samples under 3 and 90 MPa is dimple rupture. In this mechanism the alloy fail by microvoid coalescence when fractured under a continual rising load. The microvoids nucleate in the material at areas of localized high plastic deformation such as that associated with second phase particles, inclusions, and grain boundaries. As the load on the material increases, the microvoids grow, coalesce, and eventually form a continuous fracture surface. A considerable amount of energy is consumed in the process of the formation of microvoids, eventually leading to creation of cracks.

The analysis of the SEM fractography shows that the fracture behavior of squeeze cast AMC501 is influenced by applied pressure levels. As the pressure level increases, the fracture of the alloy tends to transition from brittle to ductile. The fracture surface of the 90 MPa specimen is ductile in nature, and is characterized by the presence of deep dimples compared with 3 MPa samples (Figure 4.20). The brittle behaviour of samples squeeze cast under 3 MPa can be attributed to high porosity percentage. The porosity presence cause stress concentrations where cracks form and spread rapidly over the section.

The brittle Al_2Ca segregation along the grain boundaries might be the main cause of the intergranular fracture. The damaged microstructure underneath the fractured surfaces presented in Figures 4.21 and 4.22, at least in part, supports this interpretation. Overall, the SEM observations of the fracture surfaces show a good agreement with the tensile properties of the alloy presented in sections 4.2.4.
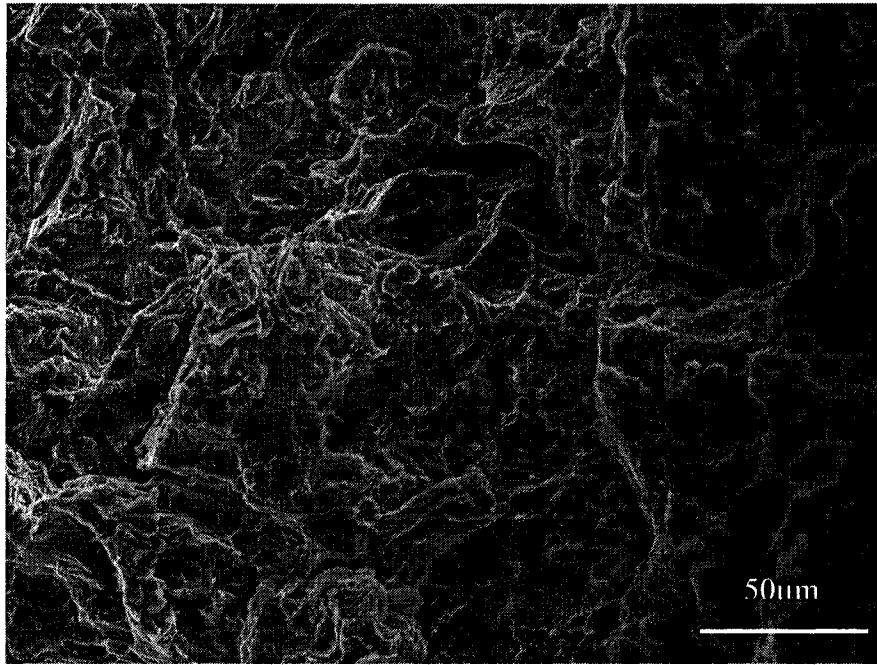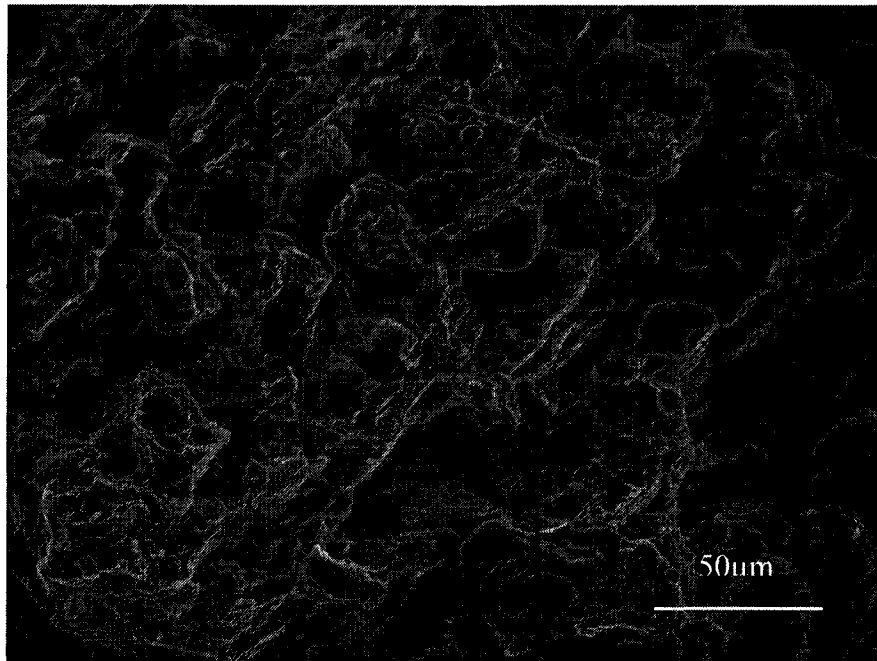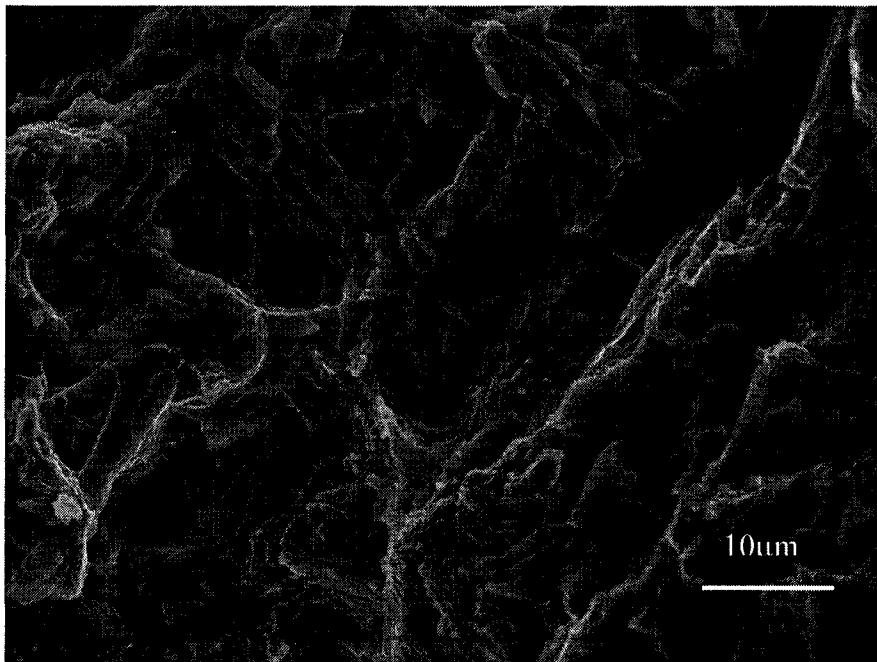
a)
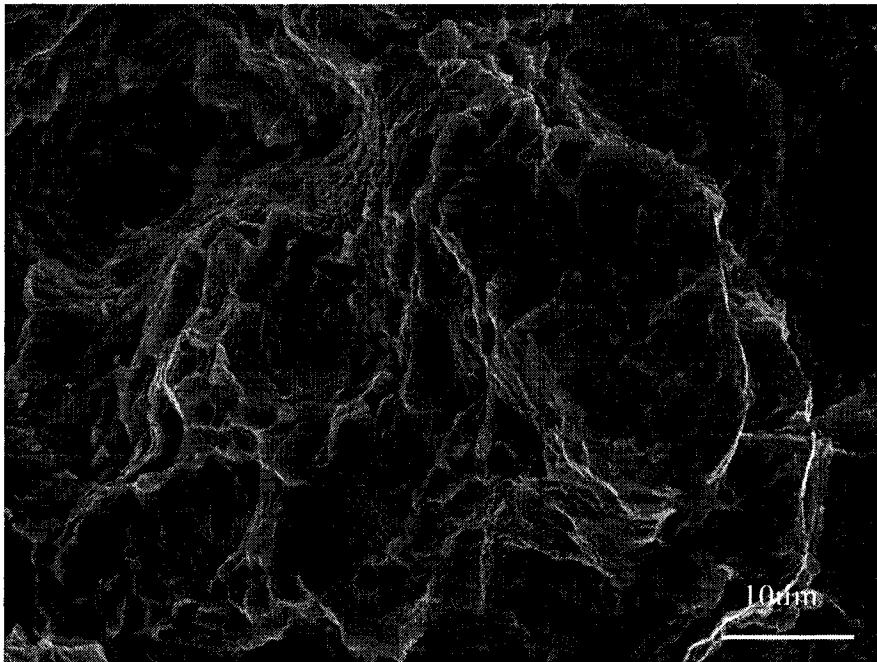
b)

Figure 4.19: SEM fractographs of squeeze cast AMC501 under 90 MPa,

a) low magnification and b) high magnification.

87

a)

b)

Figure 4.20: SEM fractographs of squeeze cast AMC501 under 3 MPa,

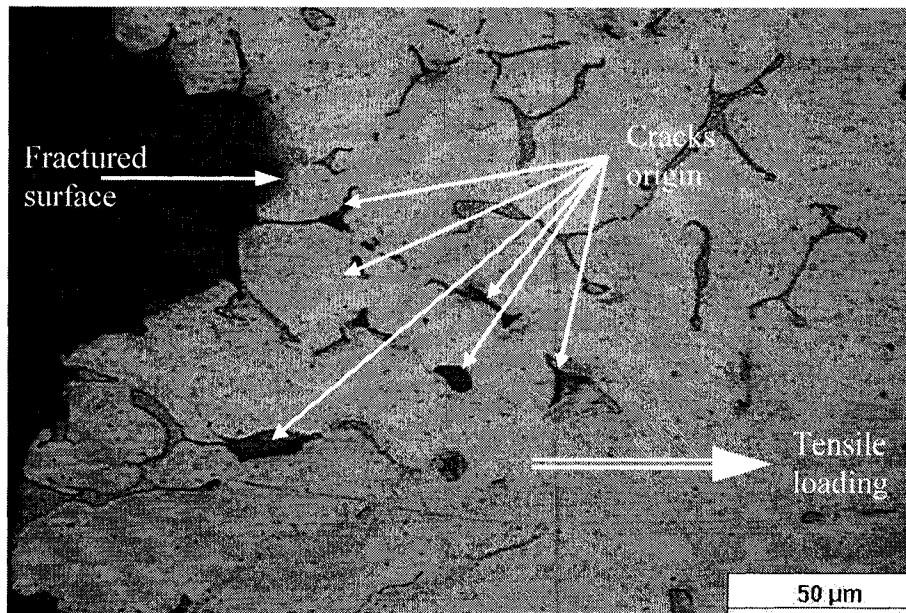a) low magnification and b) high magnification.

88

Figure 4.21: Optical micrograph showing crack origin in AMC501 squeeze cast under
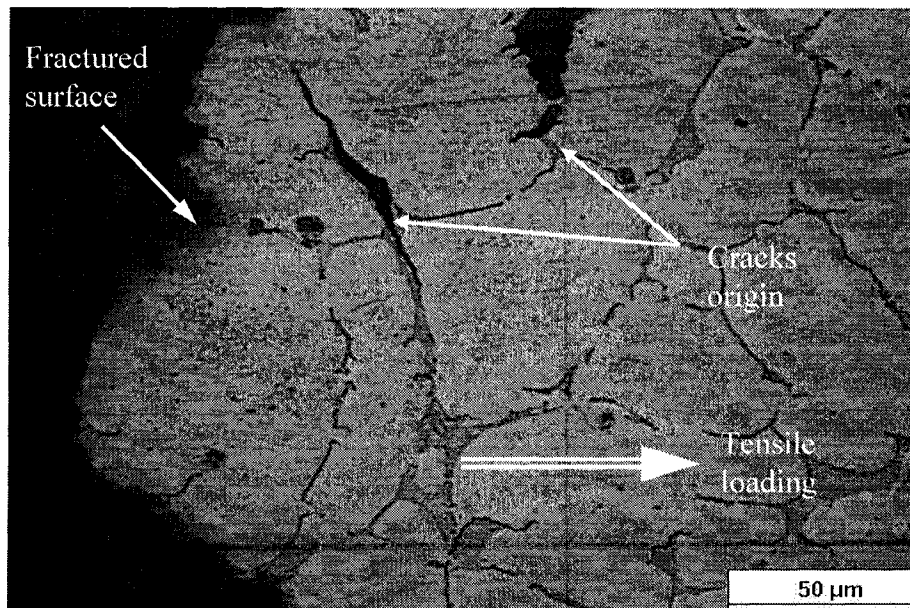
3 MPa.

Figure 4.22: Optical micrograph showing crack origin in AMC501 squeeze cast under

90 MPa.

4.2.6 Summary

The effect of pressure was investigated on microstructure and mechanical properties of squeeze cast AMC501 alloy. The microstructure for all samples contain primary α-Mg, Al_2Ca intermetallic and Mn-Al intermetallic. Due to high aspect ratio of the casting geometry no significant improvement in grain structure was observed as the applied pressures increase.

The results of tensile testing indicate that the mechanical properties, UTS, YS, and elongation, increase with an increase in applied pressures during solidification. The material densification and porosity reduction should be responsible for the increase in tensile properties.

The observation via SEM fractography and tensile results indicates that, as the applied pressures increase, the fracture mode of the alloy transits from brittle to ductile.

4.3 Effect of Calcium Contents on Tensile Properties and Microstructure of Squeeze Cast Mg-Al-Ca Alloy

To investigate the effect of calcium content on microstructure and mechanical properties, the AM50A alloys with different percentages of calcium addition, 0, 1, 2, 3, 4 wt.%, were squeeze cast under a constant pressure of 30 MPa in the second series of experiments. It was observed that the resistance of melt to ignition increased with addition of calcium to AM50A and the need for sulfur hexafluoride to protect the melt could be reduced, but more dross formed during alloying.

4.3.1 Microstructure Analysis

Figures 4.23 to 4.27 present the optical microstructure of the squeeze cast specimen of AM50A alloy with different calcium contents 0, 1, 2, 3, 4 wt.% in as-cast condition, respectively. The grain size of alloys was measured by image analysis according to ASTM E112-96. The results show that addition of calcium to AM50A alloy causes a grain refinement (Figure 4.28). The grain size decreases from 47 to 39 μm with a calcium addition of 1 wt.%, and further reduces to 35μm with an increase in the calcium to 2 wt.%. As the calcium content increases to 3 wt.%, however its influence on grain refinement becomes limited (Figure 4.28). It appears that, increasing calcium to 4 wt.% has no further effect on grain size of Mg-Al-Ca alloys (Figure 4.28).

The optical microstructural analysis of AM50A (Figure 4.23) shows that a visible white network and an irregularly shaped black dispersoids are continuously present around grain boundaries, and gray particles reside in grains. The results of SEM analysis given in Figure 4.29 reveals that the white networks are just the light reflection of grain

91

boundaries in optical microscopy and only the black dispersoids are the secondary eutectic phase.

With an addition of 1 wt.% calcium to AM50A, a semi-continuous network of secondary phases forms around grain boundaries. As calcium content increases, the amount of secondary phases present around grain boundaries become massive. As a result, a continuous network of secondary phases forms at grain boundaries. In an effort to quantitatively determine the role of calcium on phase formation, the fraction area of secondary phases in AMC alloys was measured. It can be seen from Figure 4.30 that, as the calcium contents of the alloys increase from 1 wt.% to 4 wt.%, the fraction of secondary phase increases from 9.9% to 19.5%.

SEM and EDS were utilized for the elemental analysis of microstructural features observed in this study. Figures 4.31 - 4.34 present the results of SEM and EDS analysis for AM50A. As it can be seen the β-$Mg_{17}Al_{12}$ eutectic phase (bright contrast) presents in a matrix (dark contrast) of the primary α-Mg solid solution tends to form a discontinuous network (Figure 4.31). Figures 4.32 to 4.34 show the EDS spectra for J, which is the α-Mg matrix, K and N as β-$Mg_{17}Al_{12}$ phase, and M, L and O as Al-Mn intermetallics almost identical to Al_8Mn_5 identified by Wang et al [90]. Oxygen peak which appeared on many spectra should be resulted from surface oxidation during and after sample preparation.

The SEM and EDS results for AMC502 are shown in Figures 4.35 - 4.38. Figures 4.36 - 4.38 give the EDS spectra for A, which is the α-Mg matrix, B, F, H and G as Al_2Ca phase which precipitates around grain boundaries, and C and D, the rounds, white particles, as an intermetallic phase containing aluminum and manganese. Again oxygen

92

peak which appeared on many spectra should be resulted from surface oxidation during and after sample preparation.

EDS mapping was performed on AMC502 and AM50A squeeze cast under 30 MPa to illustrate elemental distribution (Figures 4.39 – 4.45). It can be seen from Figure 4.40 and 4.41 that, in AMC502 the calcium and aluminum mostly precipitated on grain boundaries. However, manganese precipitates in the matrix (Figure 4.42). In AM50A the aluminum also precipitate mostly on grain boundaries and the manganese precipitate in the matrix (Figures 4.43 - 4.45).
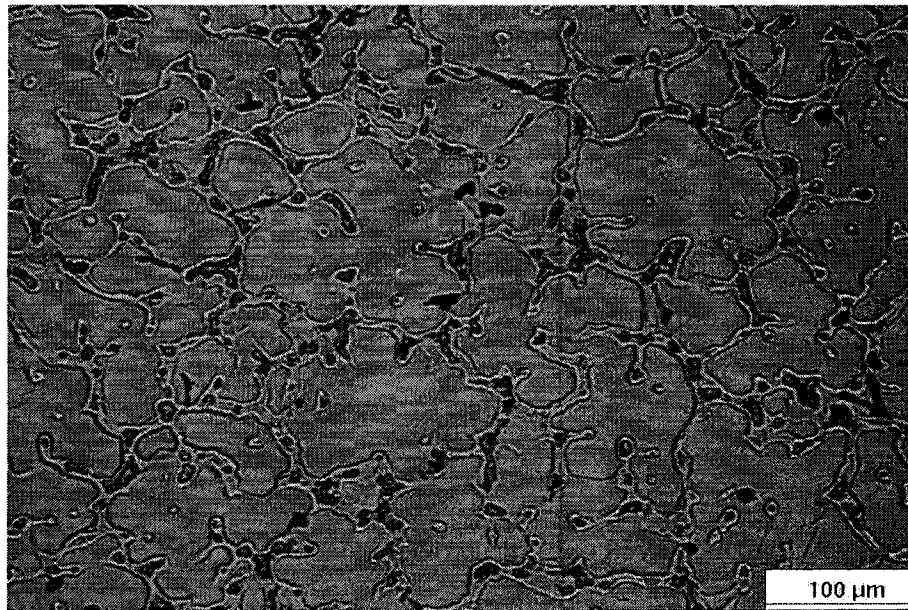
Figure 4.23: Optical micrograph showing microstructure of squeeze cast AM50A under 30 MPa.

93
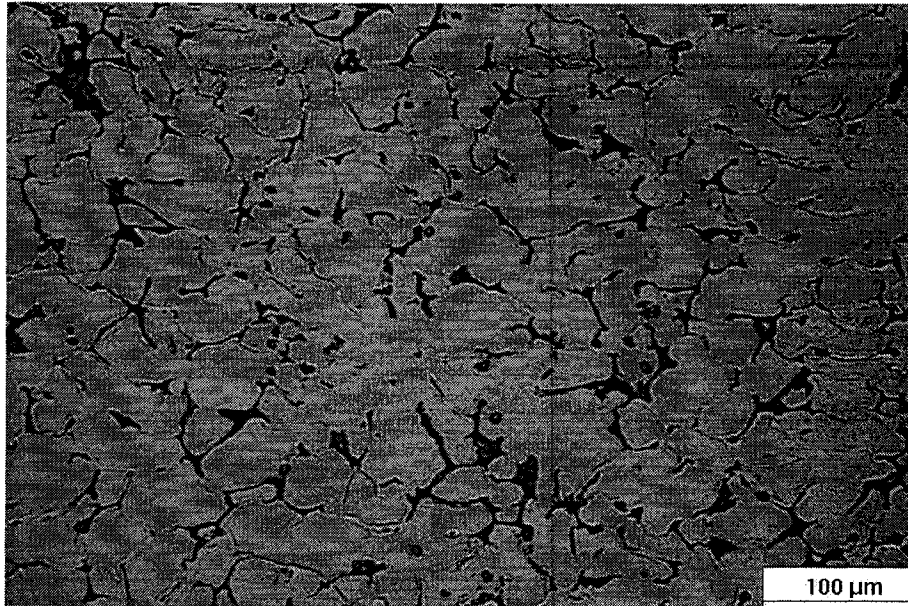
Figure 4.24: Optical micrograph showing microstructure of squeeze cast AMC501 under
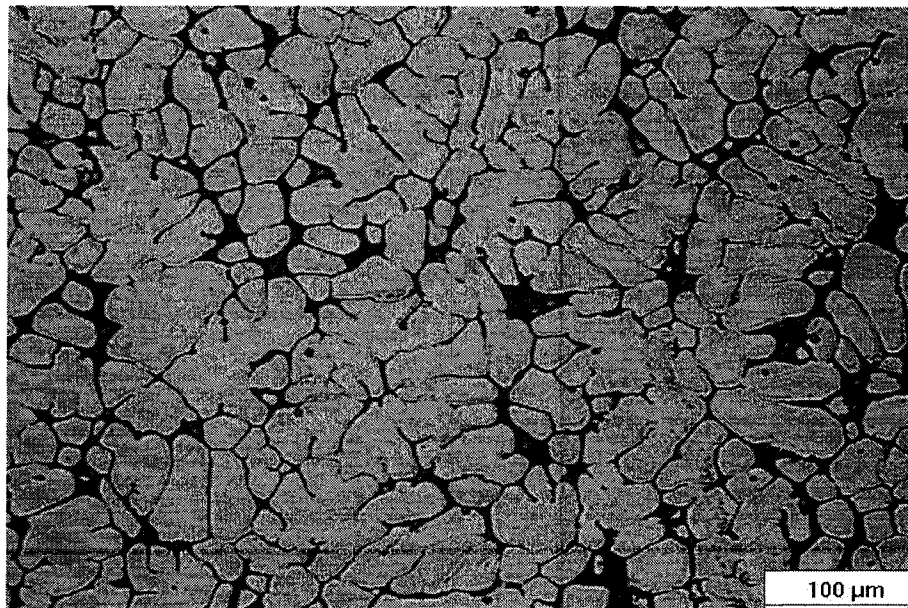
30 MPa.

Figure 4.25: Optical micrograph showing microstructure of squeeze cast AMC502 under

30 MPa.

94
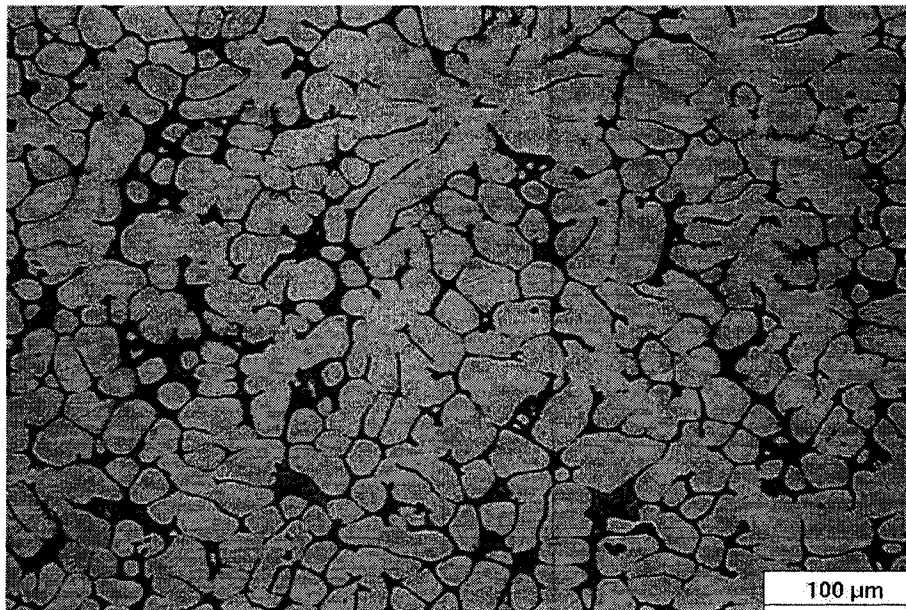
Figure 4.26: Optical micrograph showing microstructure of squeeze cast AMC503 under

30 MPa.
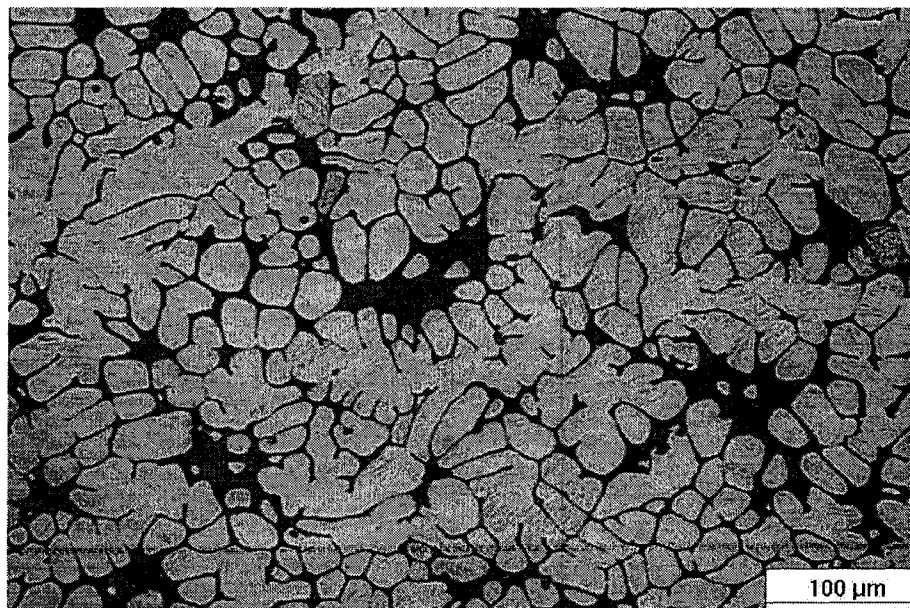
Figure 4.27: Optical micrograph showing microstructure of squeeze cast AMC504 under

30 MPa.

95
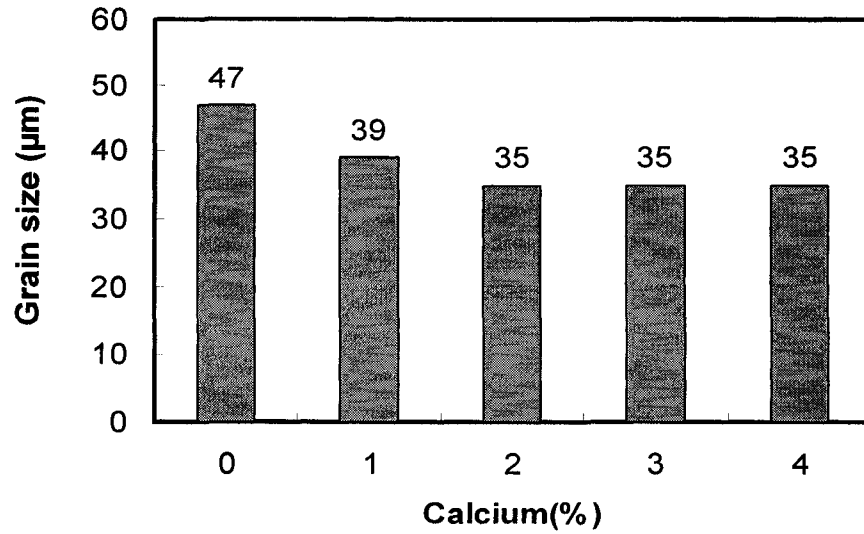
Figure 4.28: Effect of calcium content on grain size.
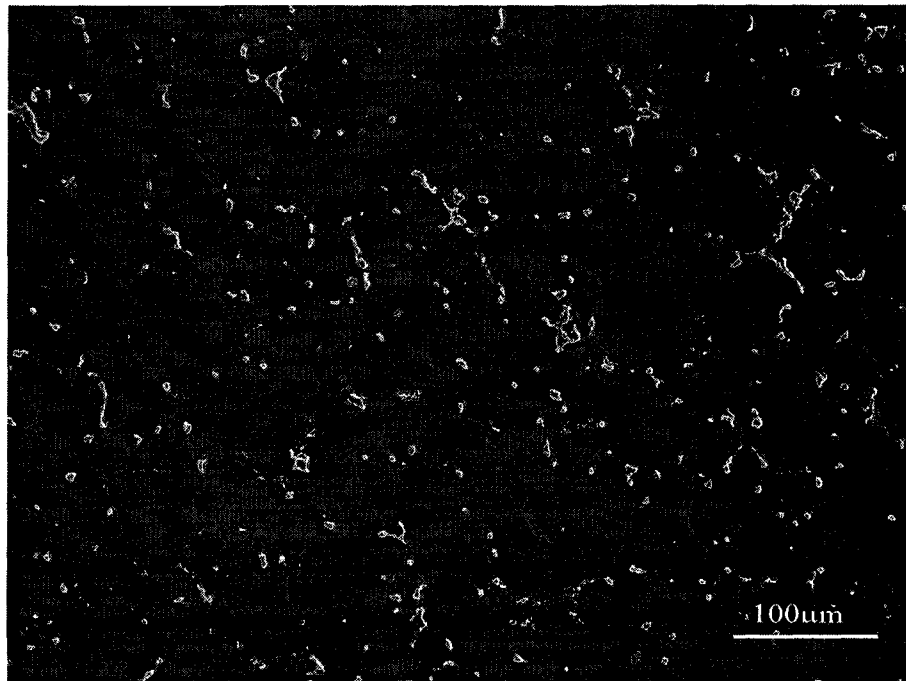
Figure 4.29: SEM micrograph showing discontinuous precipitation of secondary phases

in squeeze cast AM50A under 30 MPa.

96
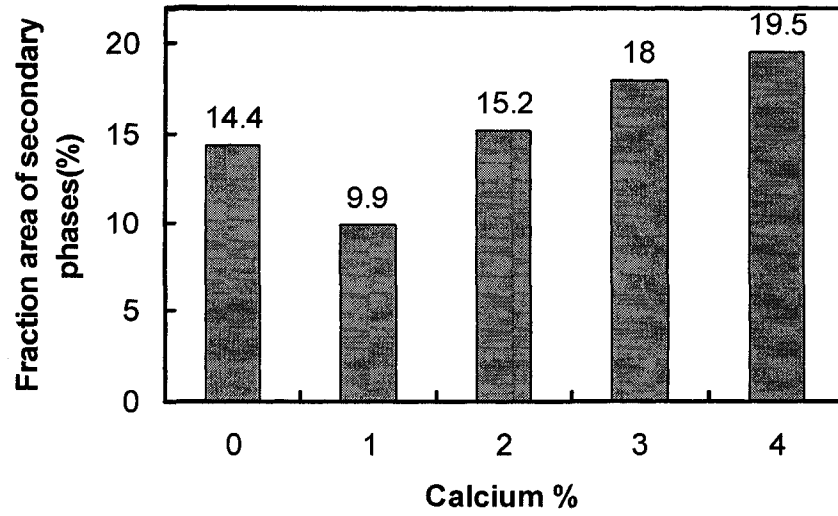
Figure 4.30: The effect of calcium content on fraction areas of secondary phases.
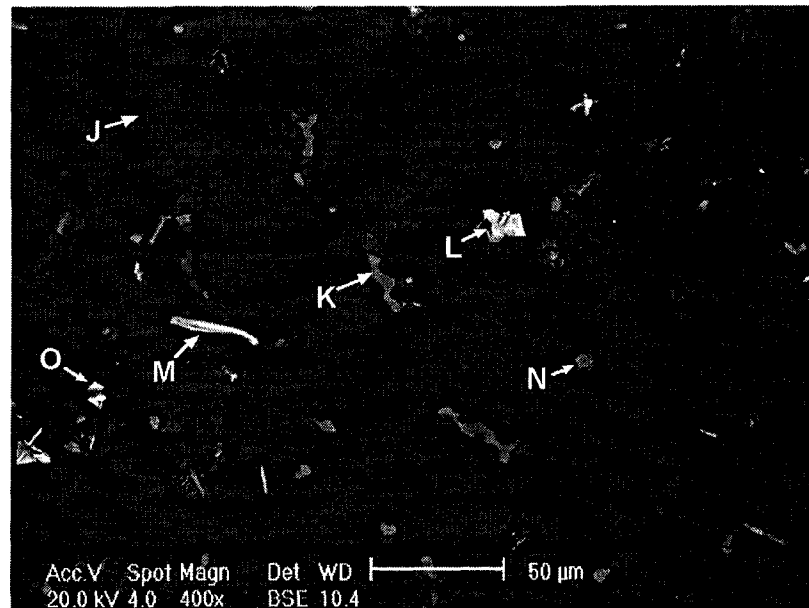
Figure 4.31: SEM micrographs showing microstructure of squeeze cast AM50A under

30MPa.

97
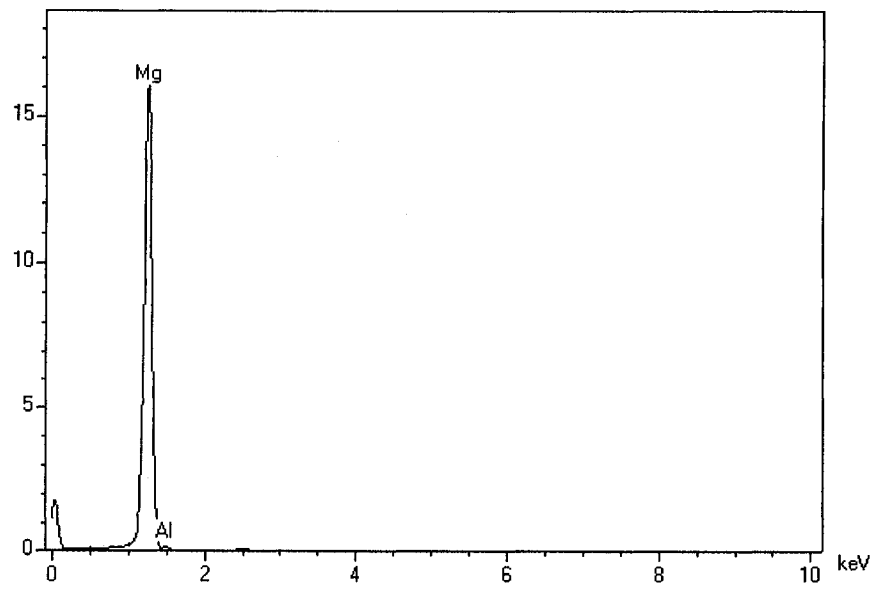
Figure 4.32: EDS spectrum from the region marked "**J**" in Figure 4.31.
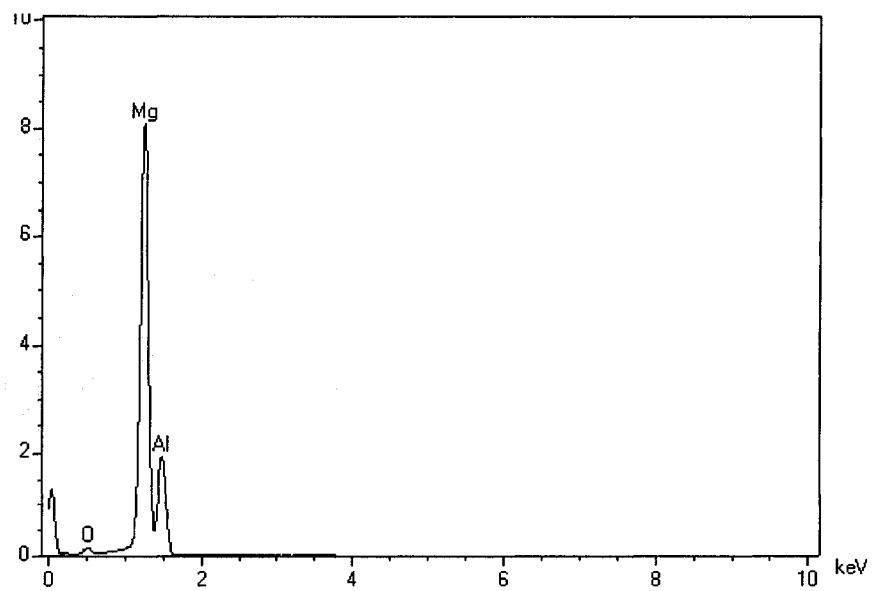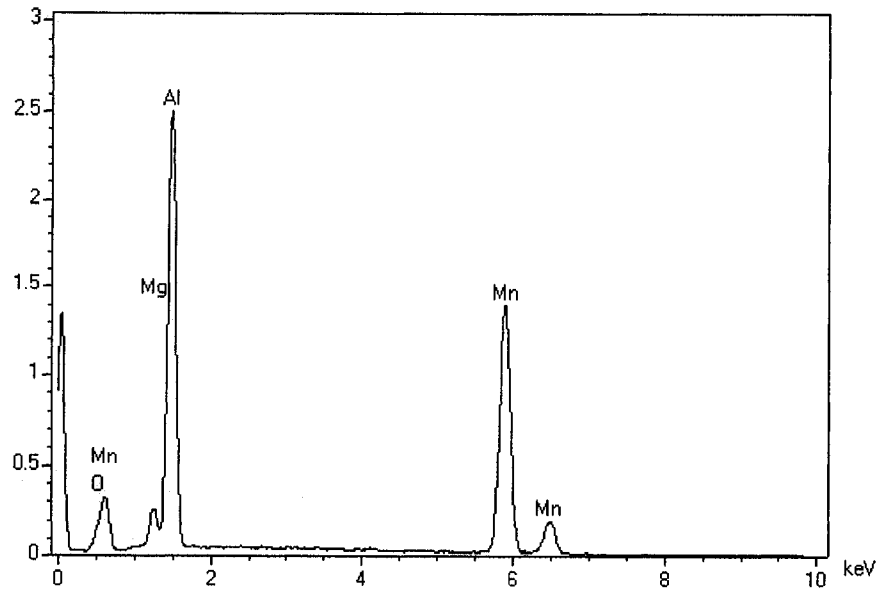

Figure 4.33: EDS spectrum from the region marked "K and N" in Figure 4.31.

98

Figure 4.34: EDS spectrum from the region marked "M, L and O" in Figure 4.31.
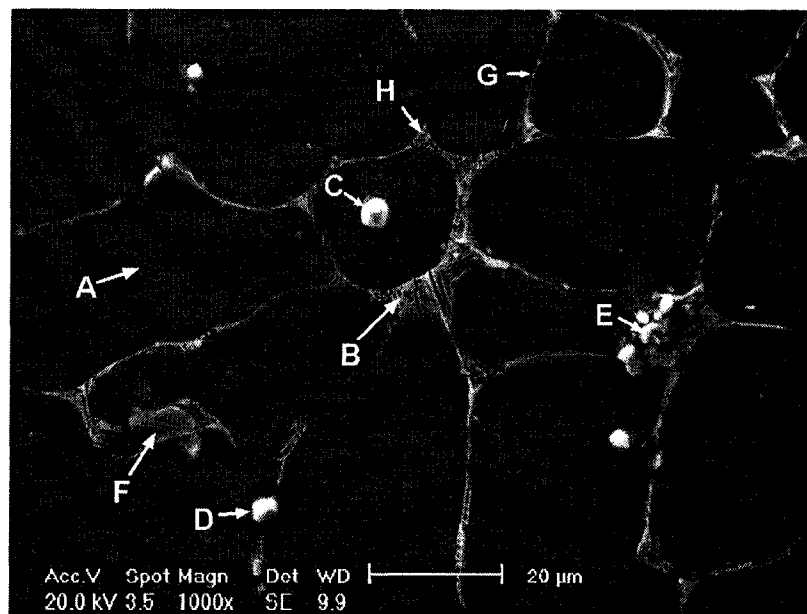

Figure 4.35: SEM micrographs showing microstructure of squeeze cast AMC502 under
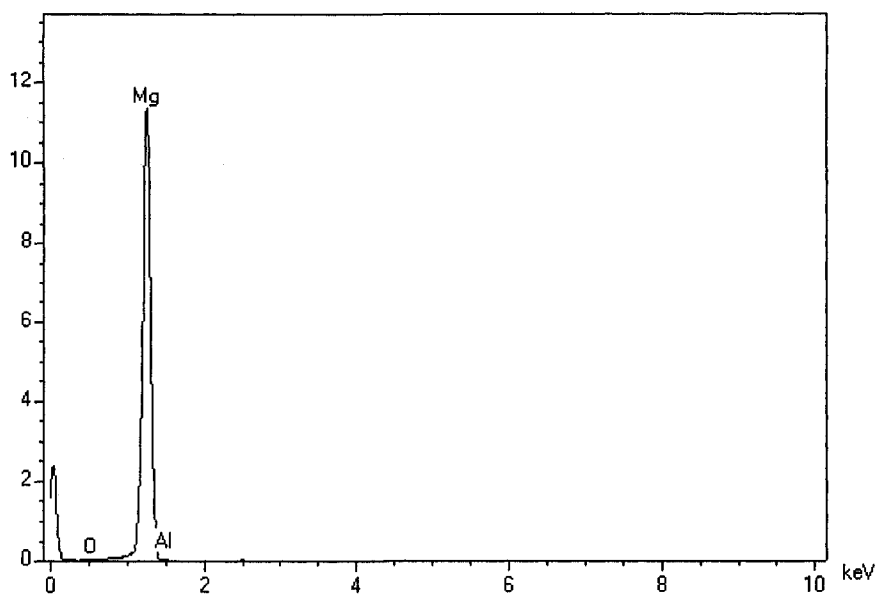
30 MPa.

99

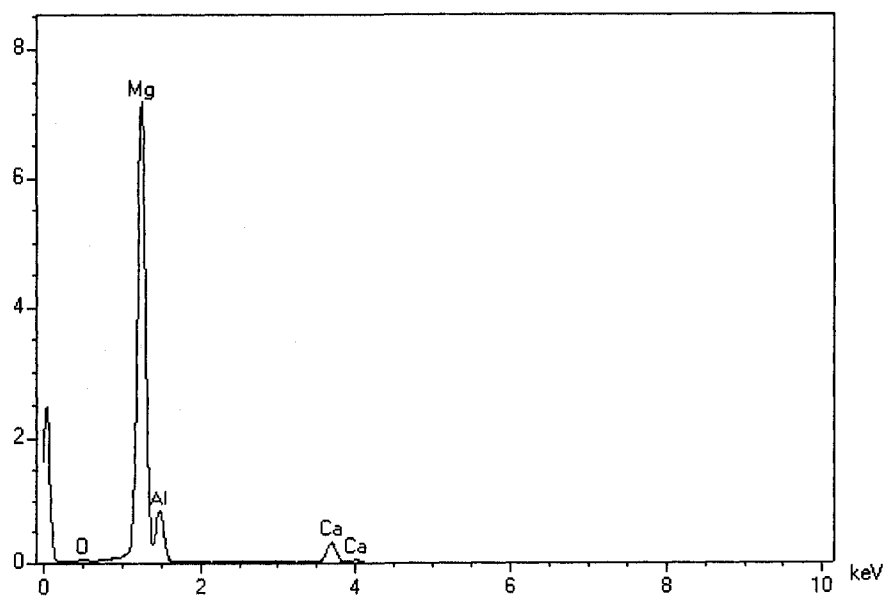Figure 4.36: EDS spectrum from the region marked "A" in Figure 4.35.

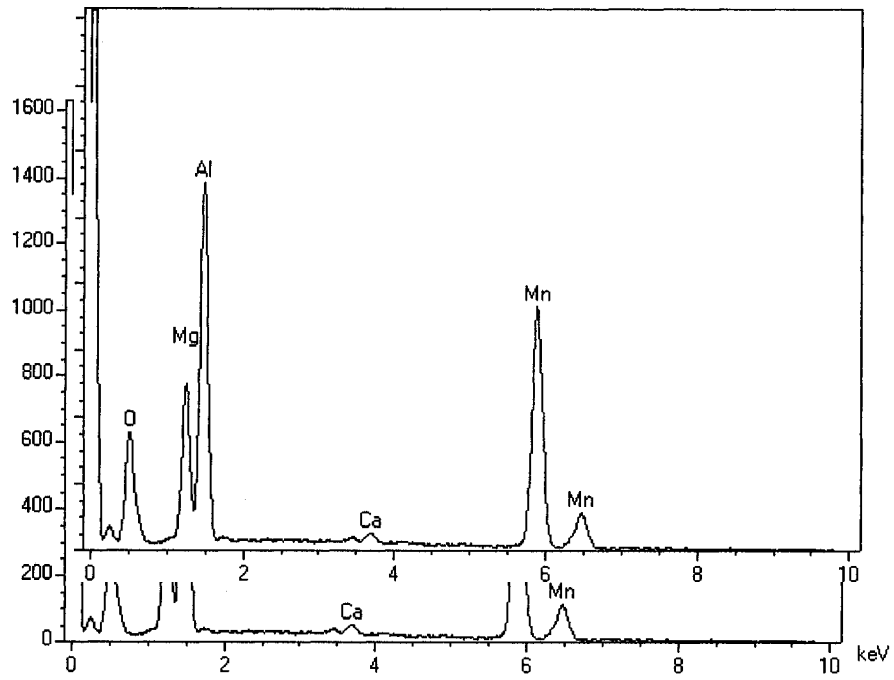Figure 4.37: EDS spectrum from the region marked "B, F, H and G" in Figure 4.35.

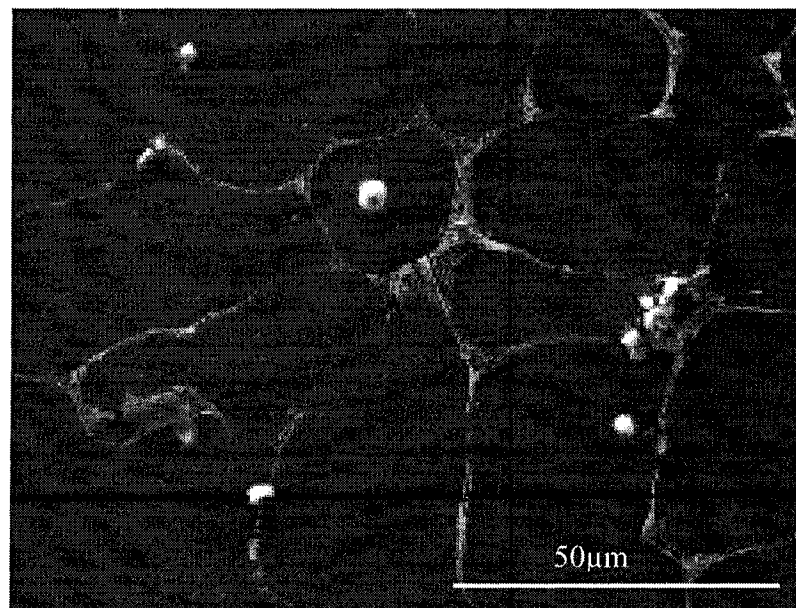Figure 4.38: EDS spectrum from the region marked "C, D and E" in Figure 4.35.

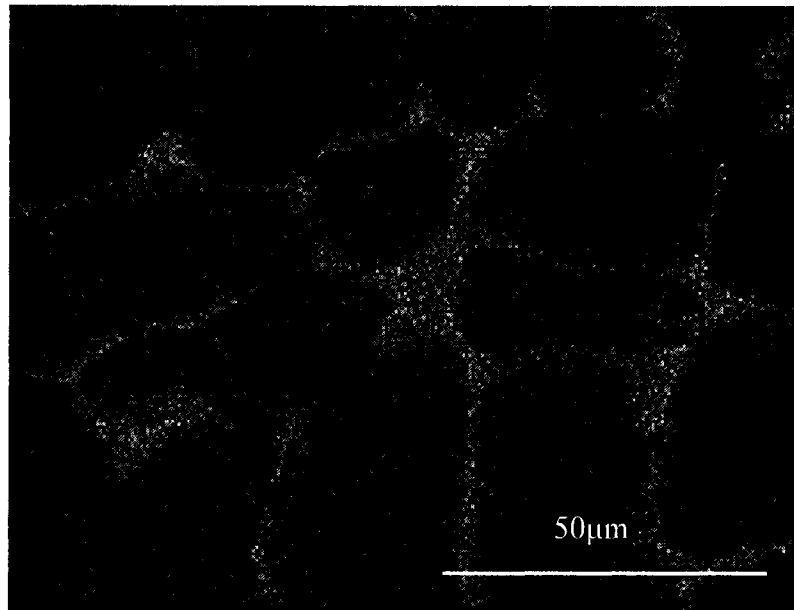Figure 4.39: Location which the EDS mapping performed on AMC502.

101

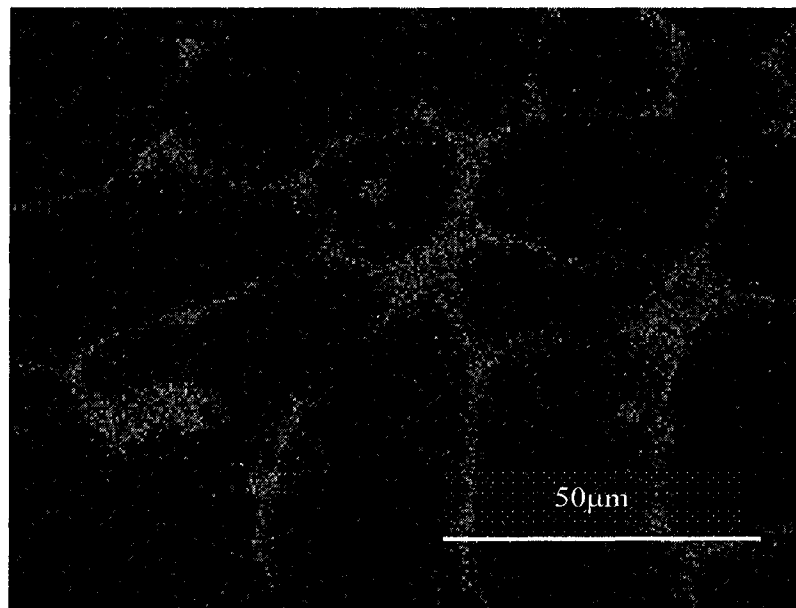Figure 4.40: Distribution of Calcium in AMC502.

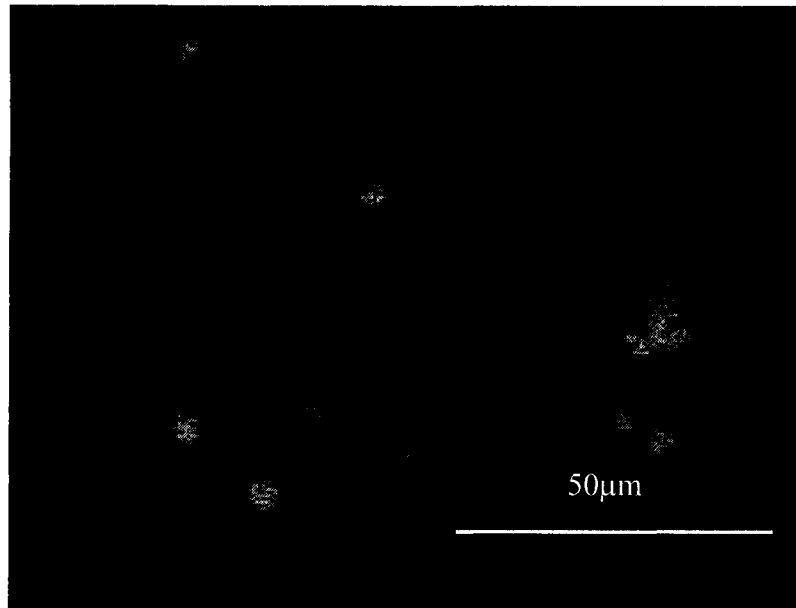Figure 4.41: Distribution of Aluminum in AMC502.

102

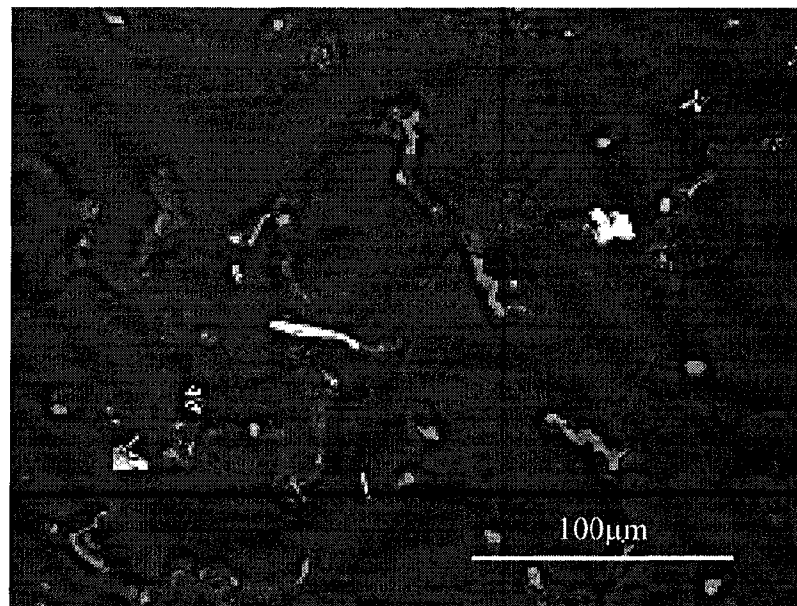Figure 4.42: Distribution of manganese in AMC502.

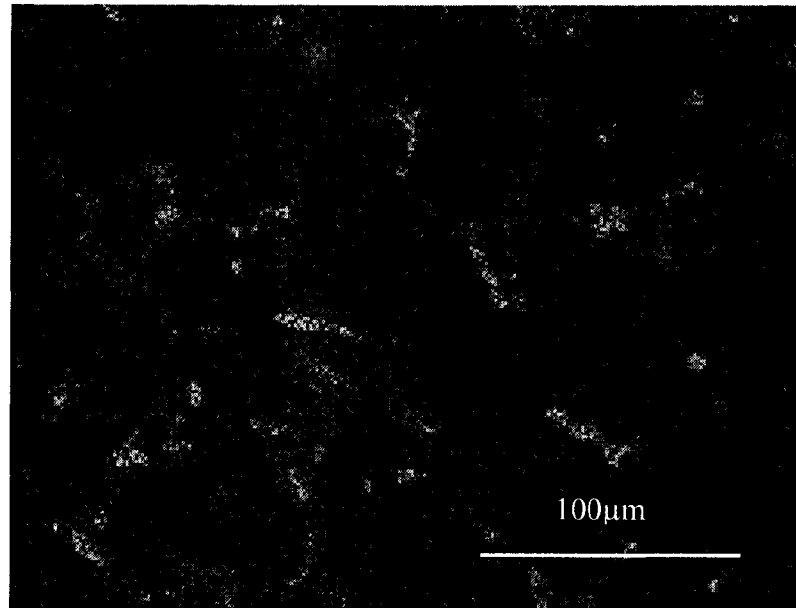Figure 4.43: Location which the EDS maps was taken from AM50A.

103

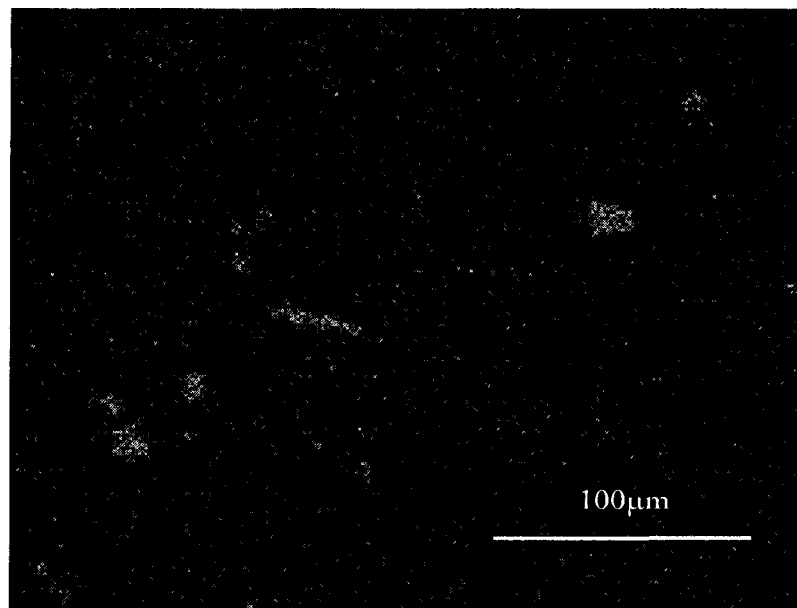Figure 4.44: Distribution of aluminum in AM50A.

Figure 4.45: Distribution of manganese in AM50A.

104

4.3.2 Tensile properties

4.3.2.1 Tensile properties at ambient temperature

Figure 4.46 shows the typical engineering stress-strain curves for AMC alloys. It is evident that the slopes of the liner portion of the curves are almost identical for all the alloys, which indicate the addition of calcium to magnesium alloy AM50 does not alter the elastic modulus of the alloy. Table 4.2 summarizes the UTS, YS and elongation of AMC alloys squeeze cast under 30 MPa.
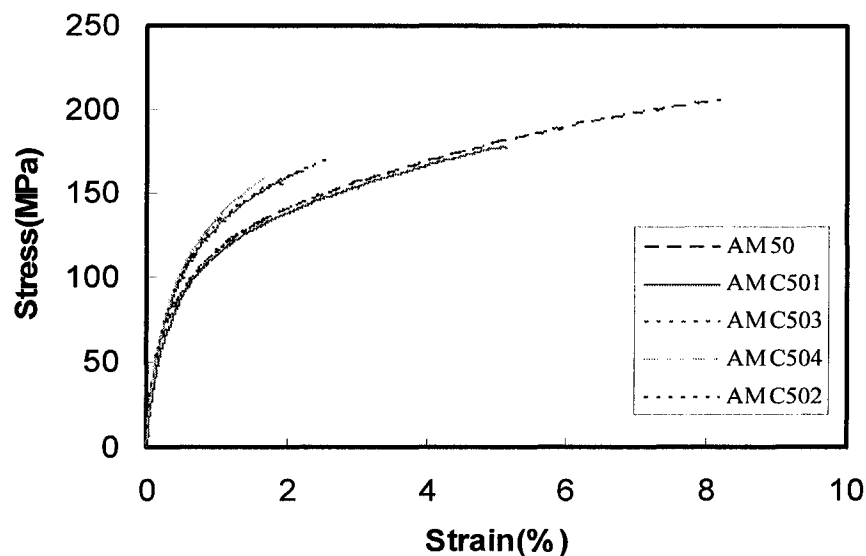
Figure 4.46: Engineering stress-strain curve for Mg-Al-Ca alloys at room temperature.

The effect of calcium contents on tensile properties of squeeze cast AMC alloy at room temperature is shown in Figure 5.47 of which data are given in Table 4.2. As the calcium content increases from 0% to 4%, the elongation and UTS at ambient temperature decrease significantly. The elongation and UTS of the alloy with 4 wt.%Ca are only 2% and 162 MPa which decrease by 325% and 27% respectively, over that of

105

alloy with 0 wt.% Ca. However the yield strength shows a slight increase. The slight increase in yield strength may be attributed to reduction in grain size and increase in k parameter due to increase in ratio of secondary phases as calcium increases, according to Hall-Petch equation relation:

$$\delta_0 = \delta_i + k\, D^{-1/2}$$

where δ_0 is the yield stress, δ_i is friction stress opposing motion of dislocation, k is " unpinning constant" measuring the extent to which dislocations are piled up at barriers, and D is the grain diameter.

Despite AMC502, AMC503 and AMC504 have the same grain size but the yield strength of AMC alloys increases as the calcium content increases. The higher yield strength as the calcium increases could be attributed to higher the fraction of secondary phases.

Table 4.2 Effect of calcium content on tensile properties at room temperature.

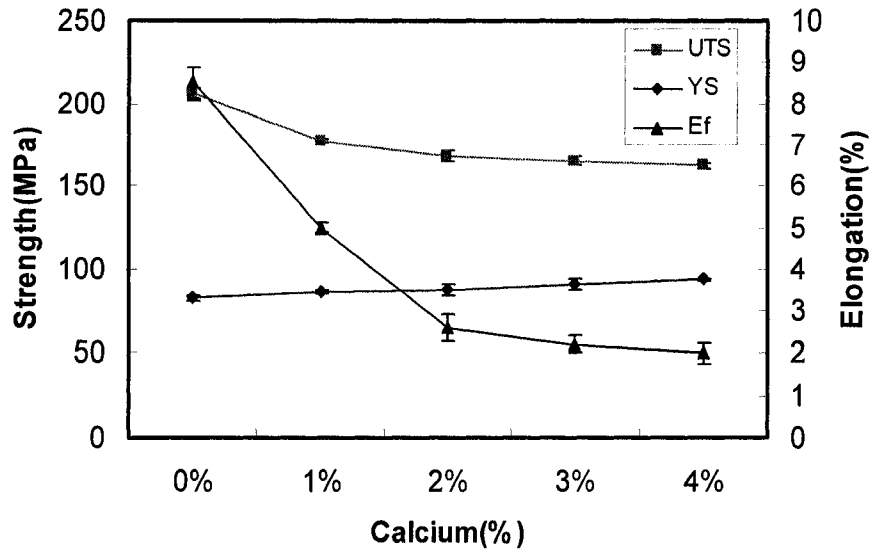| Calcium content	UTS(MPa)	Yield strength(MPa)	Elongation (%)
0%	206±4.2	82.6±1.5	8.5±0.35
1%	176.9±0.8	86.0±1	5.0±0.1
2%	168.1±3.7	87.6±3.2	2.6±0.3
3%	165±2.9	91.0±3.6	2.2±0.2
4%	162±1.7	93.6±0.6	2.0±0.2

106

Figure 4.47: Effect of calcium content on tensile properties of squeeze cast AM50 alloy at room temperature.

The decrease in UTS and elongation may be due to constituents, area fraction and distribution of secondary phases in the alloys. As discussed in section 4.3.1 in AM50A alloy, the divorced secondary phase of $Mg_{17}Al_{12}$ uniformly distributes but discontinuously around grain boundaries. However, in the Ca-containing alloys, the calcium addition encourages the precipitation of a different type of secondary phase Al_2Ca instead of $Mg_{17}Al_{12}$. The addition of 2 wt.% and more calcium leads to the formation of a continuous network of the secondary phase of Al_2Ca. From Al-Ca and Mg-Al phase diagrams [91] as shown in Figures 4.48 and 4.49, Al_2Ca identified as an intermetallic compound but $Mg_{17}Al_{12}$ as an electron compound. Intermetallic compounds are an intermediate phase which has a narrow range of composition, and is represented on the diagram as a vertical line and labelled with the chemical formula of the compound [92]. They are generally formed between chemically dissimilar metals and are combined

107

by following the rules of chemical valance. Since they generally have strong bonding (ionic or covalent), their properties are essentially nonmetallic. They usually show poor ductility and poor electrical conductivity. If the intermediate phase exists over a range of composition, it is usually an electron compound and is labelled with a Greek letter. Many electron compounds have properties resembling those of solid solutions, including a wide range of composition, relatively high ductility, and low hardness [92].

The mechanical properties of an alloy consisting of a ductile phase and a hard brittle phase often depend on how the brittle phase is distributed in the microstructure. If the brittle phase is present as a grain boundary envelope, the alloy is brittle. If the brittle phase is in the form of discontinuous particles at grain boundaries, the brittleness of the alloy is reduced somewhat. When the brittle phase is present as a fine dispersion uniformly distributed throughout the softer matrix, a condition of optimum strength and ductility is obtained [93].

Therefore the presence of continuous network of brittle secondary phase in nature in Mg-Al-Ca alloy is concluded to be responsible for their low UTS and elongation. The decreasing UTS and elongation with increasing calcium content are due to the increase in fraction area of secondary phase and the change in the distribution of Al_2Ca from a semi-continuous to continuous network around grain boundaries. The higher tensile properties (UTS and elongation) of AM50A at room temperature can be attributed to fine dispersion of β-$Mg_{17}Al_{12}$ in the soft α-Mg matrix.
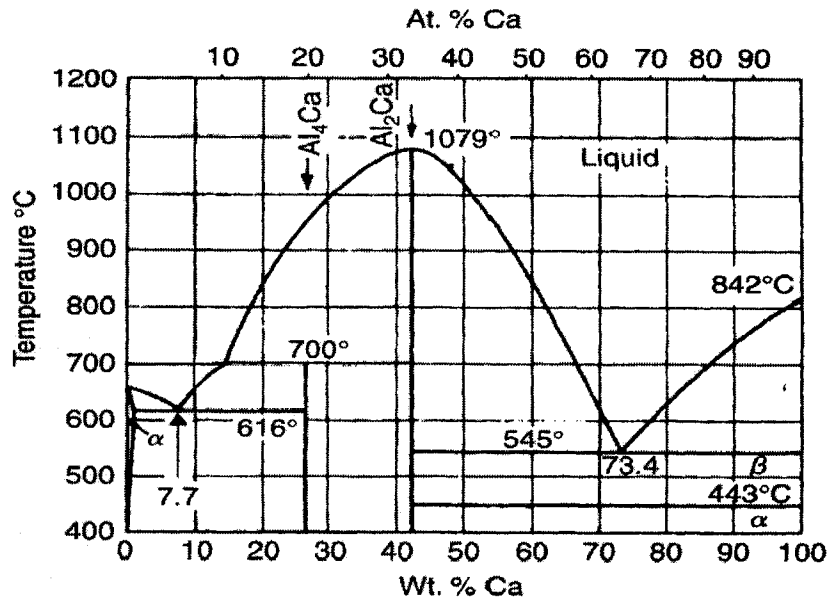
108

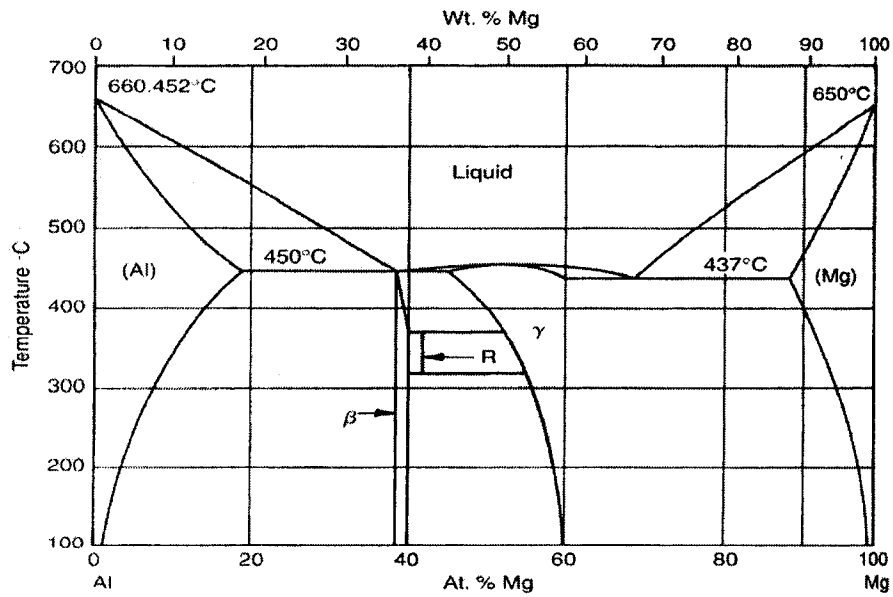Figure 4.48: Al-Ca binary phase diagram [91].

Figure 4.49: Al-Mg binary phase diagram [91].

109

Figure 4.50 gives the true stress-strain curves of AMC alloys. To elucidate the strain-hardening behaviour of the alloys, a plot of strain-hardening rate ($d\delta/d\varepsilon$) versus true plastic strain (ε), is given in Figure 4.51. It can be seen from Figure 4.51 that as the calcium content rises, the strain hardening rate of the alloys increases. It suggests that AMC alloys with high calcium content are able to strengthen themselves increasingly in response to increasing levels of plastic deformation prior to fracture. The high strain hardening rates for the alloys with high calcium contents may be attributed to smaller grain size and to a larger fraction area of secondary phases present in the alloy, which increases the resistance to slip in the magnesium matrix. The large volume fraction of secondary phases phase provides excessive barriers against dislocation slip during deformation and consequently increases strain hardening rate.

Despite the high fraction of secondary phases in AM50A the strain rate hardening of AMC50A and AMC501 are almost the same. This may be explained by the nature of secondary phases in AMC50A and AMC501. Secondary phase particles act in two distinct ways to retard the motion of dislocations. The particles could be cut either by the dislocations or the particles resist cutting and the dislocations are forced to bypass them. When particles are small and/or soft, dislocations cut and deform the particles. When the dislocation can not cut the second phase and they are forced to bypass the particles [93]. As discussed early, the secondary phase in AMC501, Al_2Ca, is identified as an intermetallic compound which should has a high hardness. But in AM50A, $Mg_{17}Al_{12}$, is identified as an electron compound which should has a low hardness. The low rate of strain hardening in AM50A suggests that dislocations may cut the secondary phases once the stress reaches a high enough value.
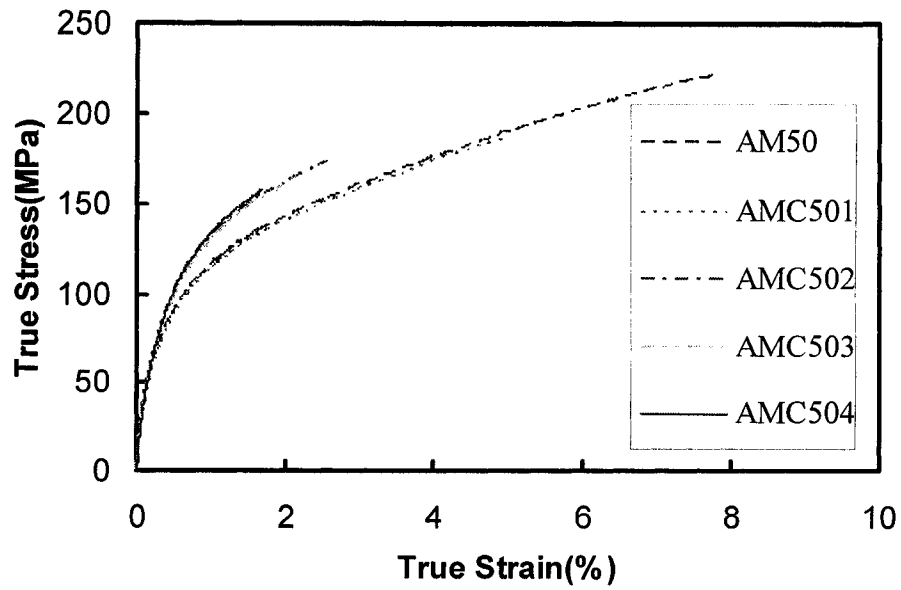
110

Figure 4.50: True stress-strain curve for Mg-Al-Ca alloys at room temperature.
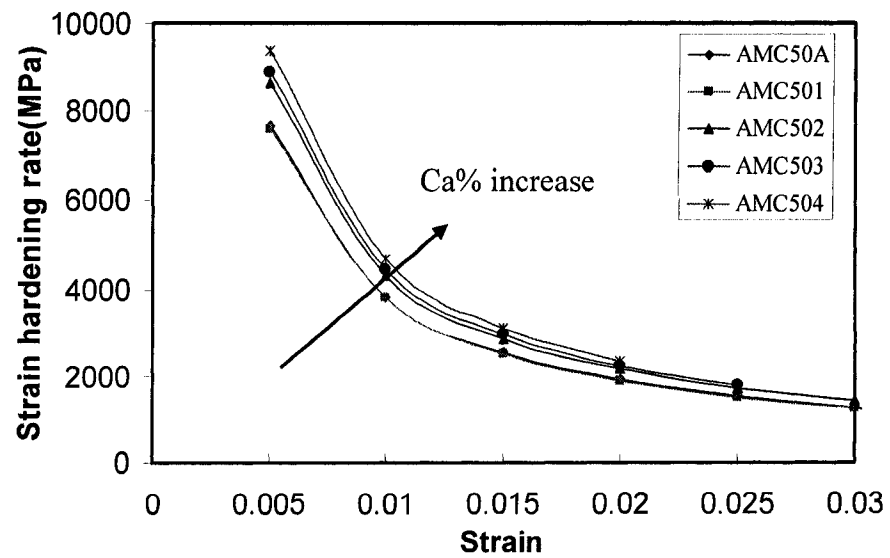

Figure 4.51: Strain hardening rate versus strain curves for Mg-Al-Ca alloys.

111

4.3.2.2 Tensile properties at elevated temperature

Figure 4.52 shows the typical engineering stress-strain curves for AMC alloys at 150 °C. Table 4.3 summarizes the UTS, YS and elongation of AMC alloys squeeze cast under 30 MPa. The effect of calcium contents on tensile properties of squeeze cast AMC alloy at 150 °C is shown in Figure 5.53.

The yield strength of the Mg-Al-Ca alloys at 150 °C was lower than that at room temperature. The yield strength of AMC501 is, only 80.3 MPa in comparison with 86.0 MPa at room temperature. Also the UTS of the Mg-Al-Ca alloys decreases with increasing testing temperature. The UTS value of AMC501, 131.3 MPa, is lower than that (176.9 MPa) at room temperature. The strain data shows that the ductility of Mg-Al-Ca alloys improve significantly at high temperature. The elongation value of AMC501 is 18.5%, while at room temperature this value is only 5.0%. Changes in strength and ductility with temperature generally can be related to the effect of temperature on slip [94]. At high temperatures (between 0.3 and 0.5 homologous temperature), thermally activated processes such as multiple slip and cross slip allow the high local stresses to be relax, and strength is decreased. For sufficiently high temperatures in excess of half of the homologous temperature, diffusion processes become important, and mechanisms such as recovery, dislocation climb, recrystalisation, and grain growth can reduce the dislocation density, prevent pileups, and further reduce strength [94]. Also certain metals show additional slip systems with increased temperature. Aluminum deforms on the {110} plane at elevated temperature, while in magnesium the {1011} pyramidal plan plays an important role in deformation by slip above 225 °C [93].

112

As the calcium content increases from 0% to 4%, the elongation at 150 °C decreases significantly. The elongation of the alloy with 4 wt.% Ca is 10.7% which decreases by 122%, over that of alloy with 0%Ca. However the yield strength and UTS show a slight increase with increasing Ca content. The slight increase in yield strength, may be attributed to reduction in grain size (according to Hall-Petch equation) and higher the fraction of secondary phases as calcium contents increase.

The decrease in elongation and increase in UTS, as the calcium contents increase, may be due to constituents, area fraction and distribution of secondary phases in the alloys.

As it was discussed in previous section the presence of continuous network of a secondary phase with a brittle nature in Mg-Al-Ca alloy should be responsible for their low elongations. The decreasing elongation with increasing calcium content should be due to the change in the distribution behaviour of Al_2Ca from a semi-continuous to continuous network around grain boundaries and increase in their fraction area. The high UTS value of Mg-Al-Ca alloys compare with AM50A at 150 °C should be attributed to the presence of thermally-stable phase, Al_2Ca, with a high melting temperature of 1073 °C, which can keep its strength to a high extent at this temperature. However, in AM50A, $Mg_{17}Al_{12}$ (β-phase) with relatively low melting temperature of 455 °C is metallurgically unstable and may soften considerably and lose its strength at 150 °C.

Figure 4.54 gives the representative true stress-strain curves of AMC alloys at 150 °C. To elucidate the strain-hardening behaviour of the alloys, a plot of strain-hardening rate ($d\delta/d\varepsilon$) versus true plastic strain (ε), is given in Figure 4.55, which is derived from true strain-stresses curves. It can be seen from Figure 4.55 that, as the

113

calcium contents rises, the strain hardening rate of the alloys increases. It means that AMC alloys with higher calcium contents are able spontaneously to strengthen themselves increasingly to large extent, in response to extensive plastic deformation prior to fracture. The higher strain hardening rate for the alloys with higher calcium contents may be attributed to larger percentage of secondary phases present in the alloy, which increases the resistance to slip in the magnesium matrix. The larger volume fraction of secondary phases provides more barriers against dislocation slip during deformation and consequently increases strain hardening rate.

It can be observed that the strain hardening of Mg-Al-Ca alloys is much lower in 150 °C than those at room temperature. It may be due to the effect of temperature on slip during plastic deformation. At elevated temperature, thermally activated processes such as multiple slip and cross slip allow the high local stresses to be relax, which decreases strengths.. Meanwhile, diffusion processes become important, and mechanisms such as recovery, dislocation climb, recrystalisation can reduce dislocation density and therefore decrease the strain hardening rate [94].
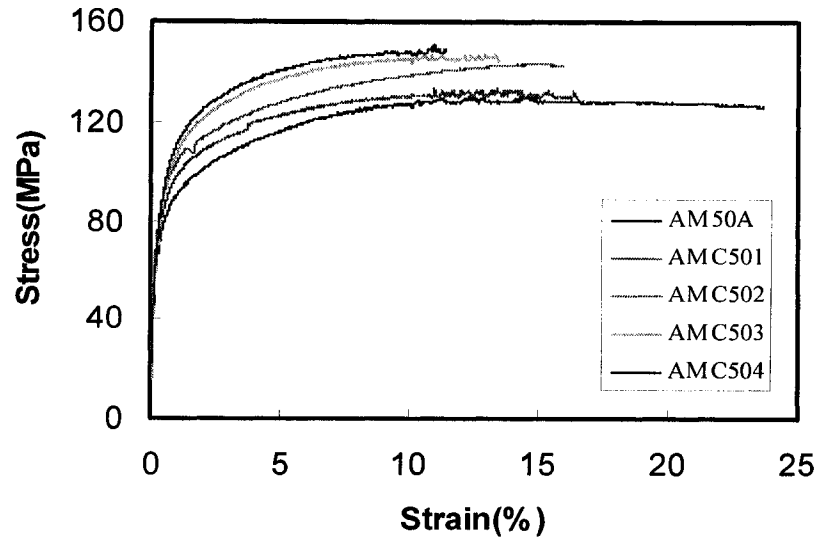
114

Figure 4.52: Engineering stress-strain curves for Mg-Al-Ca alloys at 150 °C.

Table 4.3 Effect of calcium content on tensile properties at elevated temperature.

Calcium content	UTS(MPa)	Yield strength(MPa)	Elongation (%)
0%	124± 1	73±2	23.8±0.35
1%	131.3±2.1	80.3±1.1	18.5±2.2
2%	136.6±2.9	85±1	14.6±1.8
3%	142±2.6	87±1.5	12.7±1
4%	145±2.5	91±1.5	10.7±2.7

115
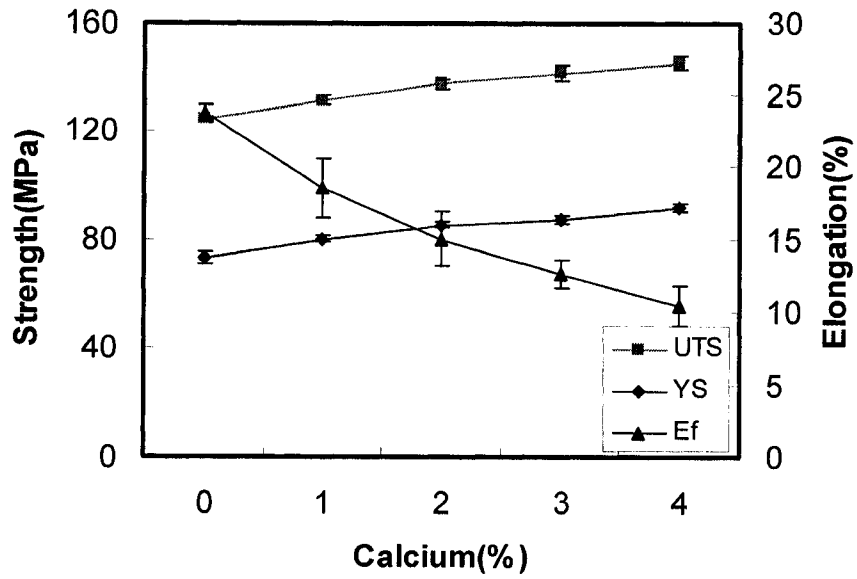
Figure 4.53: Effect of calcium content on tensile properties of squeeze cast AM50 alloy at elevated temperature.
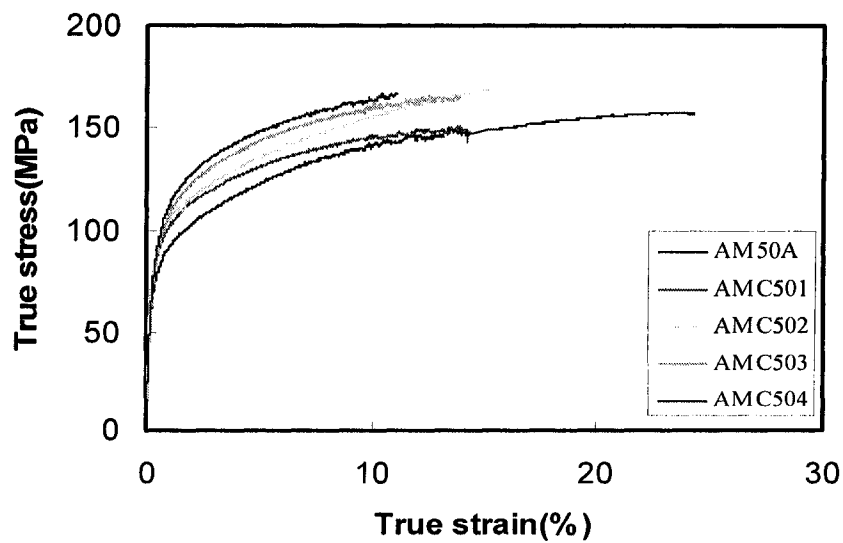
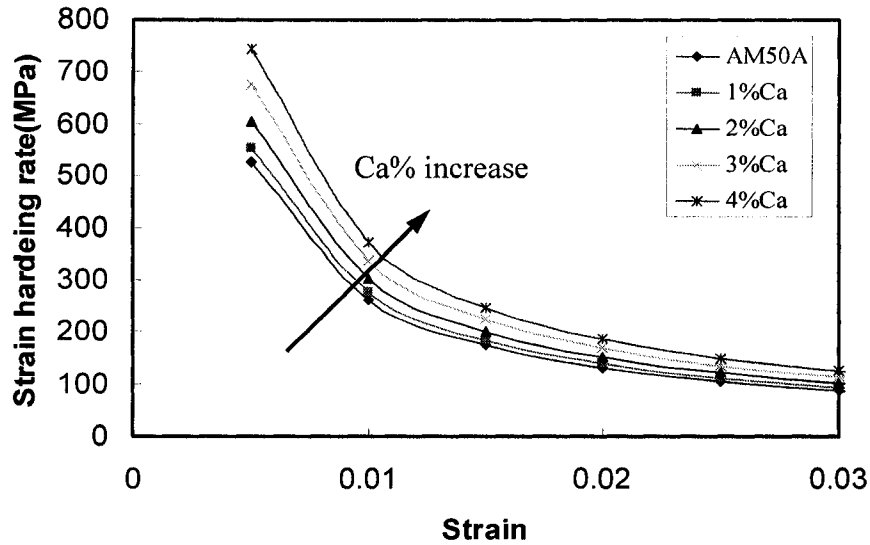Figure 4.54: True stress-strain curves for Mg-Al-Ca alloys at 150 °C.

116

Figure 4.55: Strain hardening rate versus strain curves for Mg-Al-Ca alloys.

4.3.3 Fracture behaviour

4.3.3.1 Fracture behaviour at room temperature

The tensile fractured surfaces of squeeze cast AM50A are shown in Figure 4.56. The observed fracture mode of the AM50A alloy is dimple rupture. Dimpled rupture is characterized by cup-like depressions that may be equiaxial, parabolic, or elliptical, depending on the stress state. Microvoids are initiated at secondary-phase particles, the growth of results in the fracture of ligaments between the microvoids. A considerable amount of energy is consumed in the process of the formation of microvoids, eventually leading to the creation of cracks.

The SEM fractography reveals the fractured surfaces of squeeze cast AMC alloys with 1 wt.% and 4 wt.% Ca contents as shown in Figure 4.57 and 4.58, respectively. The results indicate that the fracture behaviour of AMC alloys is influenced by the levels of Ca addition. The fracture surface of calcium AMC501 alloy shows somewhat ductile in

117

nature, which is characterized by the presence of dimple features compared with samples containing 4 wt.% Ca. As the calcium contents increases, the fracture of the alloys tends to transit from ductile to brittle.

In an effort to locate the crack origins of squeeze cast AM50A and AMC504, the region of the fractured specimens underneath the fracture surface were examined with optical microscopy in a direction normal to tensile loading, which is shown in Figures 4.59 and 4.60 . The failure in both the alloys should be mainly attributed to the intergraular fracture. The fracture starts with the initiation of voids, most commonly at second phase particles. It has been pointed out [93] that the high stresses produced at the head of a dislocation pile up behind of second phases or grain boundaries could produce fracture. The shear stress acting on the slip plane squeezes the dislocation together. At some critical value of stress the dislocations at the head of the pile-up are pushed so closed together that they coalesce into an embryonic crack or cavity dislocation. From the appearance of the fracture surface it is clear that the fracture mode of AMC504 is intergranular brittle. The intergranular brittle fracture behaviour of AMC504 should be attributed to precipitation of brittle phase, Al_2Ca, with a high volume fraction, on grain boundaries.

Overall, the SEM observations on the fractured surfaces are in good agreement with the results of tensile testing presented in the previous section.
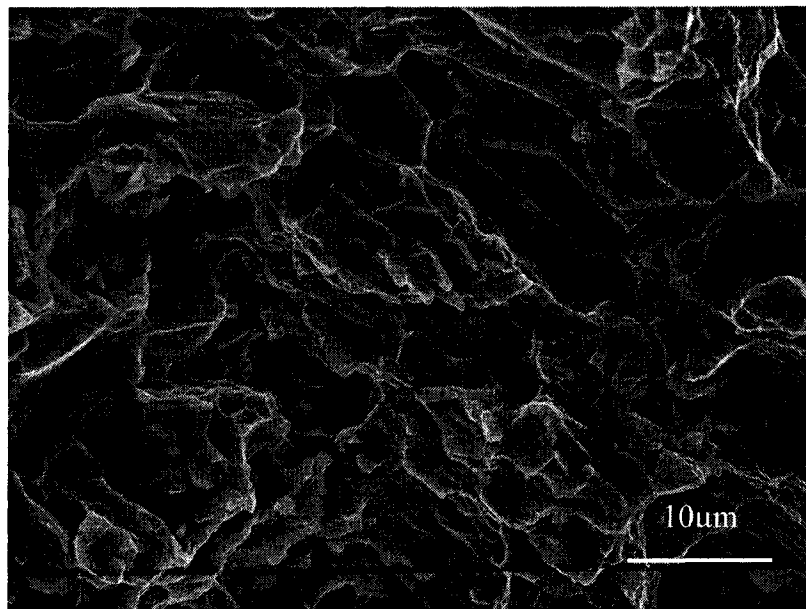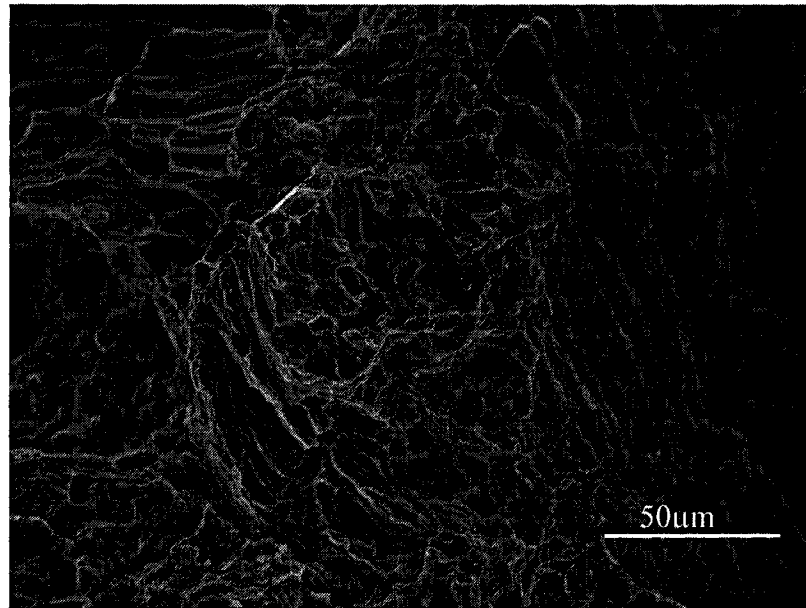
118

Figure 4.56: SEM fractographs of squeeze cast AM50A fractured at room temperature, a) low magnification and b) high magnification.
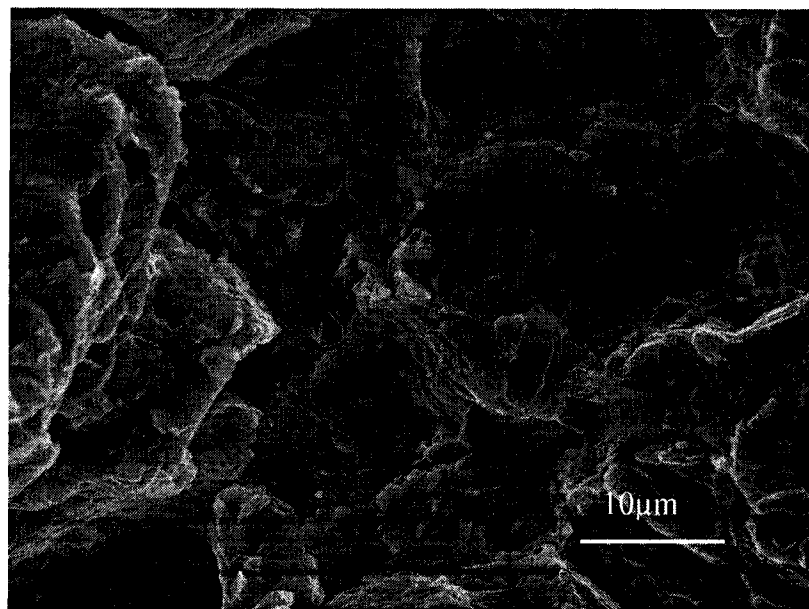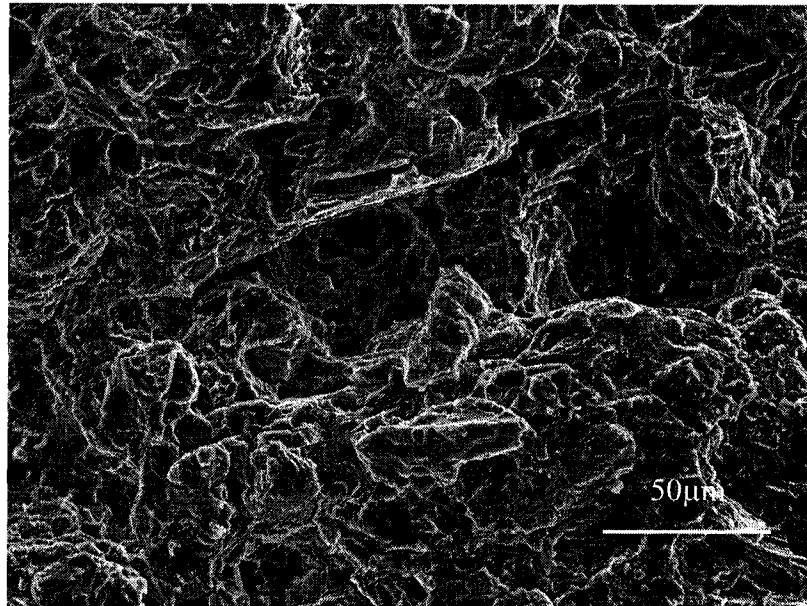
119

Figure 4.57: SEM fractographs of squeeze cast AMC501 fractured at room temperature,

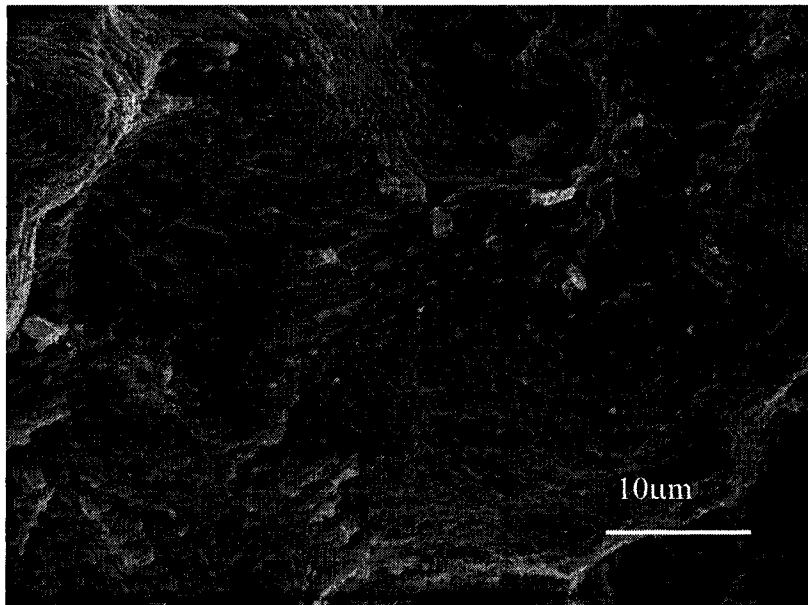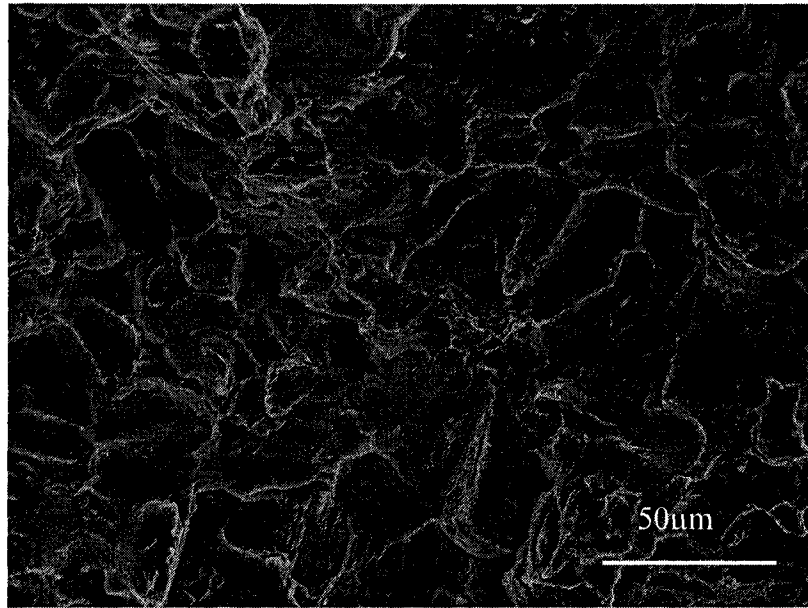a) low magnification and b) high magnification.

120

Figure 4.58: SEM fractographs of squeeze cast AMC504 fractured at room temperature, a) low magnification and b) high magnification.
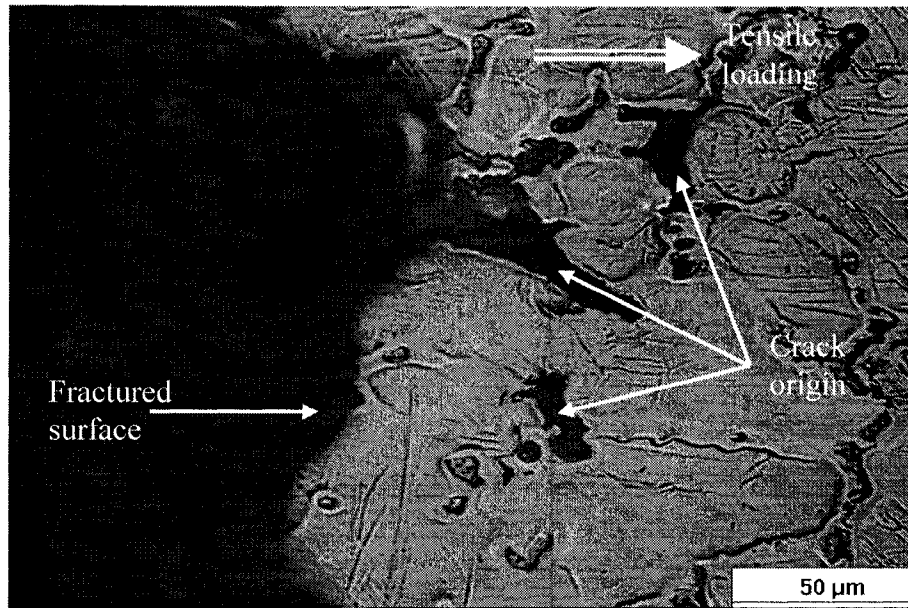
121

Figure 4.59: Optical micrograph showing crack origin in AM50A fractured at room temperature.
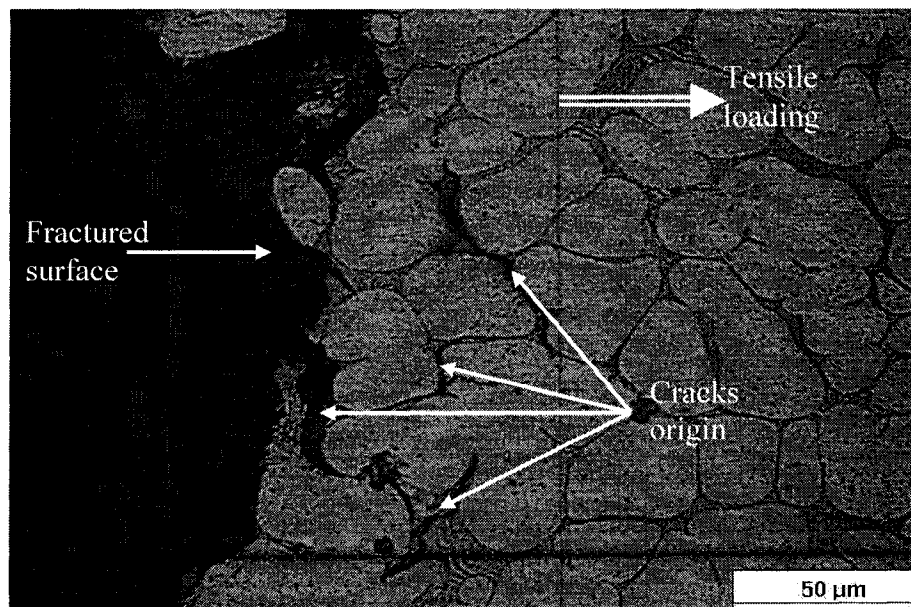

Figure 4.60: Optical micrograph showing crack origin in AMC504 fractured at room temperature.

122

4.3.4.1 Fracture behaviour at 150 °C temperature

The fractography results for high temperature tensile tests for AM50A and AMC504 are presented in Figures 4.61 and 4.62. The observed fracture mode of the AM50A and AMC504 samples at 150 °C is dimple rupture.

The analysis of SEM fractography shows the fracture behavior of squeeze cast AMC alloys is influenced by calcium contents. As the calcium content increases, the fracture of alloy tends to be less ductile. The fractured surface of AM50A shows evidently ductile in nature, which is characterized by the presence of massive deep dimples compare with AMC504 samples. The presence of brittle phase, Al_2Ca, in the grain boundaries, should be responsible for the relatively less ductile behaviour of AMC504 even at 150 °C.

In an effort to locate the crack origins of squeeze cast AM50A and AMC504, the region of the fractured specimens underneath the fracture surface were examined with optical microscopy in a direction normal to tensile loading, which is shown in Figures 4.63 and 4.64. The failure in the both alloys should be considered intergraular fracture. The fracture starts with the initiation of voids, most commonly at second phase particles.

Overall, the SEM observations of the fracture surfaces show a good agreement with the tensile behaviour of the alloy at elevated temperature as discussed in sections 4.2.4.
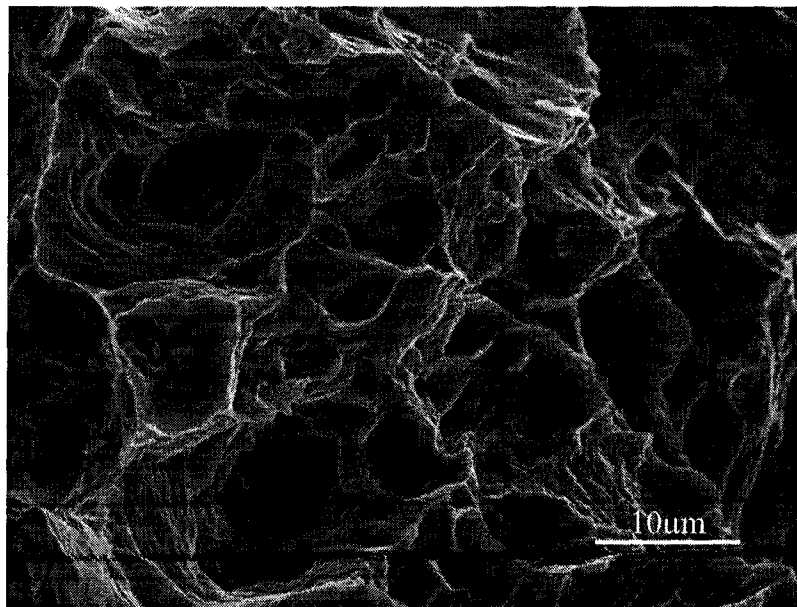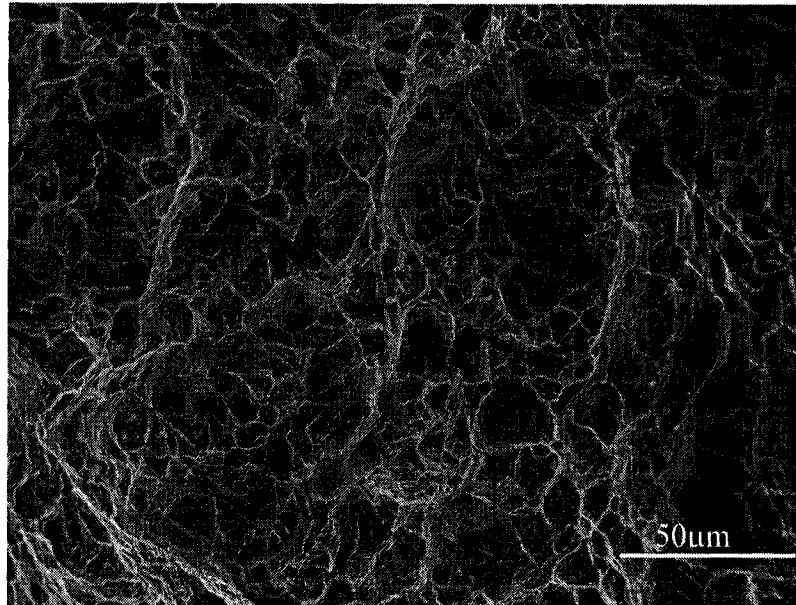
Figure 4.61: SEM fractographs of squeeze cast AM50A fractured at 150 °C,

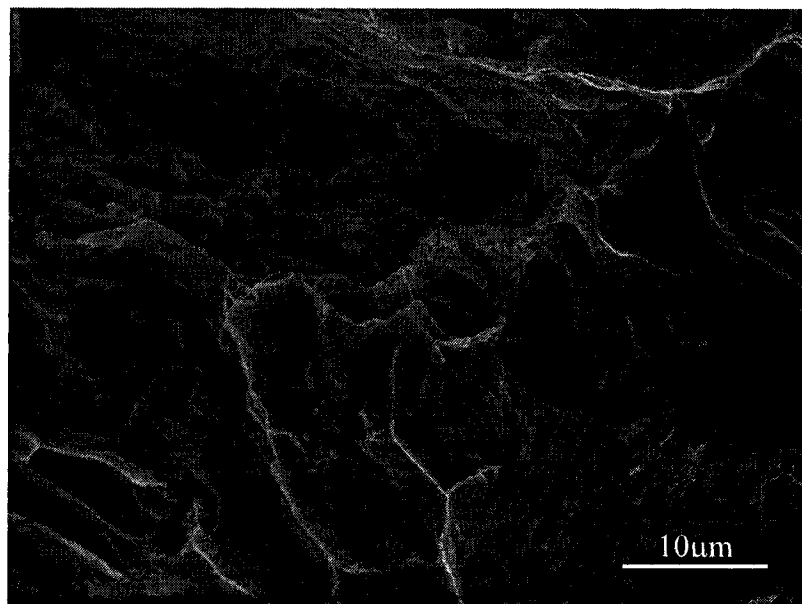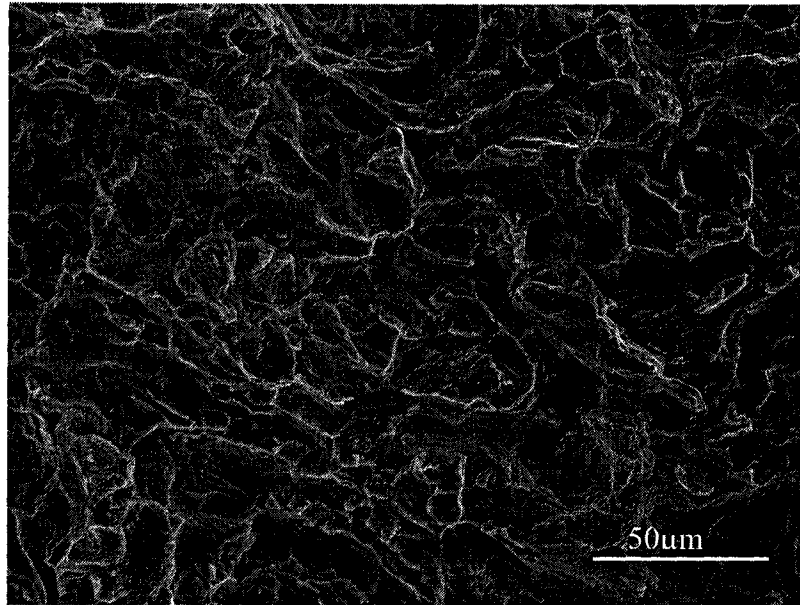a) low magnification and b) higher magnification.

124

Figure 4.62: SEM fractographs of squeeze cast AMC504 fractured at 150 °C,
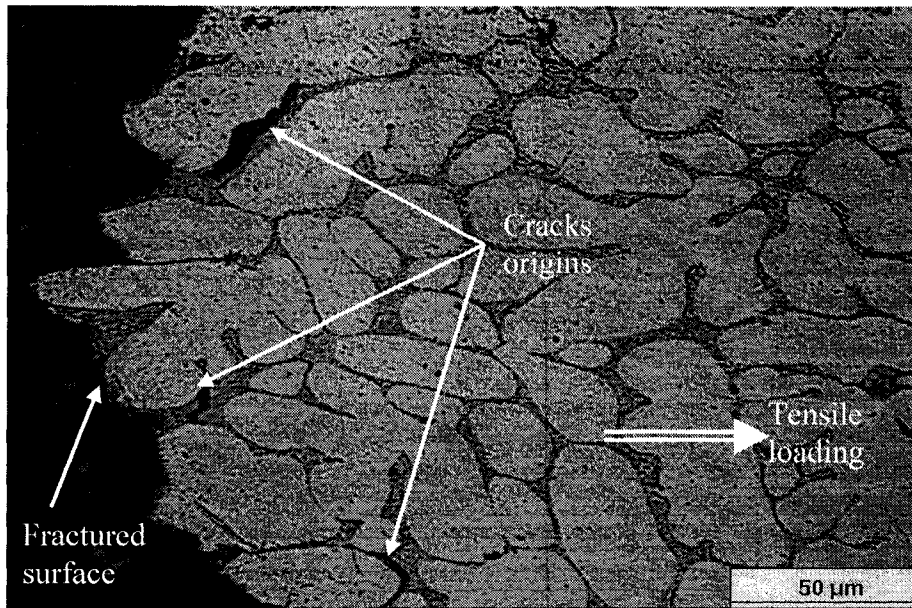
a) low magnification and b) higher magnification.

125

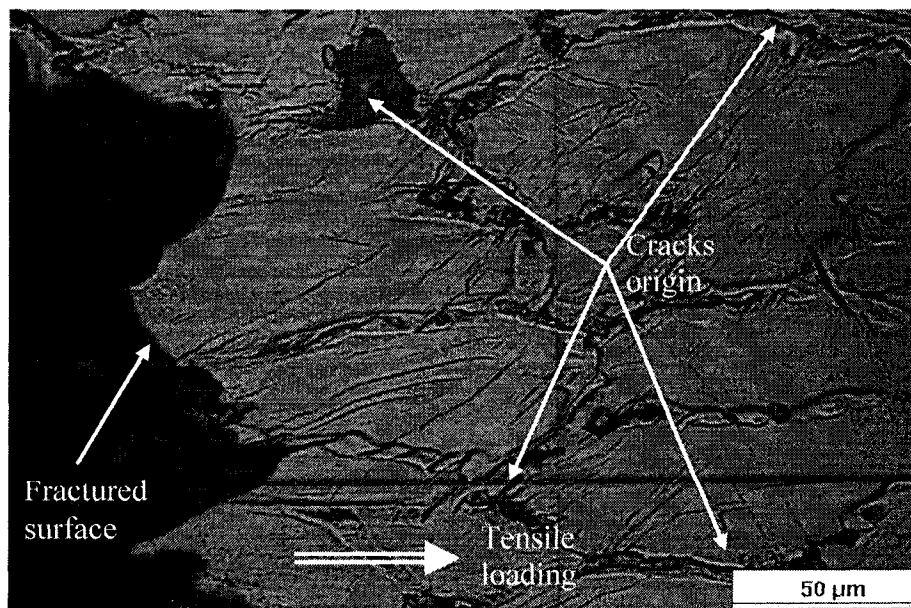Figure 4.63: Optical micrograph showing crack origin in AMC504 at 150 °C.

Figure 4.64: Optical micrograph showing crack origin in AM50A at 150 °C.

126

4.3.5 Summary

The effect of calcium contents was investigated on microstructure and tensile properties of squeeze cast Mg-Al-Ca magnesium alloy at both room and elevated temperatures. The addition of calcium refines the grain structure of Mg-Al-Ca magnesium alloys. The microstructure of all the AMC alloys with different calcium contents consists of the primary α-Mg, Al_2Ca intermetallic, and Mn-Al intermetallic. But for the base alloy, AM50A, they are the primary α-Mg, $Mg_{17}Al_{12}$ and Mn-Al intermetallic.

The results of tensile testing indicate that, the room temperature tensile properties, UTS and elongation, decrease with an increase in calcium contents. But at 150 °C, as the calcium contents increase, their UTS increases but still the elongation decreases. This may be due to the presence of brittle phase, Al_2Ca in the AMC alloys. The addition of calcium increases the strain hardening rate of Mg-Al-Ca alloys at both room and high temperature.

The observation of SEM fractography indicates that the fracture mode of the AMC alloys transit from ductile to brittle as their calcium contents increase, which is consistent with the tensile results.

127

CHAPTER V

CONCLUSIONS

The conclusions drawn from this study can be classified into two categories based on two research objectives:

I. Effect of pressure levels on tensile behaviour and microstructure of squeeze cast magnesium alloy AMC501:

1. The microstructure of the alloy contains of the primary α-Mg, Al_2Ca intermetallic and Mn-Al intermetallic;

2. Due to the high aspect ratio of the casting geometry, no significant microstructal change was observed as the applied pressures increase;

3. The results of tensile testing indicate that the mechanical properties, UTS, YS, and elongation, increase from 153.7, 80 MPa and 3.26% to 183.7, 90.5 and 5.42% with an increase in the applied pressures from 3 to 90 MPa. The material densification and porosity reduction should be responsible for the increase in tensile properties.

II. The effect of calcium contents was investigated on microstructure and tensile properties of squeeze cast Mg-Al-Ca magnesium alloys:

1. The addition of calcium refines the grain structure of Mg-Al-Ca magnesium alloys. But the grain refining effect diminishes as Ca content increases to and beyond 2 wt.%;

2. The microstructure of all the AMC alloys with different calcium contents consists of the primary α-Mg, Al_2Ca intermetallic and Mn-Al intermetallic;

128

3. As the calcium content increases, the fraction area of secondary phases increases in the microstructure;

4. EDS mapping shows that, in alloy AMC502, the calcium and aluminum mostly precipitated on grain boundaries; however manganese precipitates in the matrix. Similarly in AM50A, the aluminum precipitates mostly on grain boundaries and the manganese precipitate in the matrix.

5. The results of tensile testing at room temperature indicate that the tensile properties, UTS and elongation, decrease from 206 MPa and 8.5% to 162 MPa and 2.0%, with an increase in calcium contents from 0 to 4 wt.%. This may be due to the presence of continuous network of Al_2Ca in the AMC alloys;

6. unlike the room temperature results, the results of tensile testing at 150 $^\circ$C indicate that UTS increases from 124 to 145 MPa as the calcium content increases from 0 to 4 wt.%. This is due to presence of Al_2Ca which can keep its strength to a high extent at 150 $^\circ$C. But elongation decreases from 23.8% to 10.7% with an increase in calcium contents from 0 to 4 wt.%, this maybe attributed to presence of continuous network of Al_2Ca in the AMC alloys;

7. As the calcium content increases from 0 to 4 wt.%, the yield strengths of Mg-Al-Ca alloys increase from 82.6 and 73 to 93.6 and 91 MPa both at room and high temperature, respectively. This is due to reduction in grain size and increase in fraction area of secondary phases as calcium content increases.

8. The addition of calcium increases the strain hardening rate of Mg-Al-Ca alloys at both room and high temperatures. This could be attributed to increase in fraction area of secondary phases as calcium content increases.

129

CHAPTER VI

FUTURE WORK

The future work for this study can be classified into two primary research areas:

I. Effect of process parameters and geometry of squeeze casting on tensile behaviour and microstructure of squeeze cast Mg-Al-Ca alloys:

1. the effect of die and pouring temperatures should be investigated; and

2. the effect of casting geometry such as aspect ratio and section thicknesses on tensile behaviour and microstructure of squeeze cast magnesium alloy AMC alloys should be studied.

II. The effect of calcium contents was investigated on microstructure and tensile properties of squeeze cast Mg-Al-Ca magnesium alloy:

1. Tensile behaviour of squeeze cast Mg-Al-Ca magnesium alloy should be investigate at temperature over 150 $^{\circ}$C;

2. TEM technique also needs to be employed to characterize microstructural features of squeeze cast Mg-Al-Ca magnesium alloy in details; and

3. The effect of heat treatment, in T4 and T6 conditions, on microstructure and tensile properties of squeeze cast Mg-Al-Ca magnesium alloys should be investigated.

130

REFERENCES

1) D. M. Stefanescu, J. R. Davis and J. D. Destefani, "Metals Handbook",Ninth Edition. Vol.15- Casting, ASM International, Metals Park, Ohio 44073, USA, 1988, pp. 937.

2) T. Rolland, "Squeeze Casting: a Literature Review", Gov. Res. Announc. Index (USA), ISSN 0097-9007, 1993, pp. 58.

3) G. A. Chadwick, "Casting Technology" The Institute of Materials, Future Developments of Metals and Ceramics (UK), 1992, pp. 179-199.

4) M. R. Ghomashchi, A. Vikhrov, "Squeeze casting: an overview" Journal of Materials Processing Technology (Netherlands). Vol. 101, no. 1-3, 14 Apr. 2000, pp. 1-9.

5) T. M. Yue, G. A. Chadwick, "Squeeze casting of light alloys and their composites" Journal of Materials Processing Technology (Switzerland). Vol. 58, no. 2-3, 15 Mar. 1996, pp. 302-307.

6) H. Hu, "Squeeze casting of magnesium alloys and their composites" Journal of Materials Science. Vol. 33, no. 6, 15 Mar. 1998, pp. 1579-1589.

7) K. U. Kainer, E. Bohm, "Optimizing of properties of magnesium alloys by squeeze casting" 29th International Symposium on Automotive Technology and Automation. Vol.I, Florence, Italy, 3-6 June 1996, pp. 653-660.

8) G. A. Rozak, D. M. Goddard, "Yield and Tensile Strengths of Squeeze Cast and Heat Treated AZ91 Magnesium and A356 Aluminum" 17th International Die Casting Congress and Exposition, Cleveland, Ohio, USA, 18-21 Oct. 1993, pp. 419-428.

9) J. F. Wallace, Q. Chang and D. Schwam, "Process control in squeeze casting" Die Casting Engineer (USA), Vol. 44, no. 6, Nov.-Dec. 2000, pp. 42-48.

10) J. F. Wallace and D. Schwam, "Squeeze casting of aluminum and magnesium alloys" 20th International Die Casting Congress; 1999 NADCA Congress; Cleveland, OH; USA; 1-4 Nov. 1999, pp. 41-45.

11) G. A. Rozak, J. J. Lewandowski, J. F. Wallace, and A. Altmisoglu, "Effects of Casting Conditions and Deformation Processing on A356 Aluminum and A356--20 vol.% SiC Composites", Journal of Composite Materials (USA). Vol. 26, no. 14, 1992, pp. 2076-2106.

12) V. P. Seredenko and T. P. Malei, "Pressing of Components from Liquid Steel" Dokl. Akad. Nauk SSSR 5, 1961, 253-255 (BISI Translation 2827, 1962).

13) V. M Plyatskii, "extrusion casting" (primary source, New York, 1965)

14) G. S. Reddy and G. R. K. Murthy, "Liquid Forging of an Aluminum Alloy" Transactions of the Indian Institute of Metals. Vol. 31, no. 5-6, Oct.-Dec. 1978, pp. 484-487.

15) B. B. Gulyaev, "crystallization of steel under mechanical pressure" Liteinoe proizvodstov, 1960, 12-33.

16) W. Meyer "Squeeze Forming-Process for Producing High Quality Castings" , Metall, , 30, (1), Jan. 1976, pp. 46-54.

17) D. K. Chernov, "Reports of the imperial Russian metallurgical society" December 1878.

18) V. G. Welter, Z. Metallkd, 23 (1931) 255

19) H. Hu, A. Yu, N. Li and J. E. Allison, "Potential Magnesium Alloys for High Temperature Die Cast Automotive Applications: A Review." Materials and Manufacturing Process, Vol18, No. 5, 2003, pp. 687-717.

132

20) G. V. Ranyor, "The Physical Metallurgy of Magnesium and its Alloys", Pregamon Press: Oxford, UK, 1959, pp. 348.

21) F. Hollrigl-Rosta, E. Just, J. Kohler and H. J. Melzer, "Magnesium in the Volkswagen", Light Metal Age. Vol. 38, no. 7-8, Aug. 1980, pp. 22-29.

22) H. J. Fuch, "Magnesium Alloys Having a High Resistance to Permanent Creep deformation at Elevated Temperatures" British Patent 847,992, 1960.

23) M. O. Pekguleryuz, and A. Luo, "Creep Resistant Magnesium Alloys for Powertrain Applications", patent PCT/CA96/00091, Aug 22, 1996.

24) M. O. Pekguleryuz, and A. Luo, "Creep Resistant Magnesium Alloys for Die Casting", patent WO9625529, 1995.

25) R. Ninomiya, T. Ojiro and K. Kubota," Improved heat resistance of Mg-Al alloys by the calcium addition" Acta Metall. Mater. Vol. 43, no. 2, Feb. 1995, pp. 669-674.

26) K. Y. Sohn, W. Jones, J. J. Berkmortel, H. Hu and J. E. Allison, "Creep and bolt load retention behavior of die cast magnesium alloys for high temperature applications: part 2 of 2" SAE 2000 World Congress Detroit, Michgan, March 6-9, No. 2000-01-1120.

27) K. Y. Sohn, W. Jones and J. E. Allison, "The effect of calcium on creep and bolt load retention behavior of die-cast AM50 alloy" Magnesium Technology, TMS Annual Meeting; Nashville, TN; USA; 12-16 Mar. 2000, pp. 271-278.

28) M. O. Pekgulryuz and J. Renaud "Creep resistance in Mg-Al-Ca casting alloys" Magnesium Technology, TMS Annual Meeting Nashville, TN, USA; 2000, pp. 279-284.

29) T. Yoshihiro, I. Naoya, S. Rie, S. Tatsuo and O. Koichi, " Creep characteristics of Ca-added Die –cast AM50 magnesium alloys" Materials Science Forum Vols. 419-422, 2003, pp. 459-464.

30) Y. Terada, R. Sota, N. Ishimatsu, T. Sato and K. Ohori, " a thousand fold creep strengthening by Ca addition in die-cast AM50 magnesium alloy" Metallurgical and Materials Transactions A, Vol. 35A, Sep 2004, pp. 3029-3032.

31) J. J. Berkmortel, H. Hu, J. E. Kearns and J. E. Allison, "die castability assessment of magnesium alloys for high temperature applications: part 1 of 2", SAE 2000 world Congress Detroit, Michigan, March 2000, Technical Paper Series 2000-01-1119.

32) B. R. Powell, A. Luo, B. L. Tiwari and V. Rezhets, "The die castability of calcium-containing magnesium alloys: thin-wall computer case", Magnesium Technology 2002 as held at the 2002 TMS Annual Meeting; Seattle, WA; USA; 17-21 Feb. 2002. pp.123-129.

33) A. A. Das and S. Chatterjee, "Squeeze Casting of an Aluminum Alloy Containing Small Amounts of Silicon Carbide Whiskers ", Metall. Mater. Technol. Vol. 13, no. 3, Mar. 1981, pp. 137-142.

34) G. Williams and K. M. Fisher, "Squeeze Forming of Aluminium-Alloy Components" Met. Technol. Vol. 8, no. 7, July 1981, pp. 263-267.

35) S. Rajagopal, "Squeeze Casting: a Review and Update" J. Appl. Metalwork. Vol. 1, no. 4Jan. 1981, pp. 3-14.

36) H. U. Ha, "Squeeze casting of Magnesium-based Alloys and their metal matrix composites," PhD dissertation, July 1989, Southampton University, ISSN 0419-4217.

37) G. A. Rozak, "Effects of processing on the properties of aluminum and magnesium matrix composites" PhD. Dissertation, case Western Reserve University, Cleveland, Ohio 1993.

38) N. A. Kudrin and P. N. Bidulya, "Mould and die life in pressure diecasting and squeeze casting of molten steel" Russian Castings Production, no 1, Jan, 1965, p 31-34.

134

39) F. Weinberg, "Squeeze Casting", Solidification Technology in the Foundry and Cast House; Coventry; England; 15-17 Sept., 1980, pp. 131-136.

40) H. R. Hashemi, H. Ashoori, and P. Davami, "Microstructure and tensile properties of squeeze cast Al-Zn-Mg-Cu alloy " Materials Science and Technology (UK). Vol. 17, no. 6, June 2001, pp. 639-644.

41) M. S. Yong and A. J. Clegg, "Process optimisation for a squeeze cast magnesium alloy." Journal of Materials Processing Technology. Vol. 145, no. 1, 1 Jan. 2004, pp. 134-141.

42) J. R. Franklin and A. A. Das, "Squeeze Casting--a Review of the Status" Br. Foundryman. Vol. 77, no. 3, Apr.1984, pp. 150-158.

43) T. N. Lipchin and P. A. Bykov, "Alloy Strengthening by Solidification Under Pressure" Liteinoe Proizv , no. 3, Mar. 1973, pp. 31-33.

44) J. A. Sekhar, "Solidification by Pressure Application" Scr. Metall. Vol. 19, no. 12, Dec. 1985, pp. 1429-1433.

45) "Squeeze Casting = Casting + Forging", Precis. Met., Sept, 32, (9), 1974, pp. 36-38.

46) O. G. Epanchintsev, "Structure and properties of metals solidified under pressure" Russian Casting Productions, 1972, p 34-37.

47) T. N. Lipchin, "The Degree of Solid Solution Alloying in Pressure-Solidified Alloys" , Metalloved. Term. Obrab. Met , no. 4, 1986, pp. 43-46.

48) M. A. Taha, N. A. E. Mahallawy, M. L. Zamzam and S. E. Mardy, "Effect of Pressure on Structure and Mechanical Properties of Al-18wt.%Si Squeeze Cast Alloy", Solidification Processing 1987; Sheffield; UK; 21-24 Sept. 1987, pp. 409-412.

135

49) G. R. K. Murthy and K. R. Satyanarayan, "Effect of Pressure Solidification on Structure and Properties of Some Eutectic Alloys" Trans. Indian Inst. Met. Vol. 41, no. 1, Feb. 1988, pp. 65-77.

50) N. Fujii, S. Okada, S. Morimoto and M. Fujii, "Solidification Phenomena and Quality of Al--Si Alloy AC8A in Squeeze Casting" Jpn. Inst. Light Met. Vol. 33, no. 7, July 1983, pp. 392-398.

51) G. A. Rozak, J. J. Lewandowski, J. F. Wallace, and A. Altmisoglu, "Effects of Casting Conditions and Deformation Processing on A356 Aluminum and A356--20 vol.% SiC Composites " Journal of Composite Materials (USA). Vol. 26, no. 14, 1992, pp. 2076-2106.

52) J. Sobczak, "The Structural Aspects of Squeeze Cast Metal" Prace Institutu Odlewnictwa (Poland). Vol. 41, no. 1-2, 1991, pp. 39-60.

53) P. Balan, R. M. Pillai, K. G. Satyanarayana and B. C. Pai, "The structure and properties of squeeze-cast eutectic Al-Si plates" International Journal of Cast Metals Research (UK). Vol. 6, no. 3, 1993, pp. 131-136.

54) G. C. Lee, K. H. Baik, B. T. Lee and K. S. Han, "Study of Squeeze Casting Conditions and Microstructure in Pure Aluminum" Research Institute of Industrial Science and Technology (Pohang City) Technical Research Report. Vol. 4, no. 3, Sept. 1990, pp. 191-198.

55) A. A. Das, Z. B. Zantout and A. J. Clegg, "Solidification Processing by Squeeze Casting" Solidification Processing 1987; Sheffield; UK; 21-24 Sept. 1987. pp. 472-475.

56) L. A. Luo H. Hu and S. H. J. Lo, "Microstructure and mechanical properties of squeeze cast AZ91D magnesium alloy" Light Metals 1996; Montreal, Quebec; Canada; 25-29 Aug. 1996, pp. 375-387.

57) M. S. Yong and A. J. Clegg, "Evaluation of squeeze cast magnesium alloy and composite", Foundryman (UK). Vol. 92, no. 3, Mar. 1999, pp. 71-75.

58) M. Zhou, H. Hu, N. Li and J. Lo, "Microstructure and tensile properties of squeeze cast magnesium alloy AM50" Journal of Materials Engineering and Performance, v 14, n 4, August, 2005, p 539-545

59) M. M. Avedesian and H. Baker, "Magnesium and Magnesium Alloys ", ASM International, Member/Customer Service Center, Materials Park, OH 44073-0002, USA, 1999, pp. 314.

60) M. S. Dargusch, G. L. Dunlop, and K. Pettersen, "Mg alloys and their applications", B. L. Mordike, K. U. Kainer, Eds, Werkstoff-Inforamtionsgesllschaft, Germany, 1998, pp. 277-282.

61) S. Beer, G. Frommeyer and E. Schmid, "Mg alloys and their applications" DGM, B. L. Mordike, F. Hehman, Eds, April 1992, pp 317-324.

62) M O Pekguleryuz, A. Lou, C. Aliravci, "Modification of Sand Cast AS41Magnesium Alloy" Light Metals Processing and Applications; Quebec City, Quebec; Canada; 29 Aug.-1 Sept. 1993, pp. 409-416.

63) F. Hollrigl-Rosta, E. Just, J. Kohler and H. J. Melzer, "Magnesium in the Volkswagen" Light Metal Age. Vol. 38, no. 7-8, Aug. 1980, pp. 22-23 and 26-29.

64) G. S. Foerster, "Designing diecasting alloys", Light Metals Age, v.30, 9-10, 1972, pp. 11-13.

65) M. S. Dargusch and G. L. Dunlop, Materials 98, Inst.Mtls Eng, Australasia ltd. Ed. Michale Ferry, Australia, 1998, pp. 579.

66) W. Blum, B. Watzinger and P. Weidinger, "Mg alloys and their applications", B. L. Mordike, K. U. Kainer, Eds, Werkstoff-Inforamtionsgesllschaft, Germany, 1998, pp. 49-60.

67) T. K. Aune and T. J. Ruden, "High temperature properties of magnesium die casting alloys" Source: SAE Technical Paper Series, 1992, 920070, pp. 1-7.

68) K. Pettersen, H. Westengen, J. I. Skar, M. Videm and L. Y. Wei, "Mg alloys and their applications", K. U. Kainer, Ed. DGM, Wiley-VCH, Weinheim, Germany, 2000, pp. 29-34.

69) T. K. Aune and H. Westengen, "Property update on magnesium die casting alloys", SAE Transactions: Journal of Materials & Manufacturing vol. 104. Society of Automotive Engineers, 400 Commonwealth Dr , Warrendale, PA 15096, USA, 1995 pp. 332-342.

70) W. Mercer, SAE 900788, Detroit, Michigan, Feb, 1990.

71) I. J. Polmear, "Light Alloys--Metallurgy of the Light Metals". 3nd Edition Edward Arnold, a division of Hodder and Stoughton, 41 Bedford Square, London WC1B 3DQ, UK, 1995.

72) O. Holta, M. Videm, H. Westengen and D. L. Albright, "Diecasting innovation" NADCA, Indianapolis T95-053, Oct 1995, pp. 177-182.

73) L. Y. Wei and G. L. Dunlop, "The solidification behaviour of Mg-Al-rare earth alloys", Journal of Alloys and Compounds (Switzerland). Vol. 232, no. 1-2, 1 Jan. 1996, pp. 264-268.

74) G. Pettersen, H. Westengen, R. Hoier and O. Lohne, "Microstructure of a pressure die cast magnesium-4wt.% aluminium alloy modified with rare earth additions" Materials Science and Engineering A (Switzerland). Vol. 207, no. 1, 15 Mar. 1996, pp. 115-120.

75) B. R. Powell, R. V. Rezhets, M. P. Balogh and R. A. Waldo, "Microstructure and creep behavior in AE42 magnesium die-casting alloy" JOM (USA). Vol. 54, no. 8, Aug. 2002, pp. 34-38.

76) P. Bakke, P. K. Pettersen and H. Westengen, "Enhanced ductility and strength through RE addition to magnesium die casting alloys.", Magnesium Technology 2003 as held at the 2003 TMS Annual Meeting; San Diego, CA; USA; 2-6 Mar. 2003. pp. 171-176.

77) B. R. Powell, A. Luo, V. Rezhets, J. J. Bommarito and B. L. Tiwari "Development of creep-resistant magnesium alloys for powertrain applications: Part 1 of 2", Society of Automotive Engineers, SAE Transactions: Journal of Materials & Manufacturing (USA). Vol. 110, 2001, pp. 406-413.

78) A. A. Luo, M. P. Balogh and B. R. Powell, "Tensile creep and microstructure of magnesium-aluminum-calcium based alloys for powertrain applications" - part 2 of 2 Society of Automotive Engineers, SAE Transactions: Journal of Materials & Manufacturing (USA). Vol. 110, 2001, pp. 414-422.

79) M. O. Pekguleryuz and E. Baril, " Development of creep resistant Mg-Al-Sr alloys" Magnesium Technology 2001 as held at the 2001 TMS Annual Meeting; New Orleans, LA; USA; 11-15 Feb. 2001. pp. 119-125.

80) M. O. Pekguleryuz, "Magnesium Diecasting alloys for high temperature applications" Magnesium Technology 2004 as held at the 2004 TMS Annual Meeting; Charlotte, NC; USA; 14-18 Mar. 2004. pp. 281-287.

81) Y. Fasoyinu, T. Castles, R. Bouchard, S. M. Sahoo, M. Pekguleryuz, and P. Labelle, "Die cast magnesium alloys AE42 and AJ52x for high temperature applications." Magnesium Technology 2003 as held at the 2003 TMS Annual Meeting; San Diego, CA; USA; 2-6 Mar. 2003. pp. 207

82) M. Pekguleryuz, P. Labelle, D. Argo, and E. Baril, "Magnesium diecasting alloy AJ62X with superior creep resistance, ductility and diecastability.", Magnesium Technology 2003 as held at the 2003 TMS Annual Meeting; San Diego, CA; USA; 2-6 Mar. 2003. pp. 201-206.

83) P. Labelle, M. Pekguleryuz, D. Argo, M. Dierks, T. SParks and T. Waltematte, "Heat resistant magnesium alloys for power-train applications" Society of Automotive Engineers, SAE Transactions: Journal of Materials & Manufacturing (USA). Vol. 110, 2001, pp. 423-430.

84) D. Argo, M. Pekguleryuz, P. Labelle, M. Dierks, T. Sparks, and T. Waltematte, "Diecastability and properties of Mg-Al-Sr based alloys", Magnesium Technology 2001 as held at the 2001 TMS Annual Meeting; New Orleans, LA; USA; 11-15 Feb. 2001. pp. 131-136.

85) S. Koike, K. Wasizu, S. Tanaka, T. Baba and K. Kikawa, SAE Paper 200-01-1117, Detroit, March, 2000.

86) E. Aghion, B. Bronfin, F. Von Buch, S. Schumann and H. Friedrich, "Dead sea magnesium alloys newly developed for high temperature applications." Magnesium Technology 2003, TMS Annual Meeting; San Diego, CA; USA; 2-6 Mar. 2003. pp. 177-182.

87) "Standard test methods of tension testing wrought and cast aluminum- and magnesium-alloy products", B557-02, ASTM, West Conshohocken, PA, p 421-434.

88) "Standard Test Methods for determining Average Grain Size" E112-96, ASTM Standards, ASTM, Vol, 2000, pp. 251-273.

89) "Standard Test Method for Density of High-Modulus Fibers," D3800-99, ASTM Standards, ASTM, Vol 15.03, 2002, pp. 186-187.

90) R. M. Wang, A. Eliezer and E. M. Gutman, "An investigation on the microstructure of an AM50 magnesium alloy" Materials Science and Engineering A. Vol. 355, no. 1-2, 25 Aug. 2003, pp. 201-207.

91) E. A. Brandes and G. B. Brook, "Smithells Metals Reference Book" Butterworth-Heinemann Ltd, Linacre House, Jordan Hill, Oxford OX2 8DP, UK, 1992.

92) S. H. Avner, "Introduction to Physical Metallurgy" New York: McGraw - Hill, Second Edition, 1974.

93) G. E. Dieter, "Mechanical metallurgy", New York: McGraw-Hill, 1976.

94) J. R. Newby, Metals Handbook. Vol. 8, "Mechanical Testing" Ninth Edition American Society for Metals, 1985, pp. 778.

APPENDICES

142

APPENDIX I: Table of data

Table Ap1.1 Grain size of squeeze cast AMC501 under different pressure levels

No	Grain size				
	3	10	30	60	90
1	40.96425	39.72525	38.47323	39.55371	37.98706
2	41.11863	39.58246	39.68099	39.26833	39.08299
3	38.77705	39.15407	39.55003	40.05314	38.9122
4	40.21664	37.72612	39.02618	39.91044	38.84103
5	39.34918	39.82521	38.34227	38.94014	38.53503
6	38.82128	38.89704	39.12804	40.03887	38.20056
7	41.43936	39.0684	39.21535	39.69641	39.49574
8	38.87835	39.56818	39.55003	39.63933	39.52421
9	40.76165	38.76853	38.53144	39.68214	39.16839
10	40.87579	39.45394	40.05932	38.96868	38.59907
11	41.21821	39.19691	40.10298	39.15418	39.35342
12	39.93414	40.12508	40.07388	39.23979	39.31072
13	39.86281	41.05325	39.36086	38.08399	39.19685
14	40.13389	39.33971	39.37541	38.16961	39.29648
15	40.07682	40.45351	38.1531	38.1268	39.42458
16	41.16114	39.6253	40.62683	38.26949	38.71294
17	39.90561	39.89661	39.75375	40.32425	39.52421
18	40.26229	39.71098	39.47727	38.59768	38.88373
Average	40.20564	39.50021	39.35388	39.20107	39.0012

143

Table Ap1.2 Density measurement of samples cast under different pressure levels

Sample number	W_a	W_w	W_a-W_w	density	Average density
3-1	2.19445	0.95395	1.2405	1.769	
3-2	1.3101	0.5671	0.743	1.7632	1.7668
3-3	1.756	0.763	0.993	1.7683	
10-1	2.141	0.9385	1.2025	1.7804	
10-2	1.778	0.779	0.999	1.7797	1.7772
10-3	1.628	0.709	0.919	1.7715	
30-1	2.533	1.1155	1.4175	1.7869	
30-2	2.328	1.028	1.30	1.7907	1.7893
30-3	1.7715	0.7835	0.988	1.7903	
60-1	1.417	0.631	0.786	1.8027	
60-2	1.4715	0.6505	0.821	1.7923	1.7968
60-3	1.168	0.5175	0.6505	1.7955	
90-1	1.4155	0.6315	0.784	1.8054	
90-2	1.169	0.5225	0.6465	1.8081	1.8085
90-3	0.743	0.333	0.41	1.8121	

144

Table Ap1.3 Tensile properties of samples cast under different pressure levels

Pressure level	Sample No.	UTS (MPa)	YS (MPa)	ε (%)
3	3-1	160	80	3.91
	3-2	146.8	78	2.73
	3-3	154.5	82	3.15
10	10-1	167.7	81	4.36
	10-2	172.5	82	4.83
	10-3	166.9	88	3.94
30	30-1	177.8	85	5.15
	30-2	176.6	87	4.91
	30-3	176.3	86	5
60	60-1	183	93	5.21
	60-2	176.1	84	5.13
	60-3	180.8	87	5.15
90	90-1	184.6	88	5.45
	90-2	182.7	90	5.45
	90-3	183.8	93	5.38

Table Ap1.4 Grain size of squeeze cast AMC alloys squeeze cast under 30 MPa

No	Grain size				
	AM50A	AMC501	AMC502	AMC503	AMC504
1	46.94458	38.47323	34.73514	35.75676	35.64324
2	48.30662	39.68099	35.18919	35.52973	34.96216
3	48.76063	39.55003	34.73514	35.64324	35.41622
4	48.00395	39.02618	34.39459	35.18919	35.3027
5	48.15528	38.34227	34.96216	36.0973	36.21081
6	48.45796	39.12804	35.18919	35.64324	34.73514
7	48.76063	39.21535	34.84865	34.28108	35.18919
8	48.15528	39.55003	34.84865	36.32432	36.66486
9	47.85261	38.53144	35.75676	34.84865	35.98378
10	47.09592	40.05932	36.0973	34.84865	35.87027
11	47.24726	40.10298	36.32432	35.75676	35.41622
12	45.12853	40.07388	36.0973	34.62162	35.3027
13	46.18789	39.36086	36.21081	34.96216	36.55135
14	45.12853	39.37541	36.43784	34.62162	35.52973
15	46.6419	38.1531	36.55135	34.84865	35.98378
16	46.33923	40.62683	35.41622	35.41622	35.64324
17	46.03655	39.75375	36.21081	35.64324	36.21081
18	44.2205	39.47727	36.21081	35.41622	35.98378
Average	47.01	39.35	35.56	35.3	35.7

146

Table Ap1.5 Tensile properties AMC alloys at room temperature

Calcium level	Sample No.	UTS (MPa)	YS (MPa)	Elongation(%)
0%	0%-1	205.5	81	8.38
	0%-2	210.5	83	8.9
	0%-3	202	84	8.17
1%	1%-1	177.8	85	5.15
	1%-2	176.6	87	4.91
	1%-3	176.3	86	5
2%	2%-1	170	84	2.91
	2%-2	163.8	89	2.30
	2%-3	170.6	90	2.58
3%	3%-1	167.4	88	2.28
	3%-2	161.8	90	2
	3%-3	166	95	2.38
4%	4%-1	163.9	94	2.14
	4%-2	162.5	94	1.77
	4%-3	159.5	93	2.09

147

Table Ap1.6 Tensile properties AMC alloys at 150 °C

Calcium level	Sample No.	UTS (MPa)	YS (MPa)	Elongation (%)
0%	0%-1	123	73	24.2
	0%-2	124	71	23.7
	0%-3	125	75	23.5
1%	1%-1	133	81	17
	1%-2	129	81	21
	1%-3	132	79	17.5
2%	2%-1	135	85	12.5
	2%-2	140	84	15.2
	2%-3	135	86	16
3%	3%-1	139	85	13.2
	3%-2	143	87	11.5
	3%-3	144	88	13.4
4%	4%-1	143	90	7.6
	4%-2	148	93	12.4
	4%-3	144	91	12.2

148

APPENDIX II: Tensile curves of squeeze cast Mg-Al-Ca alloys

a)

b)

149
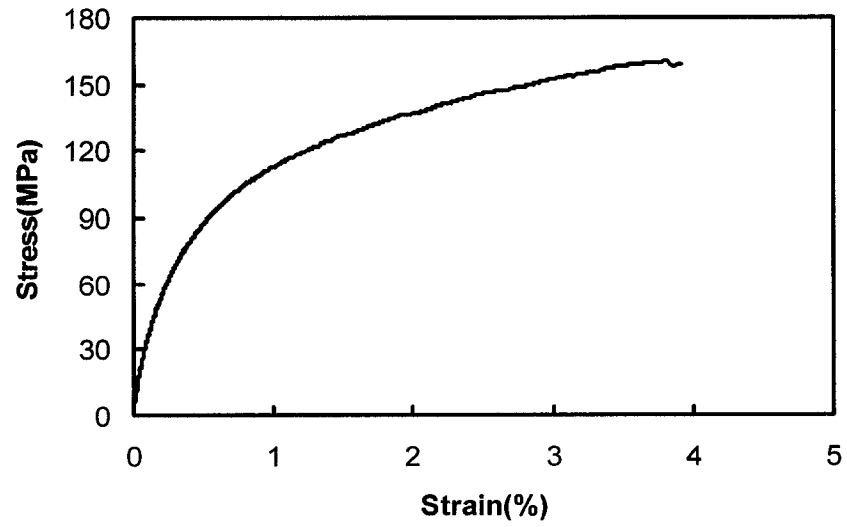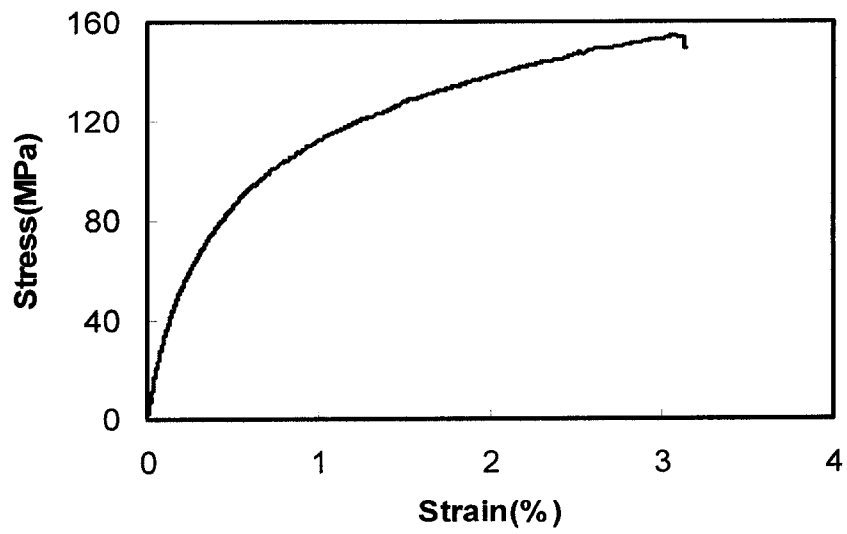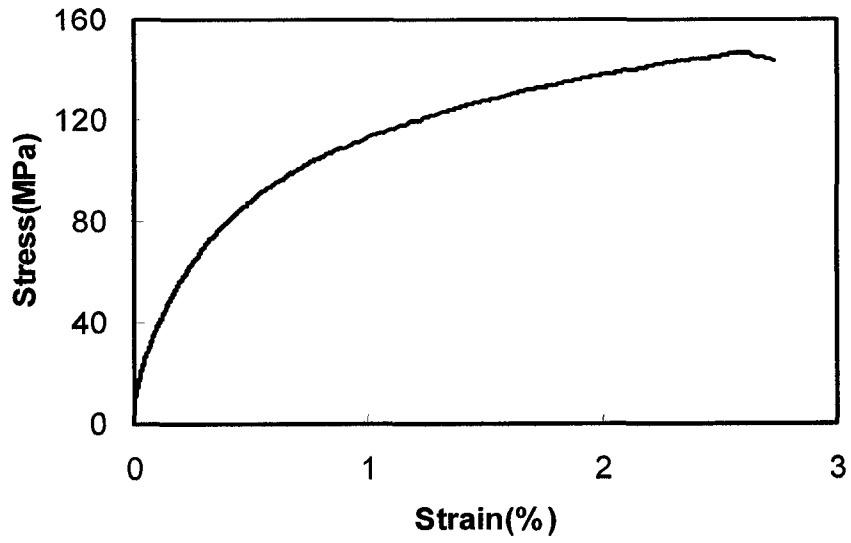
c)

Figure Ap2.1: Tensile curves of squeeze cast AMC501 under applied pressure of

3 MPa at room temperature.

a)

150
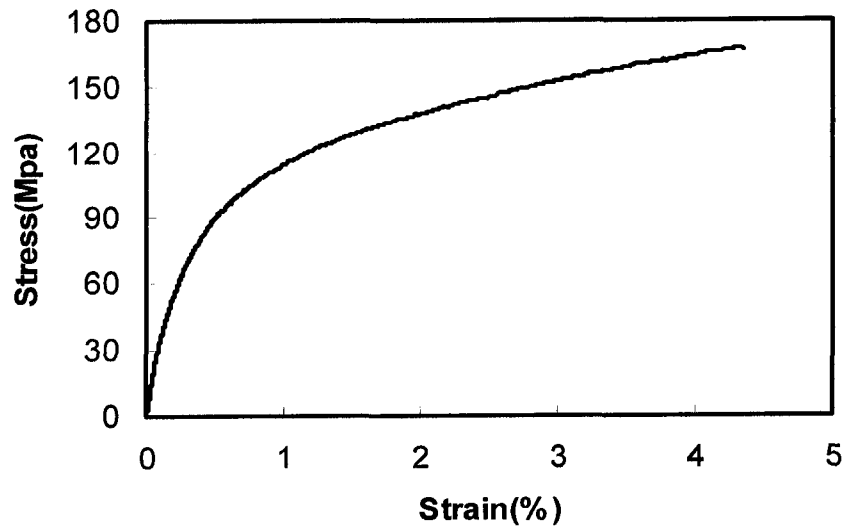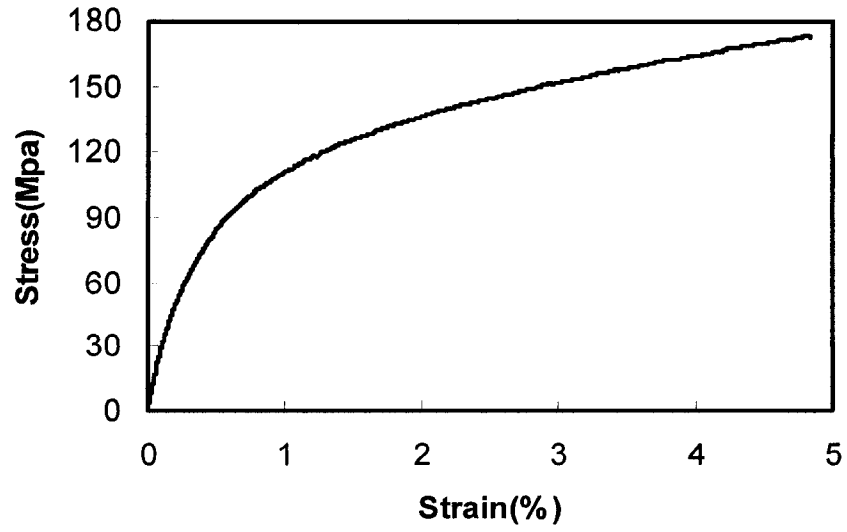
b)
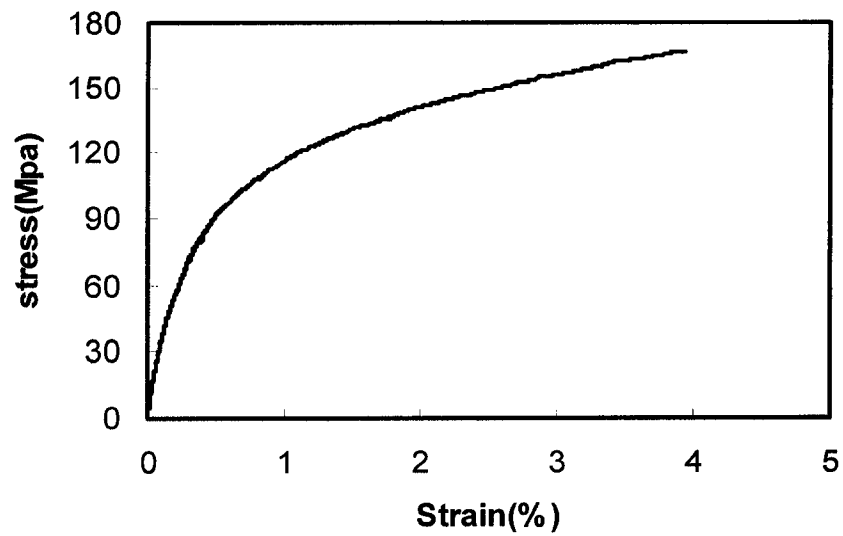
c)

Figure Ap2.2: Tensile curves of squeeze cast AMC501 under applied pressure of
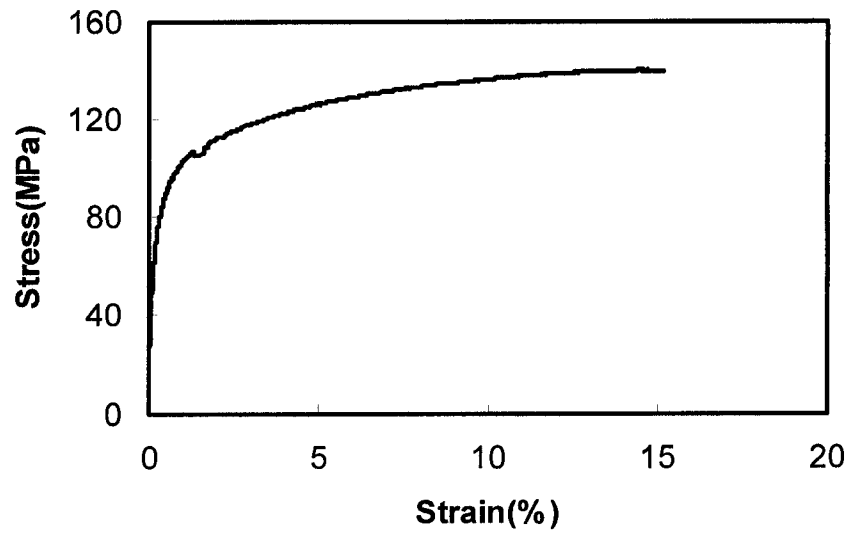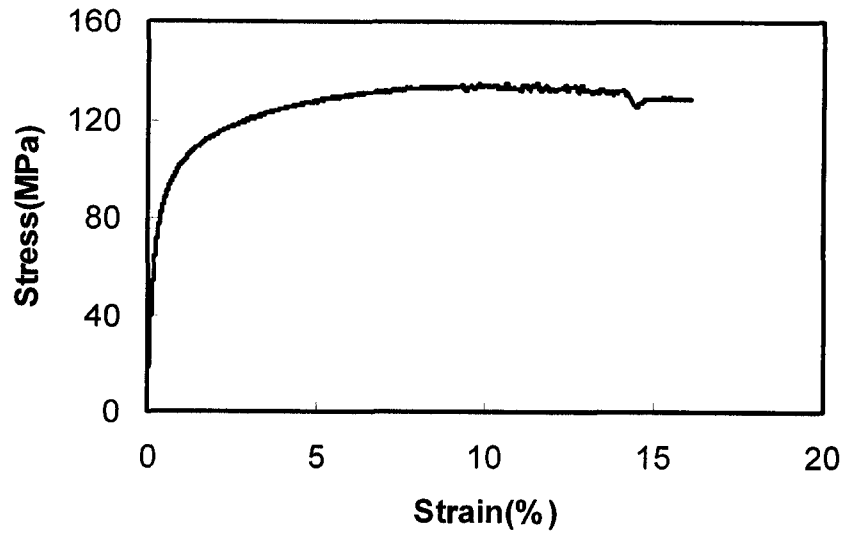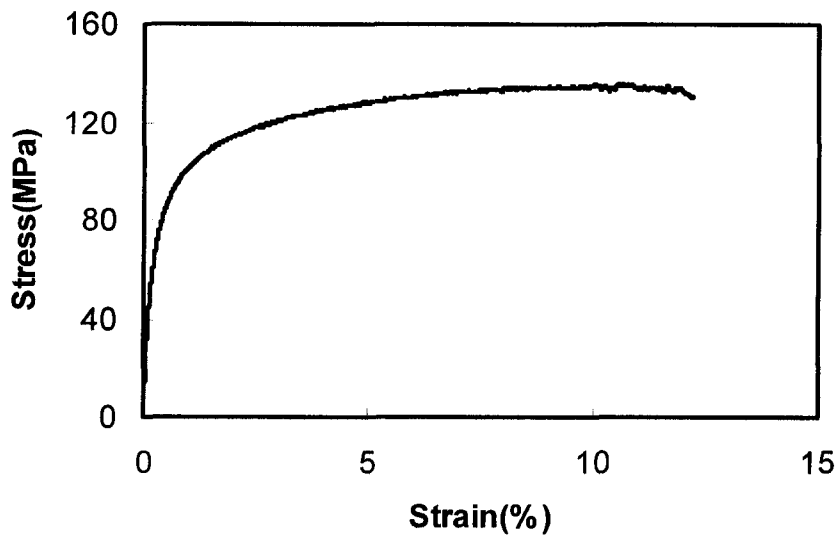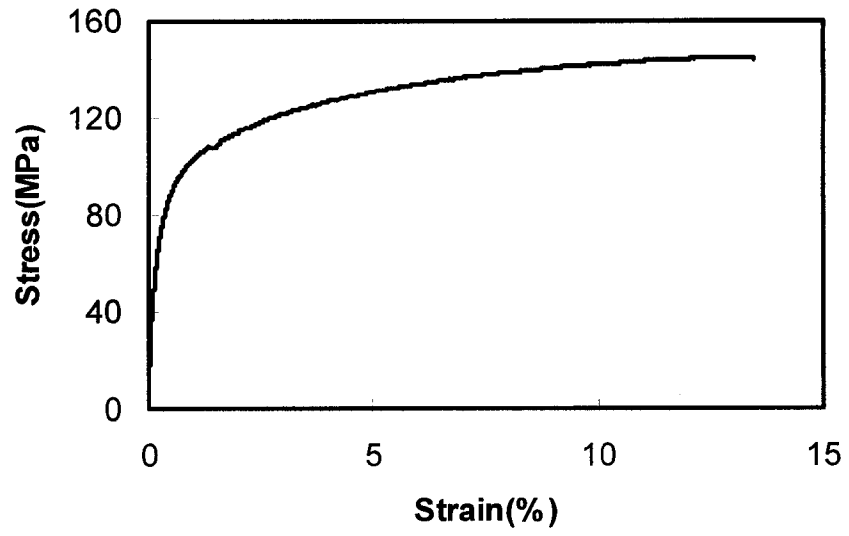
10 MPa at room temperature.

151

a)

b)

152
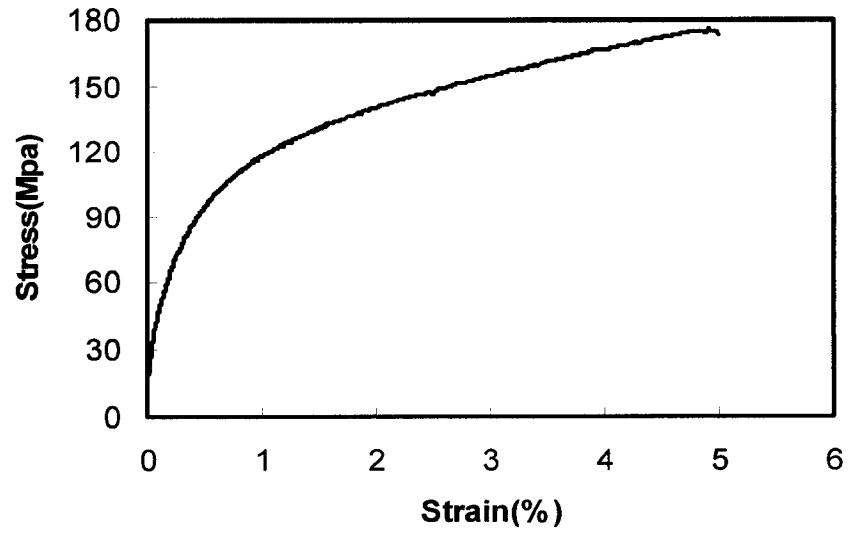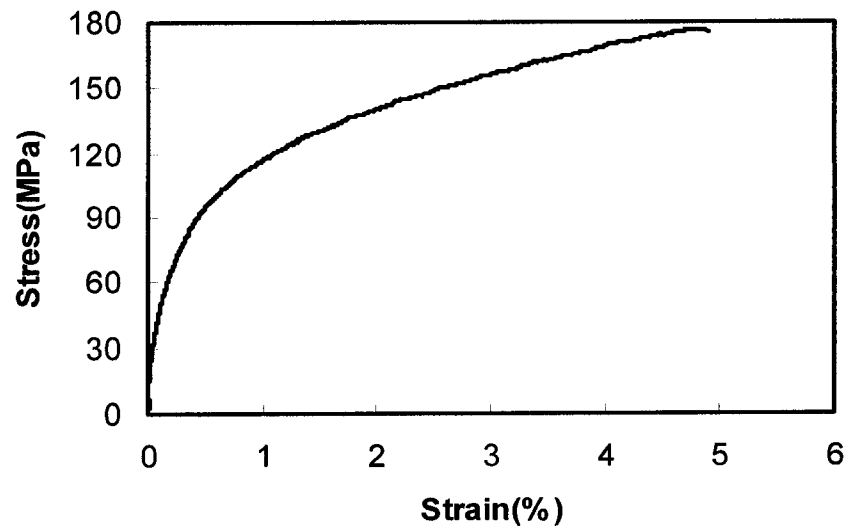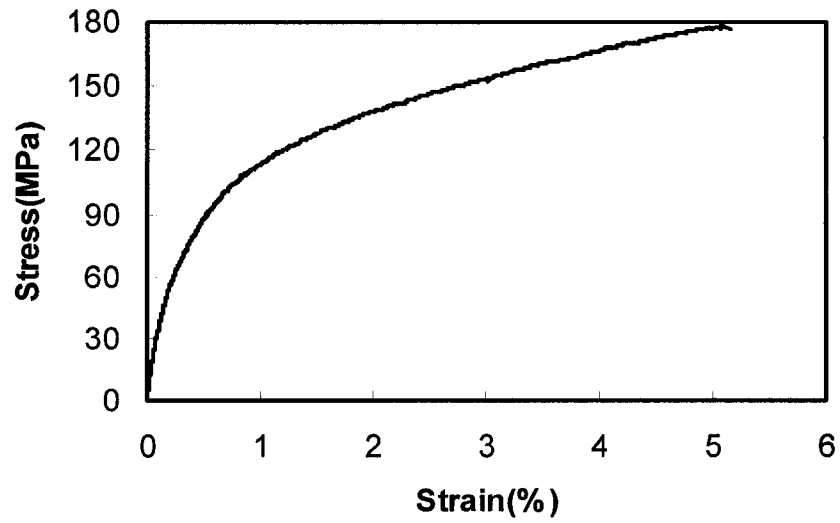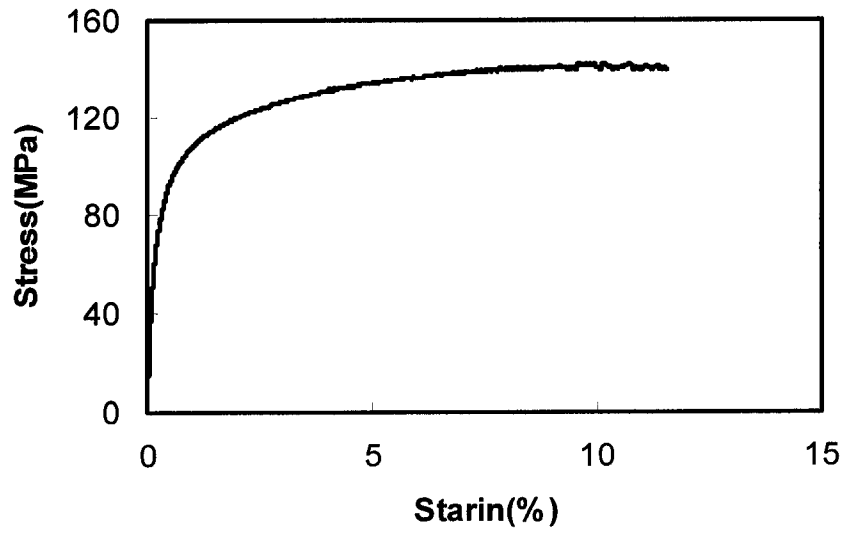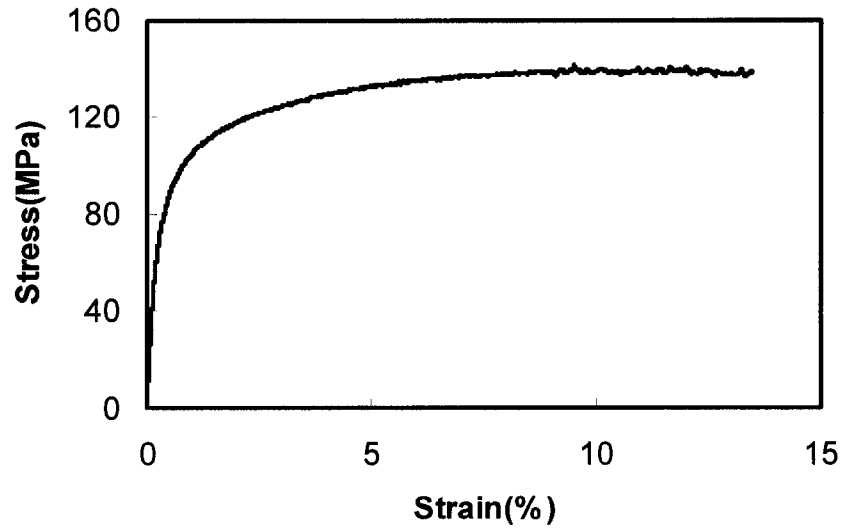
c)

Figure Ap2.3: Tensile curves of squeeze cast AMC501 under applied pressure of

30 MPa at room temperature.

a)

153
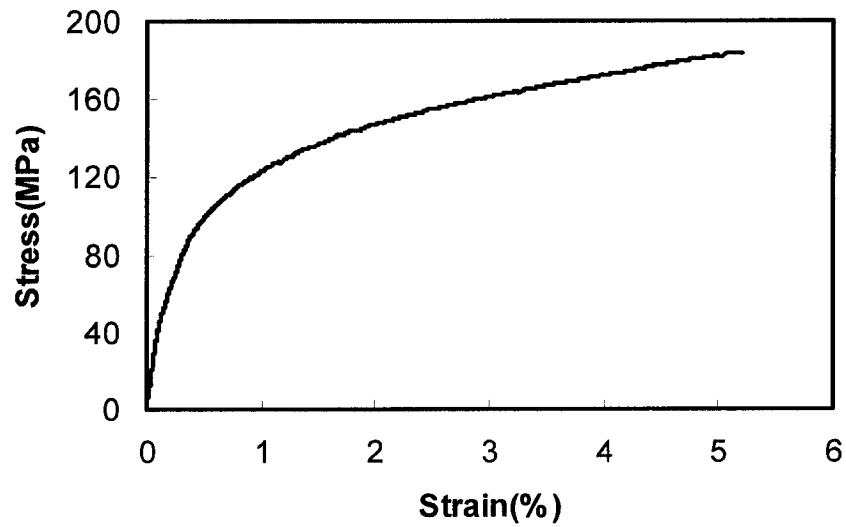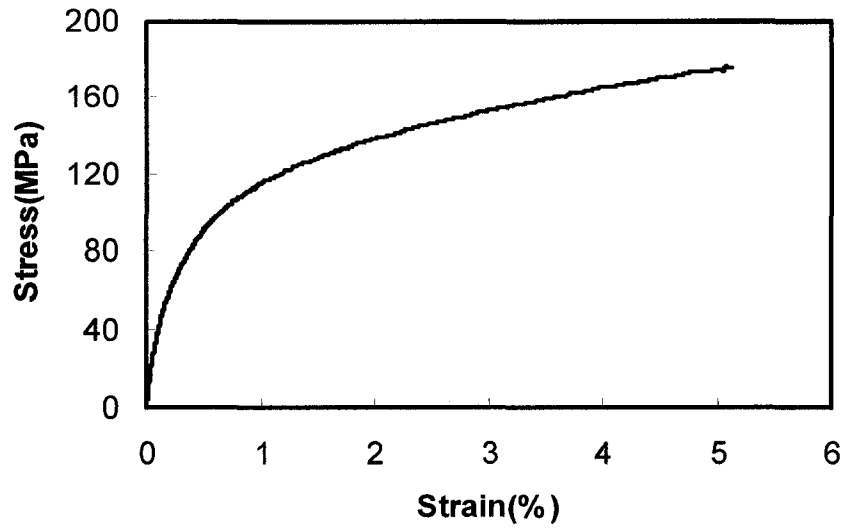
b)
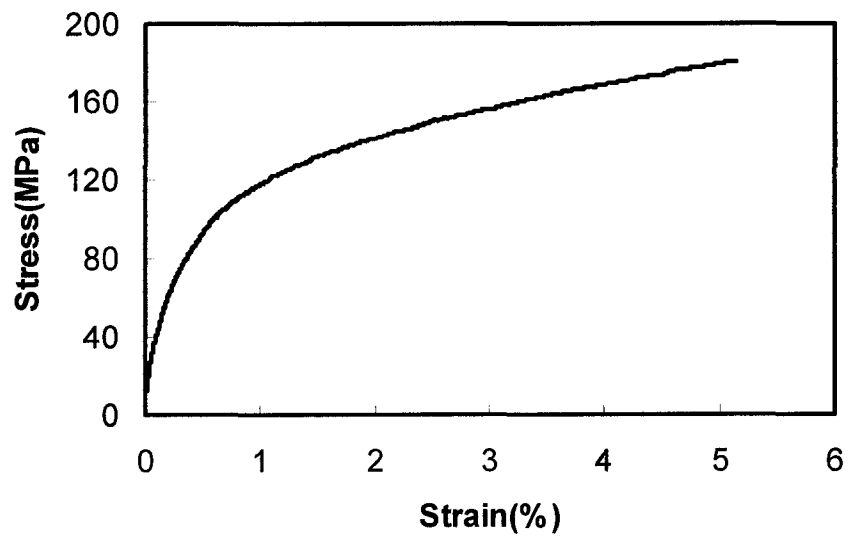
c)

Figure Ap2.4: Tensile curves of squeeze cast AMC501 under applied pressure of

60 MPa at room temperature.

154

a)

b)

155
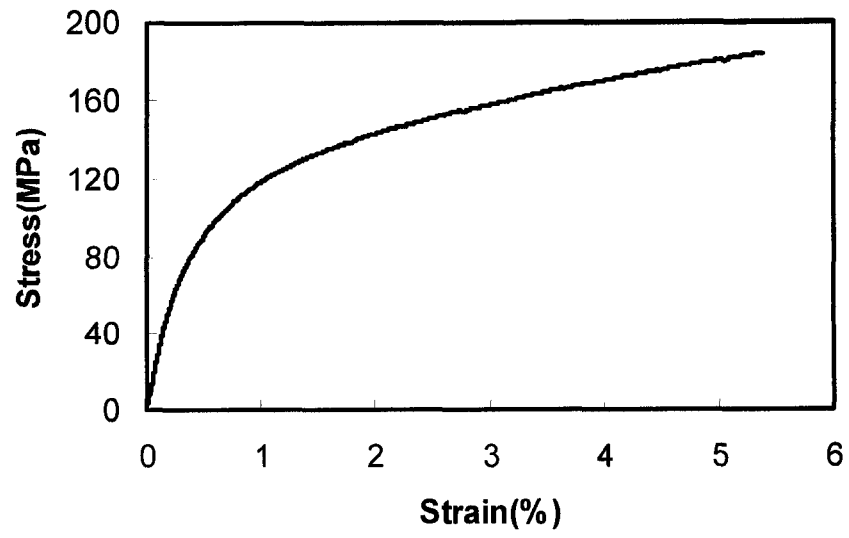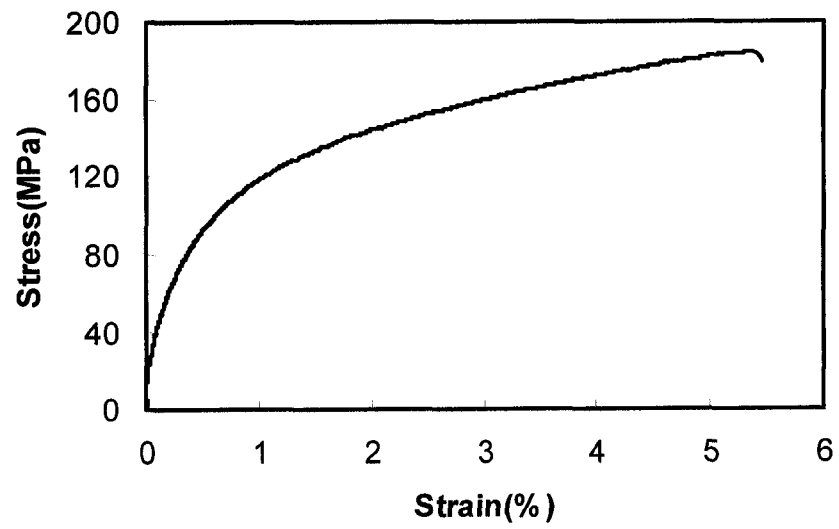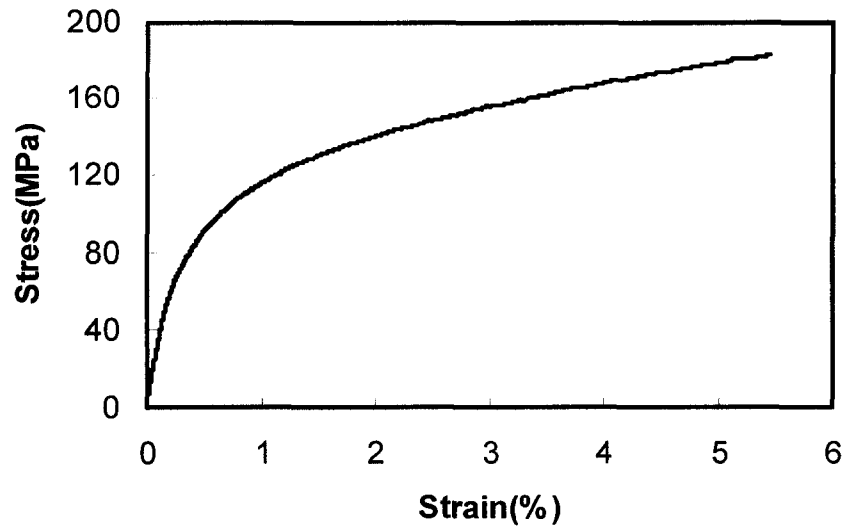
c)

Figure Ap2.5: Tensile curves of squeeze cast AMC501 under applied pressure of

90 MPa at room temperature.

a)

156
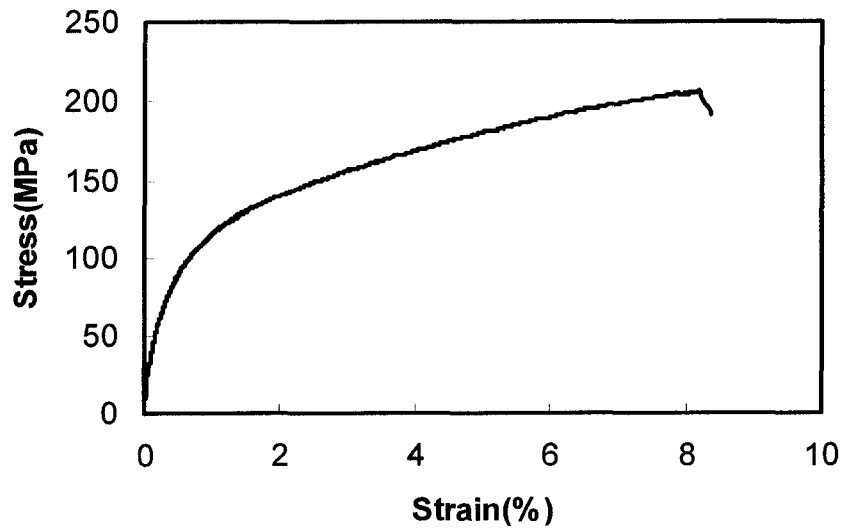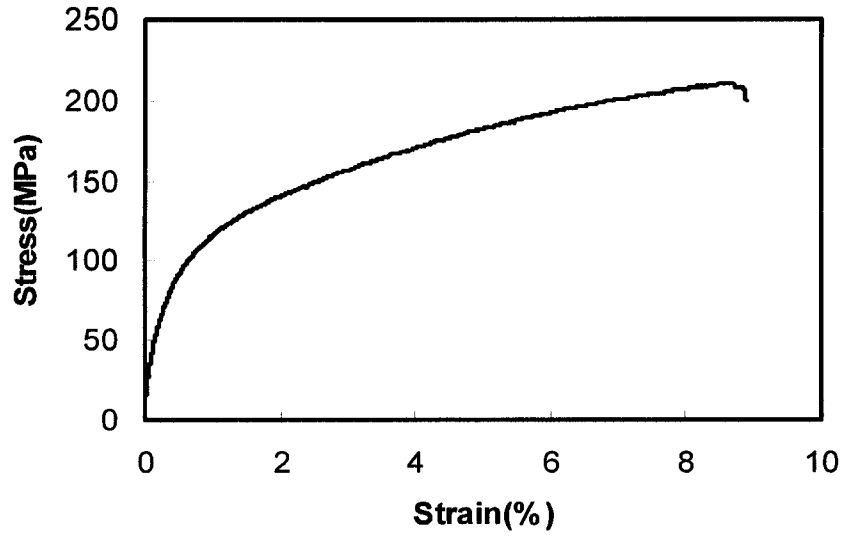
b)
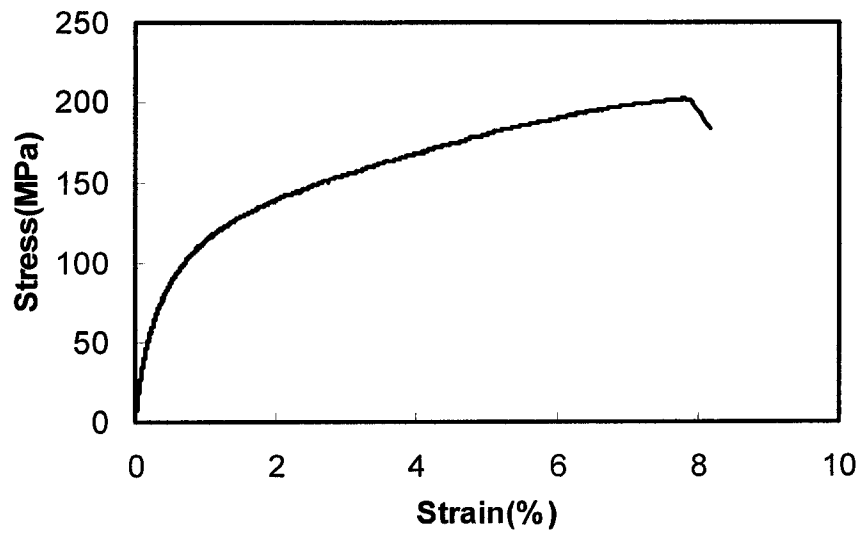
c)

Figure Ap2.6: Tensile curves of squeeze cast AM50A under applied pressure of

30 MPa at room temperature.

157

a)

b)

158
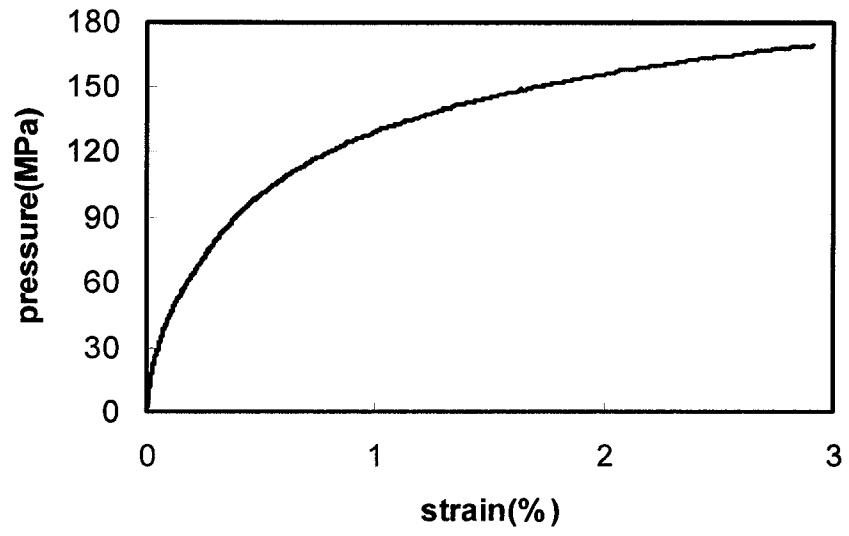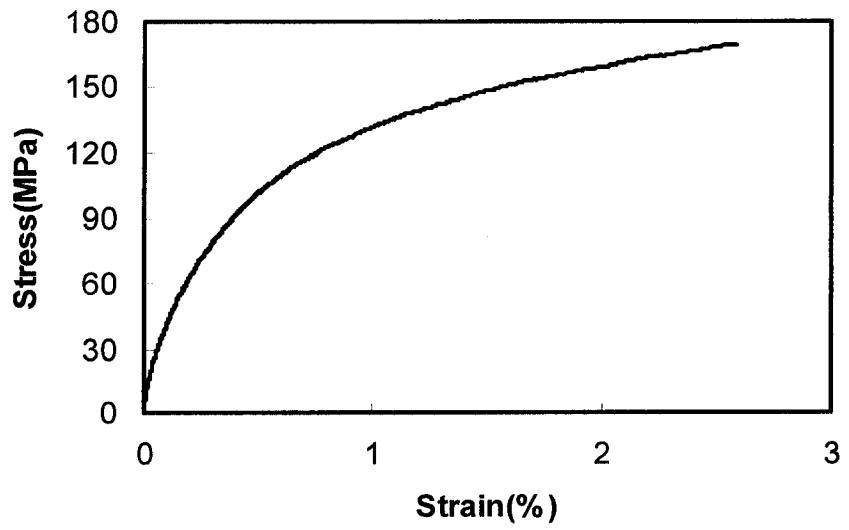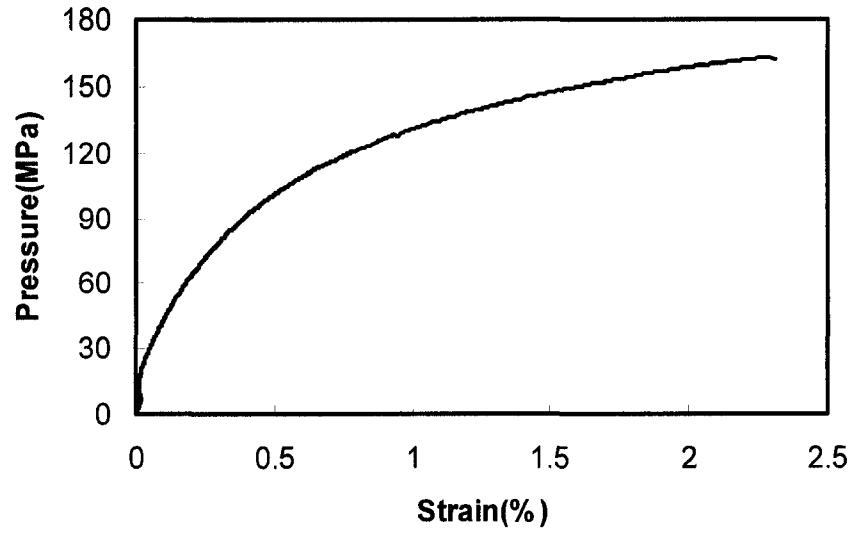
c)

Figure Ap2.7: Tensile curves of squeeze cast AMC502 under applied pressure of

30 MPa at room temperature.

a)

159
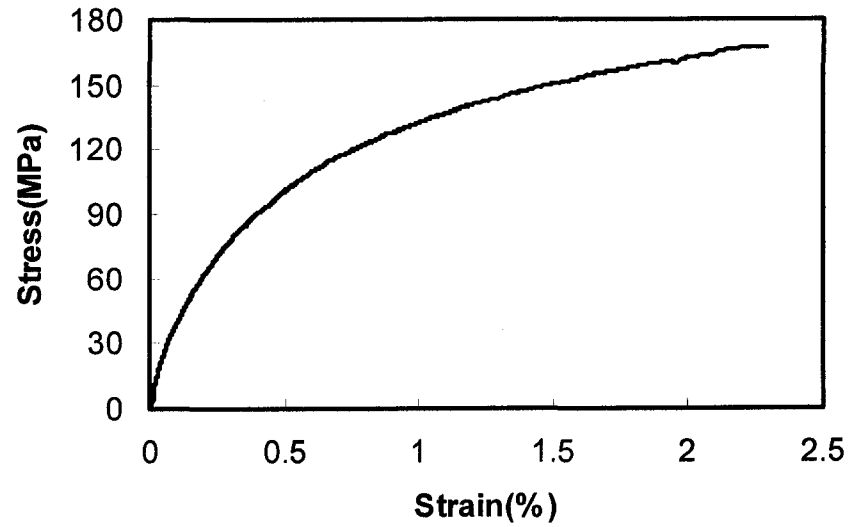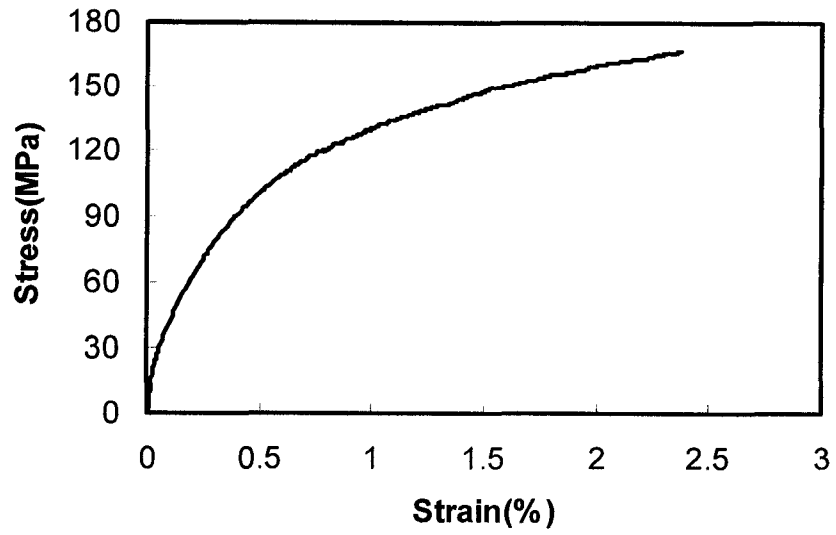
b)
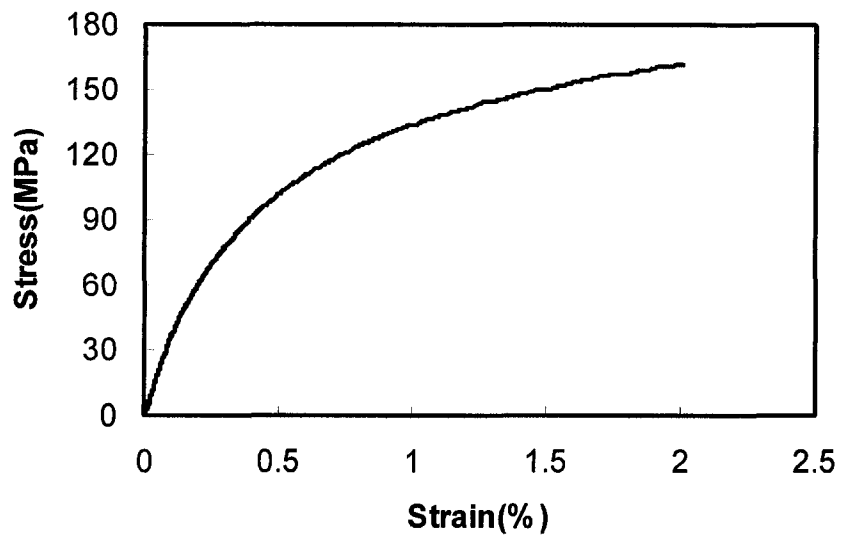
c)

Figure Ap2.8: Tensile curves of squeeze cast AMC503 under applied pressure of

30 MPa at room temperature.

160

a)

b)

161
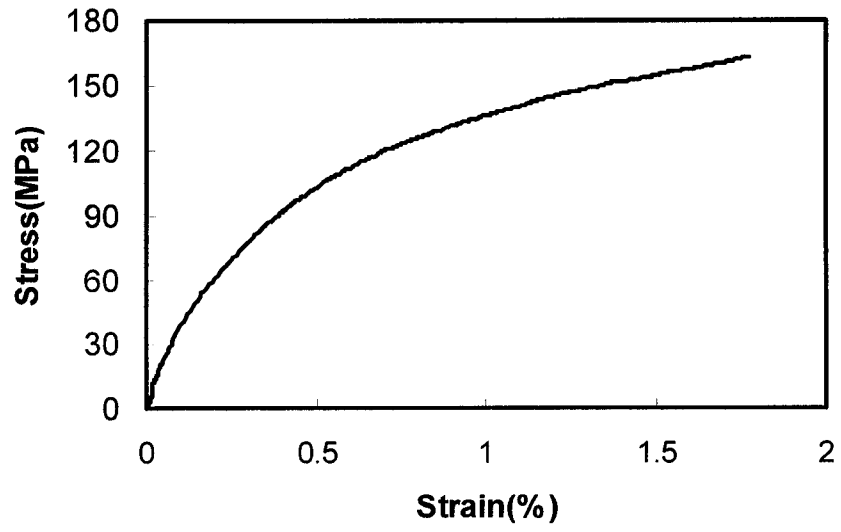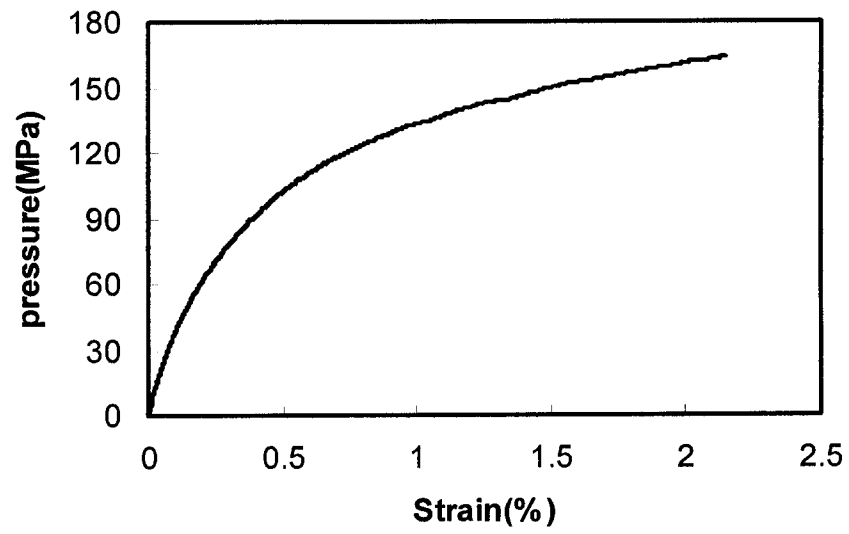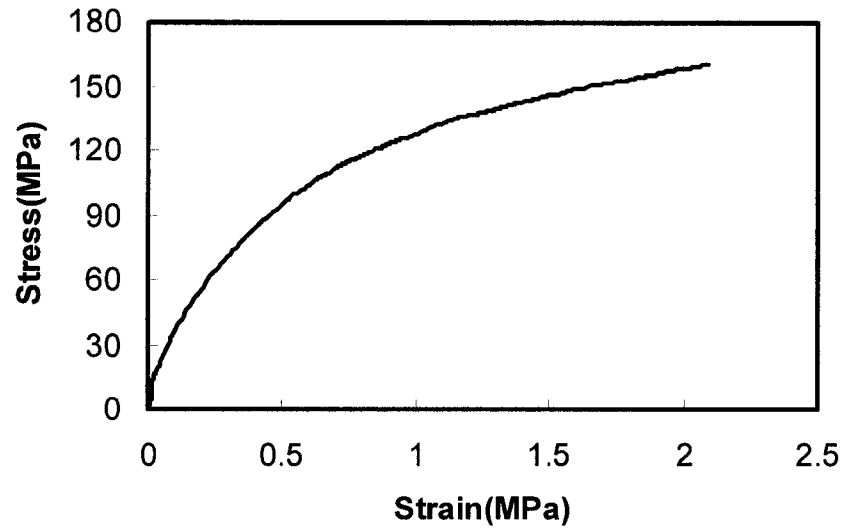
c)

Figure Ap2.9: Tensile curves of squeeze cast AMC504 under applied pressure of 30 MPa at room temperature.
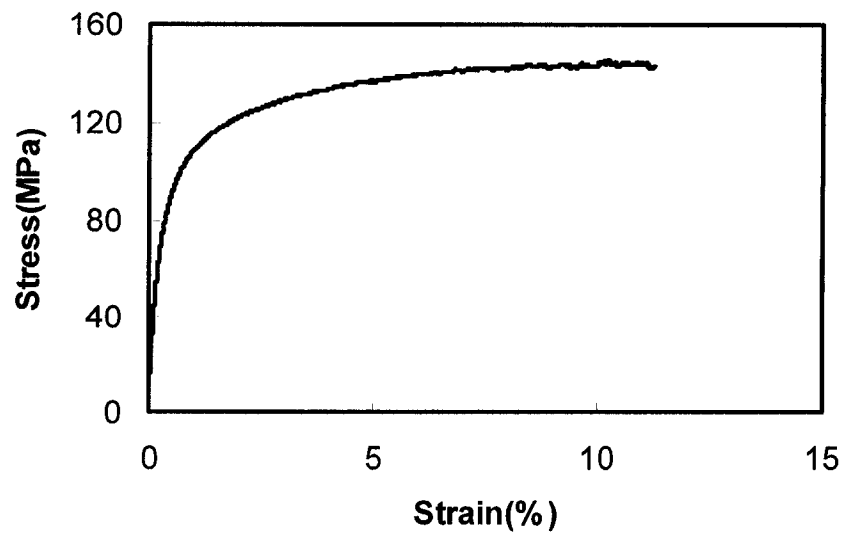

a)

162
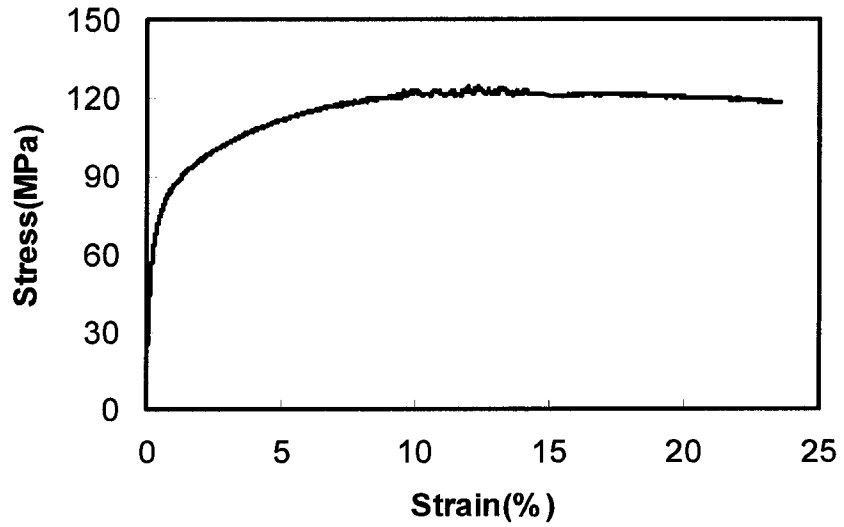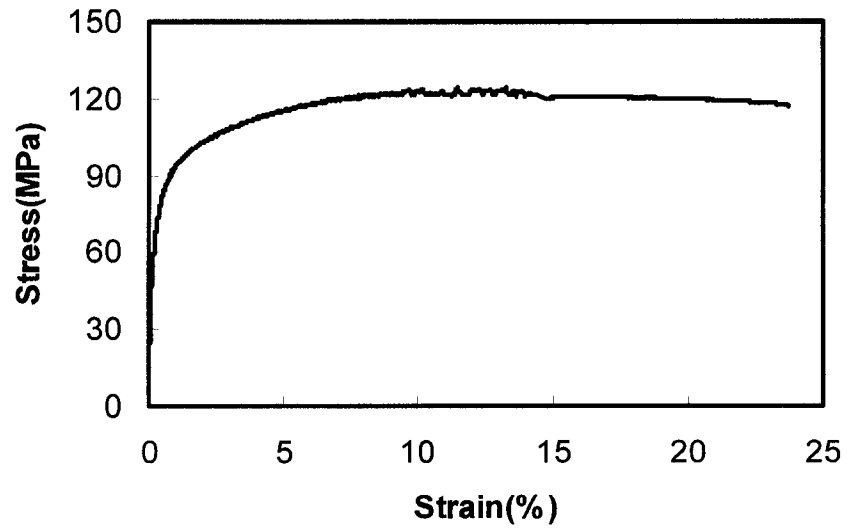
b)
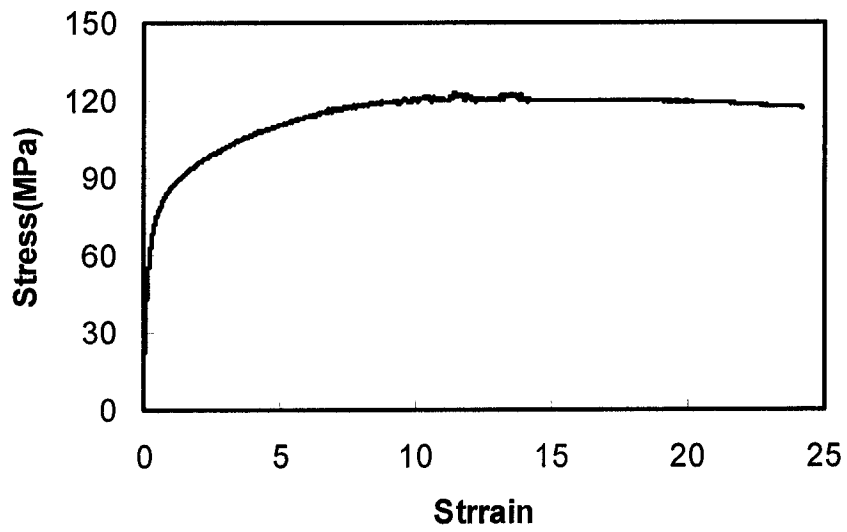
c)

Figure Ap2.10: Tensile curves of squeeze cast AM50A under applied pressure of

30 MPa at 150 °C.

163

a)

b)

164
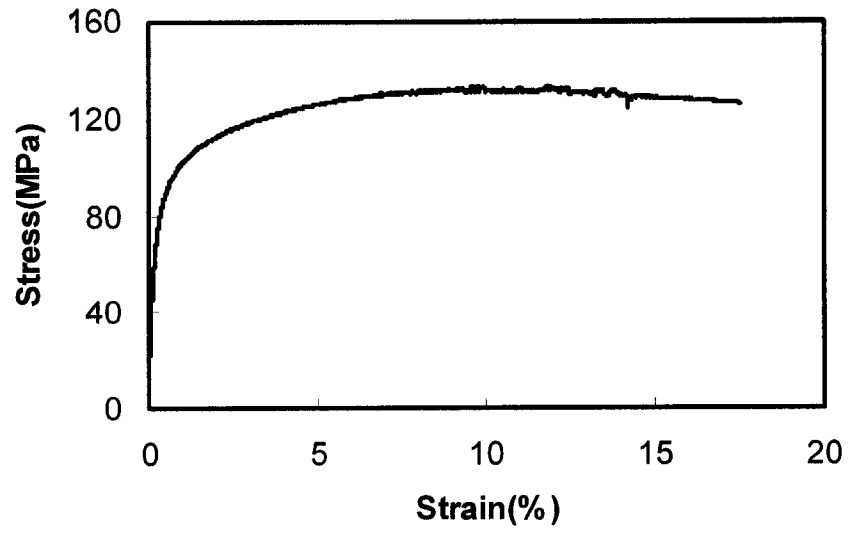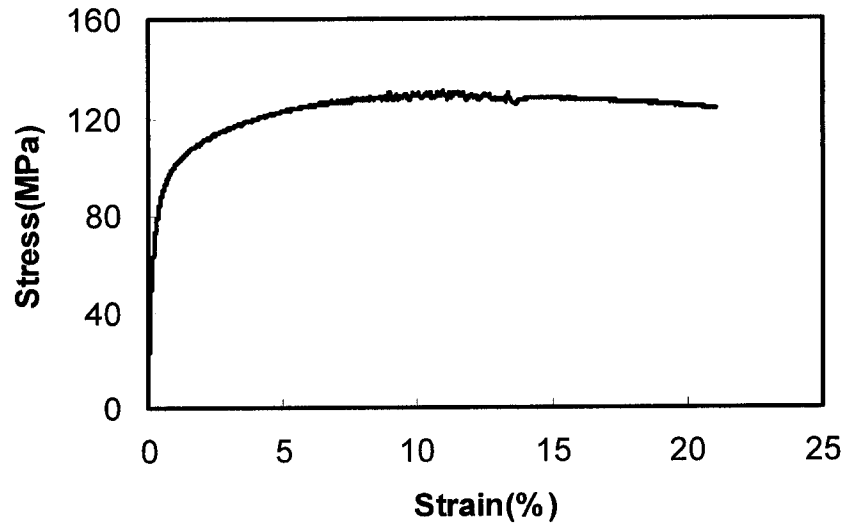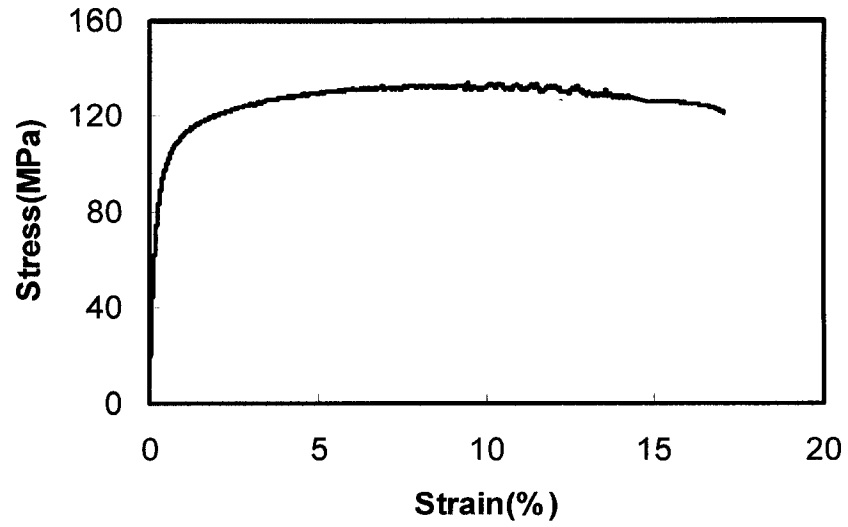
c)

Figure Ap2.11: Tensile curves of squeeze cast AMC501 under applied pressure of

30 MPa at 150°C.

a)

165

b)

c)

Figure Ap2.12: Tensile curves of squeeze cast AMC502 under applied pressure of

30 MPa at 150 °C.

166

a)

b)

167

c)

Figure Ap2.13: Tensile curves of squeeze cast AMC503 under applied pressure of

30 MPa at 150°C.

a)

168
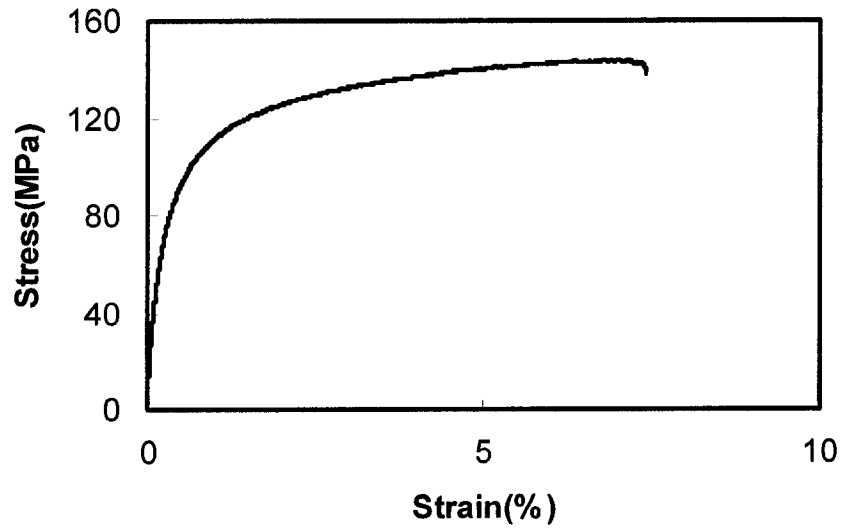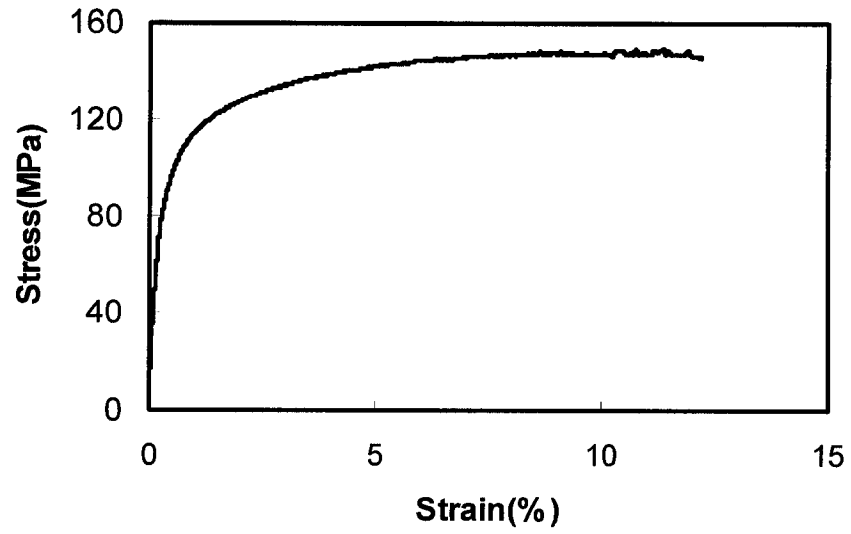
b)

c)

Figure Ap2.14: Tensile curves of squeeze cast AMC504 under applied pressure of

30 MPa at 150 °C.

169

Appendix III: Fracture surfaces
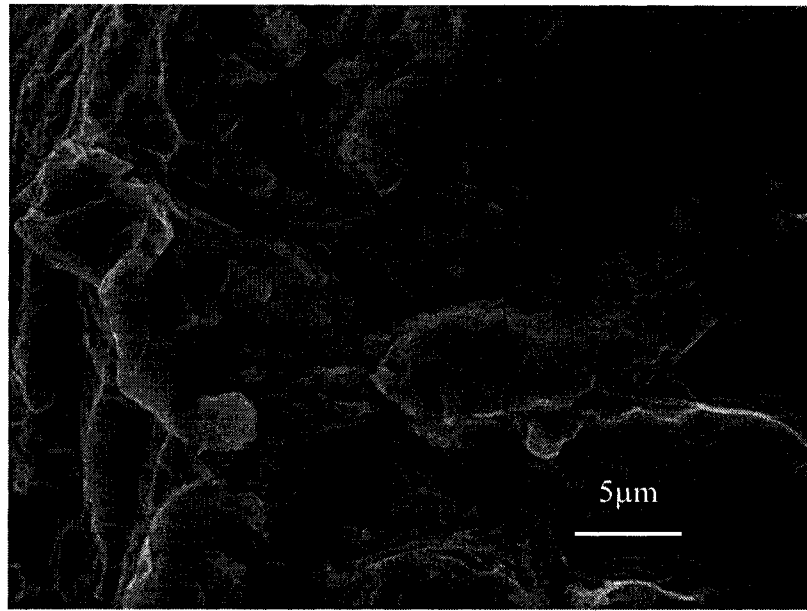
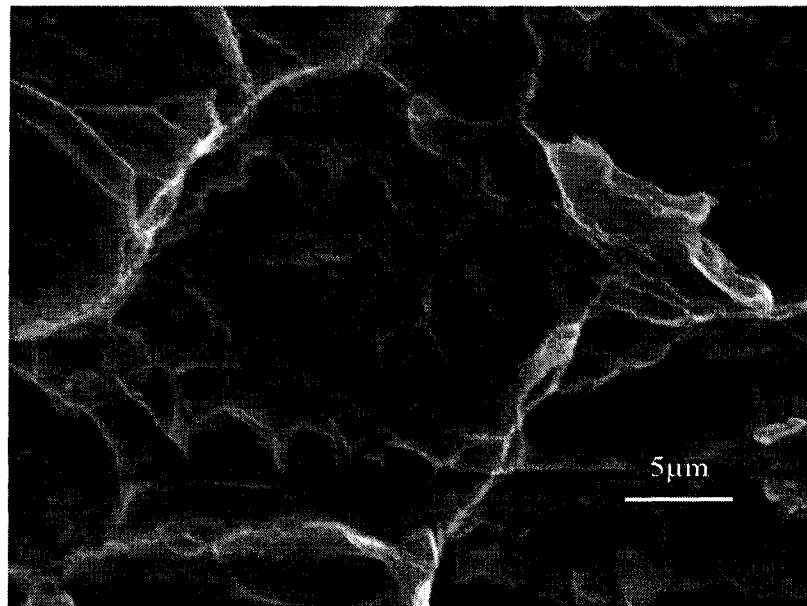Figure Ap3.1: SEM fractographs of squeeze cast AMC501 under 3 MPa.

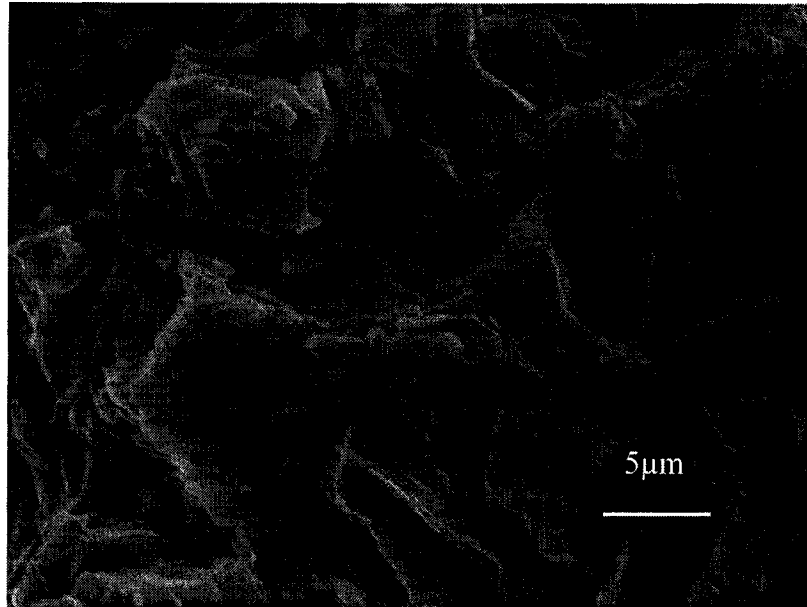Figure Ap3.2: SEM fractographs of squeeze cast AMC501 under 90 MPa.

170

Figure Ap3.3: SEM fractographs of squeeze cast AM50A under 30 MPa
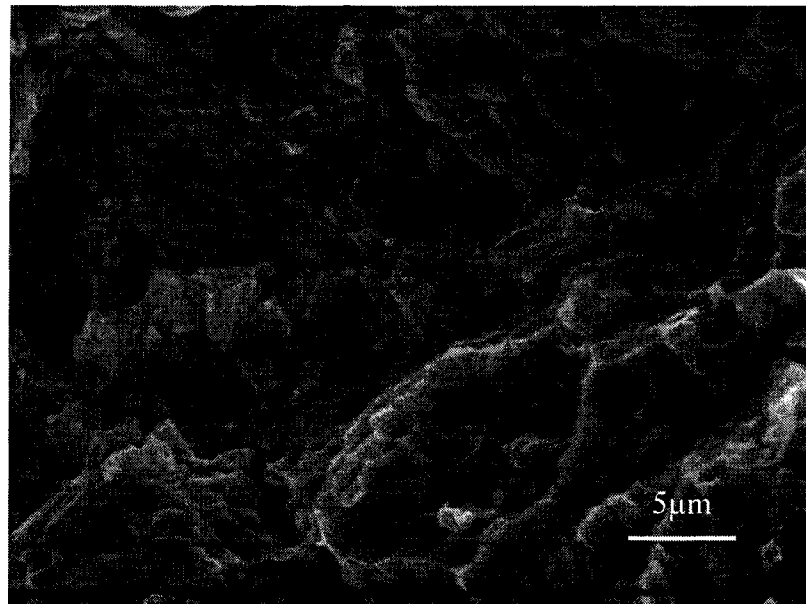
at room temperature.

Figure Ap3.4: SEM fractographs of squeeze cast AMC501 under 30 MPa
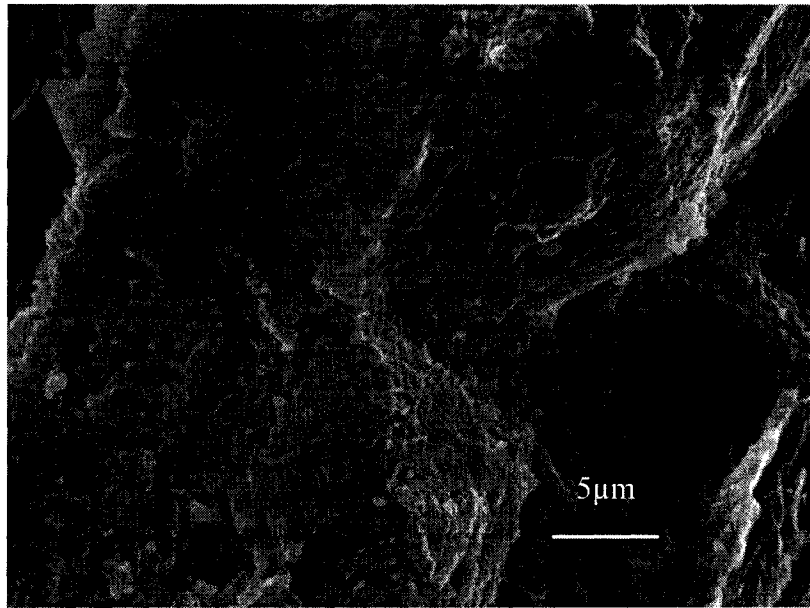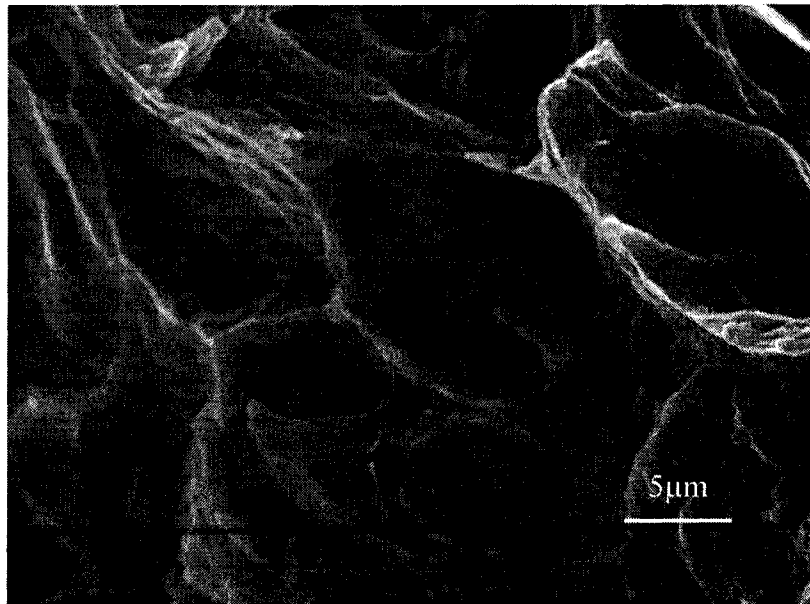
at room temperature.

171

Figure Ap3.5: SEM fractographs of squeeze cast AMC504 under 30 MPa

at room temperature.

Figure Ap3.6: SEM fractographs of squeeze cast AM50A under 30 MPa at 150 °C.

172

Figure Ap3.7: SEM fractographs of squeeze cast AMC504 under 30 MPa at 150 °C.

173

VITA AUCTORIS

NAME:	Mohsen Masoumi
PLACE OF BIRTH:	Tehran, Iran
YEAR OF BIRTH:	1971
EDUCATION:	

Iran University of Science and Technology,

Tehran, Iran

1989-1994 B.Sc.

Iran University of Science and Technology,

Tehran, Iran

1994-1997 M.Sc.

University of Windsor, Windsor, Ontario

2004-2006 M.Sc.